2020

Responses of Land Surface Phenology to Wildfire Disturbances in the Western United States Forests

Jianmin Wang
South Dakota State University

RESPONSES OF LAND SURFACE PHENOLOGY TO WILDFIRE DISTURBANCES IN THE WESTERN UNITED STATES FORESTS

BY

JIANMIN WANG

A dissertation submitted in partial fulfillment of the requirements for the

Doctor of Philosophy

Major in Geospatial Science and Engineering

Specialization in Remote Sensing Geography

South Dakota State University

2020

DISSERTATION ACCEPTANCE PAGE

Jianmin Wang

This dissertation is approved as a creditable and independent investigation by a candidate for the Doctor of Philosophy degree and is acceptable for meeting the dissertation requirements for this degree. Acceptance of this does not imply that the conclusions reached by the candidate are necessarily the conclusions of the major department.

Xiaoyang Zhang
Advisor Date

Robert Watrel
Department Head Date

Nicole Lounsbery, PhD
Director, Graduate School Date

to my wife - Meng Wang and my parents - Wenquan Wang and Baihua Hu.

ACKNOWLEDGMENTS

I would first like to express my deepest gratitude to my advisor, Dr. Xiaoyang Zhang, who has been guiding me in research and assisting me in life. Dr. Zhang provided me financial assistance in conducting this dissertation with his NASA grants (NNX14AQ18A and 80NSSC18K0626), during which he patiently gave me useful advice on scientific research and writing. Besides being a great advisor, Dr. Zhang is also a good friend in life who often goes fishing and plays card games with us. I am grateful to be a member of Dr. Zhang's group.

My gratitude also goes to Dr. David Roy and Dr. Geoffrey Henebry for being my Ph.D. committee members, teaching me classes, and giving me advice on the research. Special thanks to Dr. Roy for helping me develop an interest in fitness and to Dr. Henebry for helping me with the visa problem in 2015. I thank Dr. Michael Wimberly, a former member, for his service in my committee and for teaching me knowledge in statistics and fire. I thank Dr. Kay Cutler for being my graduate representative.

I am grateful to all my friends for the help and encouragement. Special thanks to the members of Dr. Zhang's group for the harmonious environment of research.

Last but not least, I am indebted to my family. I thank my wife, Meng, for coming into my life. Her love, encouragement, and dedication have been supporting me through the dissertation. I thank my son, Bruce, for bring me happiness. I thank my parents Wenquan and Baihua, who have always loved me unconditionally and taught me to be an upright person. I thank my sister for accompanying my parents during my study abroad. I thank my parents-in-law for visiting us and helping us take care of Bruce after his birth.

CONTENTS

ABBREVIATIONS

AVHRR	Advanced Very High Resolution Radiometer
B	Blue
BRDF	Bidirectional Reflectance Distribution Fuction
BRT	Boosted Regression Tree
BS	Burn Severity
CD	Chilling Days
DEM	Digital Elevation Model
DF	Duration of Freeze
DOY	Day Of Year
DS	Duration of Snow
EOS	End Of growing Season
EPA	Environmental Protection Agency
EVI	Enhanced Vegetation Index
EVI2	two-band Enhanced Vgetation Index
FFD	First Freeze Date
FSA	Farm Service Agency
FSD	First Snow Date
G	Green
GDD	Growing Degree Day
GEE	Google Earth Engine
GMax	seasonal Greenness Maximum
GMin	seasonal Greenness Minimum

GRatio	the Ratio of GMin to GMax
HLS	Harmonized Landsat Sentinel-2
HPLM	Hybrid Piecewise-Logistic-Model
HPLM-LPSD	hybrid piecewise-logistic-model-based LSP detection
LFD	Last Freeze Date
LOS	Length of growing Season
LSD	Last Snow Date
LSP	Land Surface Phenology
LST	Land Surface Temperature
MAD	Mean Absolute Deviation
MD	Mean Deviation
MK	Mann-Kendall
MODIS	Moderate-resolution Imaging Spectroradiometer
MSI	Multi-Spectral Instrument
MTBS	Monitoring Trends in Burn Severity
NAIP	National Agriculture Imagery Program
NASA	National Aeronautics and Space Administration
NBAR	Nadir BRDF Adjusted Reflectances
NBR	Normalized Burn Ratio
NDVI	Normalized Difference Vegetation Index
NDWI	normalized difference water index
NIR	Near-Infrared
NLCD	National Land Cover Database

OLI	Operational Land Imager
PGQ	Proportion of Good Quality
Prcp	Precipitation
QA	Quality Assessment/Assurance
R	Red
SOS	Start Of growing Season
SRad	Shortwave Radiation
SRTM	Shuttle Radar Topography Mission
TMax	Maximum Temperature
TMin	Minimum Temperature
TPV	Tree Proportion to Vegetation
US	United States
USA	United States of America
USA-NPN	USA - National Phenology Network
USDA	US Department of Agriculture
UTM	Universal Transverse Mercator
VFC	Vegetation Fractional Coverage
VI	Vegetation Index
VIIRS	Visible Infrared Imaging Radiometer Suite

LIST OF FIGURES

LIST OF TABLES

ABSTRACT

RESPONSES OF LAND SURFACE PHENOLOGY TO WILDFIRE DISTURBANCES IN THE WESTERN UNITED STATES FORESTS

JIANMIN WANG

2020

Land surface phenology (LSP) characterizes the seasonal dynamics in the vegetation communities observed for a satellite pixel and it has been widely associated with global climate change. However, LSP and its long-term trend can be influenced by land disturbance events, which could greatly interrupt the LSP responses to climate change. Wildfire is one of the main disturbance agents in the western United States (US) forests, but its impacts on LSP have not been investigated yet. To gain a comprehensive understanding of the LSP responses to wildfires in the western US forests, this dissertation focused on three research objectives: (1) to perform a case study of wildfire impacts on LSP and its trend by comparing the burned and a reference area, (2) to investigate the distribution of wildfire impacts on LSP and identify control factors by analyzing all the wildfires across the western US forests, and (3) to quantify the contributions of land cover composition and other environmental factors to the spatial and interannual variations of LSP in a recently burned landscape. The results reveal that wildfires play a significant role in influencing spatial and interannual variations in LSP across the western US forests. First, the case study showed that the Hayman Fire significantly advanced the start of growing season (SOS) and caused an advancing SOS trend comparing with a delaying trend in the reference area. Second, summarizing >800

wildfires found that the shifts in LSP timing were divergent depending on individual wildfire events and burn severity. Moreover, wildfires showed a stronger impact on the end of growing season (EOS) than SOS. Last, LSP trends were interrupted by wildfires with the degree of impact largely dependent on the wildfire occurrence year. Third, LSP modeling showed that land cover composition, climate, and topography co-determine the LSP variations. Specifically, land cover composition and climate dominate the LSP spatial and interannual variations, respectively. Overall, this research improves the understanding of wildfire impacts on LSP and the underlying mechanism of various factors driving LSP. This research also provides a prototype that can be extended to investigate the impacts on LSP from other disturbances.

CHAPTER 1: Introduction

1.1. Background

1.1.1. Overview of vegetation phenology

Phenology is the study of the timing of recurrent biological events (Lieth, 1974). For vegetation, phenology can either pertain to observable physical changes (e.g., leaf development and abscission) in vegetation structure or physiological changes regulating the seasonality of photosynthesis and evapotranspiration (Gu et al., 2003; Richardson et al., 2012). Because of its sensitivity to climatic variation and readily understandability to the public, phenology has been selected as one of the most effective indicators to track ecosystem changes in response to climate change by the Intergovernmental Panel on Climate Change (IPCC, 2014, 2007), the United States (US) Global Change Research Program (NCA, 2015, 2010), and the Environmental Protection Agency (U.S. EPA, 2016).

The climate change-induced phenological shifts have strong impacts on ecosystems and human health. First, the phenological shifts influence ecosystem productivity by regulating the processes related to photosynthesis, such as cycling of carbon (Churkina et al., 2005; Dragoni et al., 2011; Bao et al., 2019), water (Hogg et al., 2000; Stéfanon et al., 2012; Muche et al., 2019), and nutrient (Cooke and Weih, 2005; Estiarte and Peñuelas, 2015). Second, the potential difference in phenological sensitivity to temperature among species can significantly change the synchrony of interacting species (Rafferty et al., 2013; Kharouba et al., 2018). Third, phenological shifts could influence the risk of wildfire activity by changing fuel availability and moisture content (Elmore et al., 2005; Bajocco et al., 2015). Fourth, phenological shifts change climate by altering land surface energy and water flux (Jeong et al., 2009; Lian et al., 2020). For

example, advanced spring phenology raises evapotranspiration and causes extra soil drying that amplifies the frequency and intensity of summer heatwaves (Lian et al., 2020). Last but not least, phenological shifts influence human health because the timing of flowering determines exposure dynamics of allergenic pollen that triggers human allergic diseases (Li et al., 2019; Sapkota et al., 2019).

Considering the strong linkage to climate change, ecosystem, and human health, the dynamics of vegetation phenology have been extensively monitored and studied. A traditional method of monitoring and studying phenology is using ground-based human observations. The recent establishment of some national- and continental-scale phenological observations networks, such as USA National Phenology Network (USA-NPN; https://www.usanpn.org/), facilitates the collection and sharing of standardized phenological observations at a large scale. However, the ground observations of phenology are subject to some limitations: the uneven spatial distribution of observations, the limited number of observed species and individuals, the subjective observations among different observers even with a standardized protocol (Piao et al., 2019). These limitations pose a challenge to a comprehensive analysis of phenological responses of various species to climate changes at a large scale.

1.1.2. Land surface phenology

Remote sensing technique provides a robust tool to detect phenology by processing digital imagery from local to global scales with low labor intensity and limited artificial subjectivity. Providing temporally frequent, continuous, and consistent observations of land surface over a large area with little time lag, satellite data have been extensively used in phenological studies during the last few decades. The phenology

retrieved using remote sensing characterizes the seasonal dynamics of vegetation greenness in communities, which is usually referred to as land surface phenology (LSP) (de Beurs and Henebry, 2005). LSP often refers to key transition dates in the annual cycle of vegetation greenness development (LSP timing), which is distinct from the ground-observed species-specific phenology that refers to specific life cycle events of vegetation such as bud break or leaf senescence. LSP also characterizes the magnitude of vegetation greenness at a certain phenological stage (LSP greenness).

A variety of satellite data are available for investigating LSP. Giving the longest time series of daily global coverage available since 1982, the advanced very high resolution radiometer (AVHRR) data have been widely used to detect LSP at a spatial resolution from 4km-16km (Duchemin et al., 1999; Marshall et al., 2016; Moulin et al., 1997; Nagai et al., 2016; Sehgal et al., 2011). However, AVHRR data suffer from the lack of precise radiometric calibration, poor geometric registration, and peculiar spatial resampling (Goward et al., 1991; Wu et al., 2010) which impairs the accuracy of the retrieved LSP (Zhang, 2015). Since 2000, the moderate resolution imaging spectroradiometer (MODIS) data have been providing daily global observations with improved temporal, spatial, and radiometric resolutions, which have triggered numerous studies to retrieve LSP at 250 m – 5,000 m (Ganguly et al., 2010; Sakamoto et al., 2010; Zhang et al., 2003). As MODIS is aging, the visible infrared imaging radiometer suite (VIIRS) has been used as the successor of MODIS to produce regional to global LSP products (Zhang et al., 2018).

Moreover, the free and open access to Landsat archive has allowed for LSP detection at a higher spatial resolution of 30 m from 1984. However, retrieving LSP using

Landsat data is very challenging because of the 16-day revisit interval for a single Landsat (8-day when considering two Landsat satellites on orbit simultaneously) and the data gaps associated with cloud contaminations and scan-line corrector failure (on the Landsat 7 ETM+). To overcome this limitation, a dense Landsat time series for LSP retrieval has been generated with three primary methods: using the adjacent Landsat images in the overlap zones of Landsat orbits (Liu et al., 2017), merging Landsat observations from multiple years (Melaas et al., 2013), and fusing Landsat data with data of higher temporal resolution from other satellites (e.g., MODIS) (Baumann et al., 2017; Zhang et al., 2017). Recently, the European Space Agency Sentinel-2 satellites (Sentinel-2A launched in 2015 and Sentinel-2B launched in 2017) provide data with a spatial resolution of 10-20 m and revisit interval of up to 5 days and allow for studying LSP in much greater details (Misra et al., 2020). The temporal resolution of the Sentinel-2 time series can be further improved by fusing with other datasets such as Landsat 8 data (Claverie et al., 2018) and VIIRS data (Zhang et al., 2020). Particularly, the Harmonized Landsat and Sentinel-2 (HLS) project at NASA generates spatially co-registered surface reflectance products using observations from Landsat 8 (launched in 2013) and Sentinel-2A (launched in 2015) and Sentinel-2B (launched in 2017) satellites (Claverie et al., 2018). Combining these three satellites, HLS can provide observations with a nominal global median average interval of 2.9 days (Li and Roy, 2017).

More recently, the PlanetScope data provide daily-to-weekly global coverage at a 3-m spatial resolution with a constellation of 130+ CubeSats (Planet Labs Inc, 2020), which offer an unprecedented opportunity to retrieve high resolution LSP at a regional scale. For example, Cheng et al. (2020) found that PlanetScope produced LSP retrievals

with fewer spatial artifacts than that derived from Sentinel-2. However, the performance of LSP retrieval from PlanetScope could be significantly influenced by the relatively low radiometric data quality and the different spectral response functions among different sensors (Houborg and McCabe, 2018). It has been suggested that PlanetScope data need to calibrate with other rigorously calibrated data such as MODIS, Landsat-8, and Sentinel-2 (Houborg and McCabe, 2018; Latte and Lejeune, 2020; Leach et al., 2019; Wang et al., 2020).

In addition to satellite data, digital repeat photography from cameras mounted overlooking the vegetation of interest (Richardson et al., 2018) and remote sensing images from spectroradiometer aboard aerial vehicles (Yang et al., 2020) have also been used to retrieve phenology at a local or landscape scale.

Using the above remote sensing data, LSP is usually derived from time series of vegetation index (VI) which depicts seasonal vegetation greenness dynamics. The most commonly used satellite-based vegetation index is the normalized difference vegetation index (NDVI) calculated from the reflectance at red and near-infrared (NIR) bands. As NDVI is sensitive to soil background brightness and saturates over densely vegetated areas, the enhanced vegetation index (EVI) has been developed to improve the quantification of vegetation activity by including the blue band (Huete et al., 2002). EVI is further modified to the two-band EVI (EVI2), which remains the advantages over NDVI, by removing the blue band (relatively low signal-to-noise ratio) using the correlation of surface reflectance between the red and blue bands (Jiang et al., 2008).

A variety of algorithms have been developed to detect the phenological transition dates from the VI time series. A commonly used algorithm is the threshold method that

identifies transition dates by empirically setting an absolute or relative VI value (White et al., 1997). The performance of this method largely depends on the choice of thresholds. Another algorithm for LSP detection is the delayed moving average that determines key transition dates based on the intersection of the vegetation index time series and a moving average curve (Reed et al., 1994; Archibald and Scholes, 2007). The length of the time interval for moving average influences the accuracy of LSP detection. In contrast, the derivative-based or curvature-based method does not need to set up the threshold or time interval manually. Specifically, this type of method first fits the VI time series with mathematic functions (e.g., piecewise logistic function) and then detects the phenological transition dates as the inflection points in the first-order or higher-order derivatives of the VI time series (Tan et al., 2011) or as the dates with the maximal or minimal rate of change in the curvature of the VI times series (Zhang et al., 2003). Besides the LSP timing metrics mainly including start (SOS), end (EOS), and length (LOS) of growing season, the LSP greenness metrics such as seasonal greenness maximum (GMax) and minimum (GMin) can also be retrieved from the fitted VI time series (Zhang, 2018). LSP has also been retrieved using other algorithms, such as models based on growing degree days (de Beurs and Henebry, 2004; de Beurs and Henebry, 2005; Tomaszewska et al., 2020), phenology matching methods (Sakamoto et al., 2010; Zeng et al., 2016), and machine learning methods (Wang et al., 2019).

1.1.3. Recent changes in LSP

LSP changes over the past three decades have been extensively investigated, revealing a general pattern of advanced SOS, delayed EOS, and prolonged LOS with the change extent varying across regions, periods, and methods (Jeong et al., 2011). For

example, using AVHRR NDVI time series, Myneni et al. (1997) found a global advance of 8 days in SOS and a delay of 4 days in EOS from 1981 to 1990; Julien and Sobrino (2009) found an advance by 3.8 days/decade in SOS, a delay by 4.5 days/decade in EOS, and a prolongation by 8 days/decade in LOS globally during 1981-2003; Jeong et al. (2011) found SOS was advanced by 5.2 days in 1982-1999 and by 0.2 days in 2000-2008, while EOS was delayed by 4.3 days in 1982-1999 and by 2.3 days in 2000-2008. Besides, Zeng et al. (2011) found an advanced SOS (4.7 days/decade) and a delayed EOS (1.6 days/decade) during 2000-2010 across the northern high-latitude region (≥60 °N) using MODIS NDVI. Specifically, the SOS advancing rate was 11.5 days/decade in northern America and 2.7 days/decade in Eurasia, while the EOS delaying rate was 2.2 days/decade in northern America and 3.5 days in Eurasia. Using EVI2 time series from both AVHRR and MODIS, Zhang et al. (2014) revealed a general advancing trend of SOS (-2.2 to -12.1 days/decade) during periods of 1982-1999 and 2000-2010 in temperate, cold, and polar climate regions in the North Hemisphere, with one exception (8.7 days/decade) in the temperate climate – dry winter region in Asia from 2000-2010.

In contrast, some other studies found no evidence of significant LSP trends or even opposite LSP trends (i.e., a delayed SOS, advanced EOS, and shortened LOS). For example, AVHRR NDVI data records found no significant SOS trend in North America from 1982-2006 (White et al., 2009) and a delayed SOS trend by 6.6 days/decade in western central Europe from 2000-2011 (Fu et al., 2014). Moreover, Zhang et al. (2007) found SOS was advanced by 3.2 days/decade above 40 °N and delayed by 1.5 days/decade below 31 °N in North America from 1982 to 2005.

1.1.4. Drivers and mechanisms

The complex pattern of LSP variation is a manifestation of the interacted roles of different drivers in regulating the vegetation phenology. Among all the potential drivers, temperature is generally regarded as the primary control of phenology. Specifically, it is assumed that spring phenological events occur when a certain accumulation of forcing temperature is achieved. Thus, the phenological dynamics have been widely linked with growing degree days (GDDs) calculated as the accumulated temperature above a threshold in the preseason (preceding season) (de Beurs and Henebry, 2005; White et al., 1997). Spring phenology tends to occur earlier with higher temperatures and later with lower temperatures. On the other hand, some studies indicated a need for winter chilling to break the vegetation dormancy before the occurrence of spring phenology (Cong et al., 2017; Delpierre et al., 2018; Richardson et al., 2006). For example, using the AVHRR NDVI data, Zhang et al. (2007) addressed the importance of chilling requirement for SOS occurrence and insufficient chilling conditions resulted in the delaying trend of SOS below 31 °N in North America. The combination of forcing and chilling effects of temperature has partly resulted in a declining global warming effect on spring phenology (Fu et al., 2015). For the occurrence of autumn phenology, a cooling requirement is needed but the effect is still poorly understood (Delpierre et al., 2009).

Besides temperature, other environmental factors also drive the phenological variations. Specifically, phenological events are commonly modeled using photoperiod and precipitation (Fracheboud et al., 2009; Jolly and Running, 2004; Piao et al., 2019). Moreover, phenology is also partially regulated by insolation (Liu et al., 2016), extreme weather events (Qiu et al., 2020), nutrient and water availability (Estiarte and Peñuelas,

2015; Fay et al., 2012), and the snow seasonality at mid- and high- latitudes and high elevations (Tomaszewska et al., 2020; Xie et al., 2017). In addition, the spatial patterns of vegetation phenology at a local to landscape scale are altered by topographic properties (e.g., elevation and aspects) influencing topoclimatic conditions (An et al., 2018; Misra et al., 2018; Xie et al., 2017).

In contrast to these aforementioned factors controlling both ground observations and LSP, the variation in land cover composition in pixels is influencing specifically the satellite-based LSP (Chen et al., 2018; Melaas et al., 2015; Misra et al., 2018). Satellite pixels, particularly at moderate (10-250 m) and coarse (>250 m) resolutions (Thomas et al., 2020), usually consist of a mixture of land cover types and plant species with different phenological responses to environmental factors (Augspurger et al., 2005; Zhang et al., 2017). The change in sub-pixel land cover composition, which can be caused by both natural processes (e.g., disturbances, climate extremes, and species invasion) and human activities (e.g., urbanization, deforestation, and crop rotation) (Zhang et al., 2019), can lead to a great change in LSP. The LSP change could subsequently modify the direction and magnitude of the interannual phenological trend, which impairs the effectiveness of phenological trends indicating climate change.

During the past few years, increasing evidence has indeed revealed the effect of land cover composition on LSP. For example, a simulation study demonstrated that SOS of mixed pixel was substantially altered by the changes in proportions of endmembers even if there was no change in SOS of each endmember (Chen et al., 2018). Moreover, using MODIS NDVI data, Misra et al. (2018) found the EOS was linked to subpixel percentage of broadleaf forests. Cho et al. (2017) found that tree cover explained 3% of

the variance of SOS and 40% for EOS in the semi-arid savanna of Southern Africa. Zhang et al. (2019) found a delaying trend of 1.8-6.7 days/decade in SOS in agricultural ecosystems spanning the Midwest of the US from 1982 to 2014. Two-thirds of the delaying trend was attributed to the areal increases in corn and soybean that have later emergence and the areal decreases in wheat and oats that have earlier emergence and one-third to climatic variation.

These findings manifest that LSP as a climate indicator is likely influenced by the change of land cover composition. This influence could be significant because land cover changes are undergoing in most part of the Earth (Buyantuyev and Wu, 2012; de Beurs and Henebry, 2004; Romo-Leon et al., 2016; White et al., 2005). This issue severely limits our understanding of phenological variability and trends that reflect climate change across regional to global scales (White et al., 2005).

1.1.5. Wildfires in the western US

As one of the most important land disturbance agents across the world, wildfire causes variation in land cover composition at a local to regional scale and subsequently changes LSP. Wildfire impact on LSP could be complex including a quick change with the burning and a gradual change with the post-fire vegetation succession that changes plant species composition and growth conditions (Johnson et al., 2012; Laughlin et al., 2004; Pongratz et al., 2006). Wildfire impacts on the LSP have been demonstrated using MODIS data. Specifically, wildfires caused an abrupt advance in SOS, delay in EOS, and prolongation in LOS with a trend of returning to pre-fire LSP in Mt Carmel, Israel (Van Leeuwen et al., 2010) and in Northern Italy alpine forests (Di-Mauro et al., 2014), but no

significant LSP change in the Guadalest Fire area, Alicante, Spain (Van Leeuwen et al., 2010).

The western US forests are among the ecosystems most affected by wildfires. Associating with climate change, large wildfire activities have abruptly increased since the mid-1980s with higher large-wildfire frequency, longer wildfire durations, and longer wildfire seasons with the greatest increases in mid-elevation Northern Rockies Forests (Westerling et al., 2006). Considering a total of 12.3% of forests burned during 1984-2014 based on the Monitoring Trends in Burn Severity (MTBS) data, LSP could be largely influenced by wildfires in the western US forests. However, these impacts have not been studied yet. This knowledge gap needs to be filled by conducting a systematic analysis of the wildfire impacts on LSP and its trends.

1.2. Research goal, objectives, and hypotheses

The overall goal of this dissertation research is to gain a comprehensive understanding of the responses of LSP to wildfires in the western US forests. For this goal, three objectives are developed and achieved by conducting three studies.

Objective 1: quantify the impacts of a wildfire in the western US forests on the magnitudes and interannual trends of SOS by using an unburned buffer as a reference.

Although few existing studies demonstrated wildfire impacts on LSP in the burned areas (Di-Mauro et al., 2014; Van Leeuwen et al., 2010), there is no clear evidence of wildfire impacts in the western US forests. Moreover, those studies used the LSP as a proxy to study the post-fire vegetation recovery, but none of them directly quantified the wildfire impacts on LSP magnitudes and trends. This study selects a large wildfire event in the western US forest and develops a method to quantify its impact on

SOS. Specifically, a buffer that is not influenced by the wildfire surrounding the burned area is used as a reference. By comparing the burned and buffer areas, the wildfire impacts on LSP magnitudes and trends are quantified.

Objective 2: investigate the distribution of wildfire impacts on LSP and identify factors controlling the wildfire impacts by analyzing all the wildfires across the western US forests.

Analyzing an individual LSP metric in an individual wildfire event from different studies has revealed an inconsistent pattern of wildfire impacts on LSP (Di-Mauro et al., 2014; Van Leeuwen et al., 2010), but there is a lack of a systematic analysis of wildfire impacts on both LSP timing and greenness metrics over a large region. Using all the wildfires in the western US forests occurred during 2002-2014, this study conducts the first systematic analysis of forest wildfire impacts on the values and trends of LSP metrics including SOS, EOS, LOS, GMax, and GMin, which allows for the further identification of factors controlling the wildfire impacts, such as burn severity.

Objective 3: compute the contributions of land cover composition change and other environmental factors to the spatial and interannual variations of LSP in a recently burned landscape in the western US forests.

An accurate LSP modeling is critical to terrestrial biosphere models simulating the biological processes on the land surface and to accurate forecasts of vegetation responses to different future climatic scenarios (Richardson et al., 2013). Conventionally, climate and topography that are regarded as the primary controls of temporal and spatial variations of phenology, respectively. Meanwhile, increasing evidence showed the influence of land cover composition change, which can be caused by wildfires, on LSP

(Chen et al., 2018; Cho et al., 2017; Misra et al., 2018). However, the quantitative contribution of various environmental factors on LSP remains unclear. To fill the gap, this study selects a large wildfire event in the western US forests, where land cover composition experiences spatial and interannual dynamics, to investigate the contributions of land cover composition and other environmental factors to LSP variations. This investigation uses a machine learning method to model spatial and interannual variations of LSP with the change in land cover composition, climate data, and topography.

Corresponding to the three objectives, three hypotheses are outlined as the following.

Hypothesis 1: the interannual trend of SOS timing becomes earlier after the occurrence of the 2002 Hayman Fire, Colorado, USA.

The Hayman Fire, the largest wildfire in the recorded history of Colorado, which occurred in 2002, is used to perform a preliminary test of the wildfire impacts on LSP and its trend in the western US forests. As the Hayman Fire largely converted the evergreen conifer forests to shrub and grass patches, the SOS trend in the burned area is expected to be earlier after the fire occurrence.

Hypothesis 2: wildfires in the western US forests change the LSP timing in both earlier and later directions with the largest change at the moderate burn severity.

While LSP greenness is expected to decrease with wildfire burning, the wildfire impact on LSP timing is more complex with the changes in plant species composition and surface conditions caused by wildfire. Specifically, post-fire species which greens up earlier in spring and browns down in autumn than the pre-fire trees would cause an

earlier SOS and a later EOS in the post-fire landscape, and vice versa. Thus, the wildfire-caused shifts on LSP timing could be divergent and vary greatly among different wildfire events in a large region such as the western US. Moreover, burn severity is expected to be an important control on the extent of LSP changes by wildfires. Specifically, higher levels of burn severity cause both more forest loss and severer soil damage (Lewis et al., 2006), which facilitates and impedes the re-colonization of understory species, respectively. Thus, a trade-off between forest loss and soil damage could result in the largest shift in LSP timing at the moderate burn severity.

Hypothesis 3: Land cover composition and weather are the dominant drivers of the spatial and interannual variations in LSP, respectively, in the burned area of the 2002 Ponil Complex Fire, New Mexico, USA.

The 2002 Ponil Complex Fire was the largest wildfire by 2002 in New Mexico. The pre-fire vegetation was dominated by evergreen tree species of Ponderosa pine and Douglas-fir (Rodman et al., 2019). After the fire, the quick recolonization of understory species, mostly Gambel Oak, in the severely burned area and the trees in the unburned area formed patches of various vegetation types. Because of the different adaptations of understory species and trees to post-fire environmental conditions and climate change, plant species experienced considerable interannual dynamics in the burned area. Considering the phenological difference among vegetation types, the land cover composition is expected to play a more important role in controlling the spatial variation of LSP when compared with weather and topography that are widely regarded as LSP drivers. However, weather is still expected to be the dominant driver of interannual variation in LSP.

1.3. Significance of the research

This research, for the first time, systematically investigates the wildfire impacts on the magnitudes and trends of LSP at a regional scale and quantitatively analyzes the contribution of wildfire-caused land cover composition change, relative to other environmental factors, to controlling the LSP dynamics in the western US forests. The outcomes are expected to advance the field of LSP by (1) improving the understanding of the impacts of wildfire disturbance on LSP, (2) providing a novel methodology that is applicable to investigate the responses of LSP to various disturbances (e.g., insects/diseases, forest logging, grazing), (3) improving the understanding of the mechanism that various factors drive LSP dynamics, and (4) providing a prototype of quantifying the contributions of various drivers to the spatial and interannual variation of LSP using machine learning.

1.4. Organization of the dissertation

The dissertation consists of five chapters. Chapter 1 provides an overview of vegetation phenology, reviews the materials and methods for LSP detection, summaries recent changes in LSP, explains the drivers and mechanisms of LSP dynamics, addresses the wildfire impacts on LSP, outlines the research goal, objectives, and hypotheses, justifies the significance of this research, and introduces the organization of the dissertation.

Chapter 2 addresses Hypothesis 1. It quantifies the impacts of the 2002 Hayman Fire in Colorado on the magnitudes and interannual trends of LSP by using an unburned buffer as a reference. The results were published:

Wang, J., Zhang, X., 2017. Impacts of wildfires on interannual trends in land surface phenology: an investigation of the Hayman Fire. Environ. Res. Lett. 12, 054008. https://doi.org/10.1088/1748-9326/aa6ad9

Chapter 3 addresses Hypothesis 2. It investigates the distribution of wildfire impacts on LSP and identifies factors controlling the wildfire impacts by analyzing all the wildfires across the western US forests. The results were published:

Wang, J., Zhang, X., 2020. Investigation of wildfire impacts on land surface phenology from MODIS time series in the western US forests. ISPRS J. Photogramm. Remote Sens. 159, 281–295. https://doi.org/10.1016/j.isprsjprs.2019.11.027

Chapter 4 addresses Hypothesis 3. It explores the role of land cover composition change caused by the 2002 Ponil Complex Fire in New Mexico on the spatial and interannual variations of LSP, relative to other environmental factors. The results were prepared in a manuscript that was submitted for review in *Remote Sensing of Environment*:

Wang, J., Zhang, X., Rodman, K. Exploring the Contribution of Land Cover Composition to Spatial and Interannual Variations of Land Surface Phenology in a Recently Burned Landscape Using Machine Learning.

Chapter 5 summarizes the key findings in the tests of the three hypotheses in Chapters 2-4, discusses the implications and limitations and provides recommendations on potential future research.

References

An, S., Zhang, X., Chen, X., Yan, D., Henebry, G.M., 2018. An exploration of terrain effects on land surface phenology across the Qinghai–Tibet plateau using Landsat ETM+ and OLI data. Remote Sens. 10, 1069.

Archibald, S., Scholes, R.J., 2007. Leaf green-up in a semi-arid African savanna – separating tree and grass responses to environmental cues. J. Veg. Sci. 18, 583. https://doi.org/10.1111/j.1654-1103.2007.tb02572.x

Augspurger, C.K., Cheesman, J.M., Salk, C.F., 2005. Light gains and physiological capacity of understorey woody plants during phenological avoidance of canopy shade. Funct. Ecol. 19, 537–546. https://doi.org/10.1111/j.1365-2435.2005.01027.x

Bajocco, S., Dragoz, E., Gitas, I., Smiraglia, D., Salvati, L., Ricotta, C., 2015. Mapping forest fuels through vegetation phenology: The role of coarse-resolution satellite time-series. PLoS One 10, e0119811.

Bao, G., Chen, J., Chopping, M., Bao, Y., Bayarsaikhan, S., Dorjsuren, A., Tuya, A., Jirigala, B., Qin, Z., 2019. Dynamics of net primary productivity on the Mongolian Plateau: Joint regulations of phenology and drought. Int. J. Appl. Earth Obs. Geoinf. 81, 85–97.

Baumann, M., Ozdogan, M., Richardson, A.D., Radeloff, V.C., 2017. Phenology from

Landsat when data is scarce: Using MODIS and Dynamic Time-Warping to combine multi-year Landsat imagery to derive annual phenology curves. Int. J. Appl. Earth Obs. Geoinf. 54, 72–83. https://doi.org/10.1016/j.jag.2016.09.005

Buyantuyev, A., Wu, J., 2012. Urbanization diversifies land surface phenology in arid environments: interactions among vegetation, climatic variation, and land use pattern in the Phoenix metropolitan region, USA. Landsc. Urban Plan. 105, 149–159.

Chen, X., Wang, D., Chen, J., Wang, C., Shen, M., 2018. The mixed pixel effect in land surface phenology: A simulation study. Remote Sens. Environ. 211, 338–344. https://doi.org/10.1016/j.rse.2018.04.030

Cheng, Y., Vrieling, A., Fava, F., Meroni, M., Marshall, M., Gachoki, S., 2020. Phenology of short vegetation cycles in a Kenyan rangeland from PlanetScope and Sentinel-2. Remote Sens. Environ. 248, 112004. https://doi.org/10.1016/j.rse.2020.112004

Cho, M.A., Ramoelo, A., Dziba, L., 2017. Response of Land Surface Phenology to Variation in Tree Cover during Green-Up and Senescence Periods in the Semi-Arid Savanna of Southern Africa. Remote Sens. 9, 689. https://doi.org/10.3390/rs9070689

Churkina, G., Schimel, D., Braswell, B.H., Xiao, X., 2005. Spatial analysis of growing season length control over net ecosystem exchange. Glob. Chang. Biol. 11, 1777–1787. https://doi.org/10.1111/j.1365-2486.2005.001012.x

Claverie, M., Ju, J., Masek, J.G., Dungan, J.L., Vermote, E.F., Roger, J.C., Skakun, S. V.,

Justice, C., 2018. The Harmonized Landsat and Sentinel-2 surface reflectance data set. Remote Sens. Environ. 219, 145–161. https://doi.org/10.1016/j.rse.2018.09.002

Cong, N., Shen, M., Piao, S., Chen, X., An, S., Yang, W., Fu, Y.H., Meng, F., Wang, T., 2017. Little change in heat requirement for vegetation green-up on the Tibetan Plateau over the warming period of 1998-2012. Agric. For. Meteorol. 232, 650–658. https://doi.org/10.1016/j.agrformet.2016.10.021

Cooke, J.E.K., Weih, M., 2005. Nitrogen storage and seasonal nitrogen cycling in Populus: bridging molecular physiology and ecophysiology. New Phytol. 167, 19–30.

de Beurs, K.M., Henebry, G.M., 2005. Land surface phenology and temperature variation in the International Geosphere-Biosphere Program high-latitude transects. Glob. Chang. Biol. 11, 779–790. https://doi.org/10.1111/j.1365-2486.2005.00949.x

de Beurs, K.M., Henebry, G.M., 2004. Land surface phenology, climatic variation, and institutional change: Analyzing agricultural land cover change in Kazakhstan. Remote Sens. Environ. 89, 497–509. https://doi.org/10.1016/j.rse.2003.11.006

Delpierre, N., Dufrêne, E., Soudani, K., Ulrich, E., Cecchini, S., Boé, J., François, C., 2009. Modelling interannual and spatial variability of leaf senescence for three deciduous tree species in France. Agric. For. Meteorol. 149, 938–948. https://doi.org/https://doi.org/10.1016/j.agrformet.2008.11.014

Delpierre, N., Lireux, S., Hartig, F., Camarero, J.J., Cheaib, A., Čufar, K., Cuny, H., Deslauriers, A., Fonti, P., Gričar, J., Huang, J.-G.J., Krause, C., Liu, G., de Luis, M., Mäkinen, H., Martinez del Castillo, E., Morin, H., Nöjd, P., Oberhuber, W., Prislan,

P., Rossi, S., Saderi, S., Treml, V., Vavrick, H., Rathgeber, C.B.K., Luis, M. de, Mäkinen, H., Castillo, E.M. del, Morin, H., Nöjd, P., Oberhuber, W., Prislan, P., Rossi, S., Saderi, S., Treml, V., Vavrick, H., Rathgeber, C.B.K., 2018. Chilling and forcing temperatures interact to predict the onset of wood formation in Northern Hemisphere conifers. Glob. Chang. Biol. 0. https://doi.org/10.1111/gcb.14539

Di-Mauro, B., Fava, F., Busetto, L., Crosta, G.F., Colombo, R., 2014. Post-fire resilience in the Alpine region estimated from MODIS satellite multispectral data. Int. J. Appl. Earth Obs. Geoinf. 32, 163–172. https://doi.org/10.1016/j.jag.2014.04.010

Dragoni, D., Schmid, H.P., Wayson, C.A., Potter, H., Grimmond, C.S.B., Randolph, J.C., 2011. Evidence of increased net ecosystem productivity associated with a longer vegetated season in a deciduous forest in south-central Indiana, USA. Glob. Chang. Biol. 17, 886–897.

Duchemin, B., Goubier, J., Courrier, G., 1999. Monitoring phenological key stages and cycle duration of temperate deciduous forest ecosystems with NOAA/AVHRR data. Remote Sens. Environ. 67, 68–82.

Elmore, A.J., Asner, G.P., Hughes, R.F., 2005. Satellite monitoring of vegetation phenology and fire fuel conditions in Hawaiian drylands. Earth Interact. 9, 1–21.

Estiarte, M., Peñuelas, J., 2015. Alteration of the phenology of leaf senescence and fall in winter deciduous species by climate change: effects on nutrient proficiency. Glob. Chang. Biol. 21, 1005–1017.

Fay, P.A., Jin, V.L., Way, D.A., Potter, K.N., Gill, R.A., Jackson, R.B., Polley, H.W., 2012. Soil-mediated effects of subambient to increased carbon dioxide on grassland

productivity. Nat. Clim. Chang. 2, 742–746.

Fracheboud, Y., Luquez, V., Björkén, L., Sjödin, A., Tuominen, H., Jansson, S., 2009. The Control of Autumn Senescence in European Aspen. Plant Physiol. 149, 1982 LP – 1991. https://doi.org/10.1104/pp.108.133249

Fu, Y.H., Piao, S., Op de Beeck, M., Cong, N., Zhao, H., Zhang, Y., Menzel, A., Janssens, I.A., 2014. Recent spring phenology shifts in western Central Europe based on multiscale observations. Glob. Ecol. Biogeogr. 23, 1255–1263. https://doi.org/10.1111/geb.12210

Fu, Y.H., Zhao, H., Piao, S., Peaucelle, M., Peng, S., Zhou, G., Ciais, P., Song, Y., Vitasse, Y., Zeng, Z., Janssens, I. a, Huang, M., Menzel, A., Pen, J., 2015. Declining global warming effects on the phenology of spring leaf unfolding. Nature 526, 104–107. https://doi.org/10.1038/nature15402

Ganguly, S., Friedl, M.A., Tan, B., Zhang, X., Verma, M., 2010. Land surface phenology from MODIS: Characterization of the Collection 5 global land cover dynamics product. Remote Sens. Environ. 114, 1805–1816. https://doi.org/10.1016/j.rse.2010.04.005

Goward, S.N., Markham, B., Dye, D.G., Dulaney, W., Yang, J., 1991. Normalized difference vegetation index measurements from the advanced very high resolution radiometer. Remote Sens. Environ. 35, 257–277. https://doi.org/https://doi.org/10.1016/0034-4257(91)90017-Z

Gu, L., Post, W.M., Baldocchi, D., Black, T.A., Verma, S.B., Vesala, T., Wofsy, S.C., 2003. Phenology of vegetation photosynthesis, in: Phenology: An Integrative

Environmental Science. Springer, pp. 467–485.

Hogg, E.H., Price, D.T., Black, T.A., 2000. Postulated feedbacks of deciduous forest phenology on seasonal climate patterns in the western Canadian interior. J. Clim. 13, 4229–4243.

Houborg, R., McCabe, M.F., 2018. A Cubesat enabled Spatio-Temporal Enhancement Method (CESTEM) utilizing Planet, Landsat and MODIS data. Remote Sens. Environ. 209, 211–226. https://doi.org/10.1016/j.rse.2018.02.067

Huete, A., Didan, K., Miura, T., Rodriguez, E.P., Gao, X., Ferreira, L.G., 2002. Overview of the radiometric and biophysical performance of the MODIS vegetation indices. Remote Sens. Environ. 83, 195–213. https://doi.org/http://dx.doi.org/10.1016/S0034-4257(02)00096-2

IPCC, 2014. Climate Change 2014: Synthesis Report. Contribution of Working Groups I, II and III to the Fifth Assessment Report of the Intergovernmental Panel on Climate Change [Core Writing Team, R.K. Pachauri and L.A. Meyer (eds.)]. Geneva, Switzerland.

IPCC, 2007. Contribution of Working Group II to the Fourth Assessment Report of the Intergovernmental Panel on Climate Change, 2007. In M. L. Parry et al. (Ed.). Cambridge University Press, Cambridge.

Jeong, S.J., Ho, C.H., Gim, H.J., Brown, M.E., 2011. Phenology shifts at start vs. end of growing season in temperate vegetation over the Northern Hemisphere for the period 1982-2008. Glob. Chang. Biol. 17, 2385–2399. https://doi.org/10.1111/j.1365-2486.2011.02397.x

Jeong, S., Ho, C., Jeong, J., 2009. Increase in vegetation greenness and decrease in springtime warming over east Asia. Geophys. Res. Lett. 36.

Jiang, Z., Huete, A.R., Didan, K., Miura, T., 2008. Development of a two-band enhanced vegetation index without a blue band. Remote Sens. Environ. 112, 3833–3845. https://doi.org/http://dx.doi.org/10.1016/j.rse.2008.06.006

Johnson, B., Tateishi, R., Kobayashi, T., 2012. Remote Sensing of Fractional Green Vegetation Cover Using Spatially-Interpolated Endmembers. Remote Sens. 4, 2619–2634.

Jolly, W.M., Running, S.W., 2004. Effects of precipitation and soil water potential on drought deciduous phenology in the Kalahari. Glob. Chang. Biol. 10, 303–308.

Julien, Y., Sobrino, J.A., 2009. Global land surface phenology trends from GIMMS database. Int. J. Remote Sens. 30, 3495–3513. https://doi.org/10.1080/01431160802562255

Kharouba, H.M., Ehrlén, J., Gelman, A., Bolmgren, K., Allen, J.M., Travers, S.E., Wolkovich, E.M., 2018. Global shifts in the phenological synchrony of species interactions over recent decades. Proc. Natl. Acad. Sci. 115, 5211–5216.

Latte, N., Lejeune, P., 2020. PlanetScope Radiometric Normalization and Sentinel-2 Super-Resolution (2.5 m): A Straightforward Spectral-Spatial Fusion of Multi-Satellite Multi-Sensor Images Using Residual Convolutional Neural Networks. Remote Sens. 12, 2366.

Laughlin, D.C., Bakker, J.D., Stoddard, M.T., Daniels, M.L., Springer, J.D., Gildar, C.N.,

Green, A.M., Covington, W.W., 2004. Toward reference conditions: wildfire effects on flora in an old-growth ponderosa pine forest. For. Ecol. Manage. 199, 137–152. https://doi.org/10.1016/j.foreco.2004.05.034

Leach, N., Coops, N.C., Obrknezev, N., 2019. Normalization method for multi-sensor high spatial and temporal resolution satellite imagery with radiometric inconsistencies. Comput. Electron. Agric. 164, 104893.

Lentile, L.B., Morgan, P., Hudak, A.T., Bobbitt, M.J., Lewis, S. a., Smith, A.M.S., Robichaud, P.R., 2007. Post-Fire Burn Severity and Vegetaion Response Following Eight Large Wildfires Across the Western United States. Fire Ecol. Spec. Issue 3, 91–108. https://doi.org/10.4996/fireecology.0301091

Lewis, S.A., Wu, J.Q., Robichaud, P.R., 2006. Assessing burn severity and comparing soil water repellency, Hayman Fire, Colorado. Hydrol. Process. 20, 1–16. https://doi.org/10.1002/hyp.5880

Li, J., Roy, D.P., 2017. A global analysis of Sentinel-2A, Sentinel-2B and Landsat-8 data revisit intervals and implications for terrestrial monitoring. Remote Sens. 9, 902. https://doi.org/10.3390/rs9090902

Li, X., Zhou, Y., Meng, L., Asrar, G., Sapkota, A., Coates, F., 2019. Characterizing the relationship between satellite phenology and pollen season: A case study of birch. Remote Sens. Environ. 222, 267–274. https://doi.org/https://doi.org/10.1016/j.rse.2018.12.036

Lian, X., Piao, S., Li, L.Z.X., Li, Y., Huntingford, C., Ciais, P., Cescatti, A., Janssens, I.A., Peñuelas, J., Buermann, W., 2020. Summer soil drying exacerbated by earlier

spring greening of northern vegetation. Sci. Adv. 6, eaax0255.

Lieth, H., 1974. Phenology and seasonality modeling. Springer-Verlag, Berlin, p. 444.

Liu, Q., Fu, Y.H., Zeng, Z., Huang, M., Li, X., Piao, S., 2016. Temperature, precipitation, and insolation effects on autumn vegetation phenology in temperate China. Glob. Chang. Biol. 22, 644–655. https://doi.org/10.1111/gcb.13081

Liu, Y., Hill, M.J., Zhang, X., Wang, Z., Richardson, A.D., Hufkens, K., Filippa, G., Baldocchi, D.D., Ma, S., Verfaillie, J., Schaaf, C.B., 2017. Using data from Landsat, MODIS, VIIRS and PhenoCams to monitor the phenology of California oak/grass savanna and open grassland across spatial scales. Agric. For. Meteorol. 237–238, 311–325. https://doi.org/10.1016/j.agrformet.2017.02.026

Marshall, M., Okuto, E., Kang, Y., Opiyo, E., Ahmed, M., 2016. Global assessment of Vegetation Index and Phenology Lab (VIP) and Global Inventory Modeling and Mapping Studies (GIMMS) version 3 products. Biogeosciences 13, 625–639. https://doi.org/10.5194/bg-13-625-2016

Melaas, E.K., Friedl, M.A., Richardson, A.D., 2015. Multi-scale modeling of spring phenology across Deciduous Forests in the Eastern United States. Glob. Chang. Biol. n/a-n/a. https://doi.org/10.1111/gcb.13122

Melaas, E.K., Friedl, M.A., Zhu, Z., 2013. Detecting interannual variation in deciduous broadleaf forest phenology using Landsat TM/ETM+ data. Remote Sens. Environ. 132, 176–185. https://doi.org/10.1016/j.rse.2013.01.011

Misra, G., Buras, A., Heurich, M., Asam, S., Menzel, A., 2018. LiDAR derived

topography and forest stand characteristics largely explain the spatial variability observed in MODIS land surface phenology. Remote Sens. Environ. 218, 231–244. https://doi.org/10.1016/j.rse.2018.09.027

Misra, G., Cawkwell, F., Wingler, A., 2020. Status of Phenological Research Using Sentinel-2 Data: A Review. Remote Sens. 12, 2760.

Moulin, S., Kergoat, L., Viovy, N., Dedieu, G., 1997. Global-scale assessment of vegetation phenology using NOAA/AVHRR satellite measurements. J. Clim. 10, 1154–1170.

Muche, M.E., Hutchinson, S.L., Hutchinson, J.M.S., Johnston, J.M., 2019. Phenology-adjusted dynamic curve number for improved hydrologic modeling. J. Environ. Manage. 235, 403–413.

Myneni, R.B., Keeling, C.D., Tucker, C.J., Asrar, G., Nemani, R.R., 1997. Increased plant growth in the northern high latitudes from 1981 to 1991. Nature 386, 698.

Nagai, S., Nasahara, K.N., Inoue, T., Saitoh, T.M., Suzuki, R., 2016. Review: advances in in situ and satellite phenological observations in Japan. Int. J. Biometeorol. 60, 615–627. https://doi.org/10.1007/s00484-015-1053-3

NCA, 2015. National Climate Assessment & Development Advisory Committee (2011–2014) Meetings, decisions, and adopted documents.

NCA, 2010. Ecosystem Responses to Climate Change: Selecting Indicators and Integrating Observational Networks, NCA Report Series, 5a. Washington DC.

Piao, S., Liu, Q., Chen, A., Janssens, I.A., Fu, Y., Dai, J., Liu, L., Lian, X., Shen, M.,

Zhu, X., 2019. Plant phenology and global climate change: Current progresses and challenges. Glob. Chang. Biol. 25, 1922–1940. https://doi.org/10.1111/gcb.14619

Planet Labs Inc, 2020. Planet Imagery and Archive.

Pongratz, J., Bounoua, L., Defries, R.S., Morton, D.C., Anderson, L.O., Mauser, W., Klink, C.A., 2006. The impact of land cover change on surface energy and water balance in Mato Grosso, Brazil. Earth Interact. 10. https://doi.org/10.1175/EI176.1

Qiu, T., Song, C., Clark, J.S., Seyednasrollah, B., Rathnayaka, N., Li, J., 2020. Understanding the continuous phenological development at daily time step with a Bayesian hierarchical space-time model: impacts of climate change and extreme weather events. Remote Sens. Environ. 247, 111956.

Rafferty, N.E., CaraDonna, P.J., Burkle, L.A., Iler, A.M., Bronstein, J.L., 2013. Phenological overlap of interacting species in a changing climate: an assessment of available approaches. Ecol. Evol. 3, 3183–3193.

Reed, B.C., Brown, J.F., VanderZee, D., Loveland, T.R., Merchant, J.W., Ohlen, D.O., 1994. Measuring phenological variability from satellite imagery. J. Veg. Sci. 5, 703–714. https://doi.org/10.2307/3235884

Richardson, A.D., Anderson, R.S., Arain, M.A., Barr, A.G., Bohrer, G., Chen, G., Chen, J.M., Ciais, P., Davis, K.J., Desai, A.R., Dietze, M.C., Dragoni, D., Garrity, S.R., Gough, C.M., Grant, R., Hollinger, D.Y., Margolis, H. a., Mccaughey, H., Migliavacca, M., Monson, R.K., Munger, J.W., Poulter, B., Raczka, B.M., Ricciuto, D.M., Sahoo, A.K., Schaefer, K., Tian, H., Vargas, R., Verbeeck, H., Xiao, J., Xue, Y., 2012. Terrestrial biosphere models need better representation of vegetation

phenology: Results from the North American Carbon Program Site Synthesis. Glob. Chang. Biol. 18, 566–584. https://doi.org/10.1111/j.1365-2486.2011.02562.x

Richardson, A.D., Bailey, A.S., Denny, E.G., Martin, C.W., O'KEEFE, J., 2006. Phenology of a northern hardwood forest canopy. Glob. Chang. Biol. 12, 1174–1188.

Richardson, A.D., Hufkens, K., Milliman, T., Aubrecht, D.M., Chen, M., Gray, J.M., Johnston, M.R., Keenan, T.F., Klosterman, S.T., Kosmala, M., Melaas, E.K., Friedl, M.A., Frolking, S., 2018. Tracking vegetation phenology across diverse North American biomes using PhenoCam imagery. Sci. Data 5, 1–24. https://doi.org/10.1038/sdata.2018.28

Richardson, A.D., Keenan, T.F., Migliavacca, M., Ryu, Y., Sonnentag, O., Toomey, M., 2013. Climate change, phenology, and phenological control of vegetation feedbacks to the climate system. Agric. For. Meteorol. 169, 156–173. https://doi.org/10.1016/j.agrformet.2012.09.012

Richardson, A.D., O'Keefe, J., 2009. Phenological Differences Between Understory and Overstory: A Case Study Using the Long-Term Harvard Forest Records, in: Noormets, A. (Ed.), Phenology of Ecosystem Processes. Springer, New York, NY, USA, pp. 87–117. https://doi.org/10.1007/978-1-4419-0026-5

Rodman, K.C., Veblen, T.T., Chapman, T.B., Rother, M.T., Wion, A.P., Redmond, M.D., 2019. Limitations to recovery following wildfire in dry forests of southern Colorado and northern New Mexico, USA. Ecol. Appl. 0, 1–20. https://doi.org/10.1002/eap.2001

Romo-Leon, J.R., van Leeuwen, W.J.D., Castellanos-Villegas, A., 2016. Land Use and Environmental Variability Impacts on the Phenology of Arid Agro-Ecosystems. Environ. Manage. 57, 283–297. https://doi.org/10.1007/s00267-015-0617-7

Sakamoto, T., Wardlow, B.D., Gitelson, A.A., Verma, S.B., Suyker, A.E., Arkebauer, T.J., 2010. A Two-Step Filtering approach for detecting maize and soybean phenology with time-series MODIS data. Remote Sens. Environ. 114, 2146–2159. https://doi.org/https://doi.org/10.1016/j.rse.2010.04.019

Sapkota, A., Murtugudde, R., Curriero, F.C., Upperman, C.R., Ziska, L., Jiang, C., 2019. Associations between alteration in plant phenology and hay fever prevalence among US adults: Implication for changing climate. PLoS One 14, e0212010.

Sehgal, V.K., Jain, S., Aggarwal, P.K., Jha, S., 2011. Deriving crop phenology metrics and their trends using times series NOAA-AVHRR NDVI Data. J. Indian Soc. Remote Sens. 39, 373–381.

Stéfanon, M., Drobinski, P., d'Andrea, F., de Noblet-Ducoudré, N., 2012. Effects of interactive vegetation phenology on the 2003 summer heat waves. J. Geophys. Res. Atmos. 117.

Tan, B., Morisette, J.T., Wolfe, R.E., Gao, F., Ederer, G.A., Nightingale, J., Pedelty, J.A., 2011. An Enhanced TIMESAT Algorithm for Estimating Vegetation Phenology Metrics From MODIS Data. IEEE J. Sel. Top. Appl. Earth Obs. Remote Sens. 4, 361–371. https://doi.org/10.1109/JSTARS.2010.2075916

Thomas, N., Neigh, C.S.R., Carroll, M.L., McCarty, J.L., Bunting, P., 2020. Fusion Approach for Remotely Sensed Mapping of Agriculture (FARMA): A Scalable

Open Source Method for Land Cover Monitoring Using Data Fusion. Remote Sens. 12, 3459. https://doi.org/10.3390/rs12203459

Tomaszewska, M.A., Nguyen, L.H., Henebry, G.M., 2020. Land surface phenology in the highland pastures of montane Central Asia: Interactions with snow cover seasonality and terrain characteristics. Remote Sens. Environ. 240, 111675. https://doi.org/https://doi.org/10.1016/j.rse.2020.111675

U.S. EPA, 2016. Climate change indicators in the United States, 2016. Fourth edition.

Van Leeuwen, W.J.D., Casady, G.M., Neary, D.G., Bautista, S., Alloza, J.A., Carmel, Y., Wittenberg, L., Malkinson, D., Orr, B.J., 2010. Monitoring post-wildfire vegetation response with remotely sensed time-series data in Spain, USA and Israel. Int. J. Wildl. Fire 19, 75–93. https://doi.org/10.1071/WF08078

Wang, J., Yang, D., Detto, M., Nelson, B.W., Chen, M., Guan, K., Wu, S., Yan, Z., Wu, J., 2020. Multi-scale integration of satellite remote sensing improves characterization of dry-season green-up in an Amazon tropical evergreen forest. Remote Sens. Environ. 246, 111865.

Wang, H., Magagi, R., Goïta, K., Trudel, M., McNairn, H., Powers, J., 2019. Crop phenology retrieval via polarimetric sar decomposition and random forest algorithm. Remote Sens. Environ. 231, 111234.

Westerling, a. L., Hidalgo, H.G., Cayan, D.R., Swetnam, T.W., 2006. Warming and earlier spring increase western U.S. forest wildfire activity. Science 313, 940–3. https://doi.org/10.1126/science.1128834

White, M.A., De Beurs, K.M., Didan, K., Inouye, D.W., Richardson, A.D., Jensen, O.P., O'keefe, J., Zhang, G., Nemani, R.R., Van Leeuwen, W.J.D., Brown, J.F., De Wit, A., Schaepman, M., Lin, X., Dettinger, M., Bailey, A.S., Kimball, J., Schwartz, M.D., Baldocchi, D.D., Lee, J.T., Lauenroth, W.K., 2009. Intercomparison, interpretation, and assessment of spring phenology in North America estimated from remote sensing for 1982-2006. Glob. Chang. Biol. 15, 2335–2359. https://doi.org/10.1111/j.1365-2486.2009.01910.x

White, M.A., Hoffman, F., Hargrove, W.W., Nemani, R.R., 2005. A global framework for monitoring phenological responses to climate change. Geophys. Res. Lett. 32, L04705.

White, M.A., Thornton, P.E., Running, S.W., 1997. A continental phenology model for monitoring vegetation responses to interannual climatic variability. Global Biogeochem. Cycles 11, 217–234. https://doi.org/10.1029/97GB00330

Wu, X., Sullivan, J.T., Heidinger, A.K., 2010. Operational calibration of the Advanced Very High Resolution Radiometer (AVHRR) visible and near-infrared channels. Can. J. Remote Sens. 36, 602–616. https://doi.org/10.5589/m10-080

Xie, J., Kneubühler, M., Garonna, I., Notarnicola, C., De Gregorio, L., De Jong, R., Chimani, B., Schaepman, M.E., 2017. Altitude-dependent influence of snow cover on alpine land surface phenology. J. Geophys. Res. Biogeosciences 122, 1107–1122. https://doi.org/10.1002/2016JG003728

Yang, Q., Shi, L., Han, J., Yu, J., Huang, K., 2020. A near real-time deep learning approach for detecting rice phenology based on UAV images. Agric. For. Meteorol.

287, 107938.

Zeng, H., Jia, G., Epstein, H., 2011. Recent changes in phenology over the northern high latitudes detected from multi-satellite data. Environ. Res. Lett. 6, 045508. https://doi.org/10.1088/1748-9326/6/4/045508

Zeng, L., Wardlow, B.D., Wang, R., Shan, J., Tadesse, T., Hayes, M.J., Li, D., 2016. A hybrid approach for detecting corn and soybean phenology with time-series MODIS data. Remote Sens. Environ. 181, 237–250.

Zhang, X., 2018. Land Surface Phenology: Climate Data Record and Real-Time Monitoring, in: Liang, S. (Ed.), Reference Module in Earth Systems and Environmental Sciences-Comprehensive Remote Sensing. Elsevier, Oxford, pp. 35–52.

Zhang, X., 2015. Reconstruction of a complete global time series of daily vegetation index trajectory from long-term AVHRR data. Remote Sens. Environ. 156, 457–472. https://doi.org/10.1016/j.rse.2014.10.012

Zhang, X., Friedl, M.A., Schaaf, C.B., Strahler, A.H., Hodges, J.C.F.F., Gao, F., Reed, B.C., Huete, A., 2003. Monitoring vegetation phenology using MODIS. Remote Sens. Environ. 84, 471–475. https://doi.org/10.1016/S0034-4257(02)00135-9

Zhang, X., Liu, L., Henebry, G.M., 2019. Impacts of land cover and land use change on long-term trend of land surface phenology: A case study in agricultural ecosystems. Environ. Res. Lett. 14. https://doi.org/10.1088/1748-9326/ab04d2

Zhang, X., Liu, L., Liu, Y., Jayavelu, S., Wang, J., Moon, M., Henebry, G.M., Friedl,

M.A., Schaaf, C.B., 2018. Generation and evaluation of the VIIRS land surface phenology product. Remote Sens. Environ. 216, 212–229. https://doi.org/10.1016/j.rse.2018.06.047

Zhang, X., Tan, B., Yu, Y., 2014. Interannual variations and trends in global land surface phenology derived from enhanced vegetation index during 1982-2010. Int. J. Biometeorol. 58, 547–564. https://doi.org/10.1007/s00484-014-0802-z

Zhang, X., Tarpley, D., Sullivan, J.T., 2007. Diverse responses of vegetation phenology to a warming climate. Geophys. Res. Lett. 34, 1–5. https://doi.org/10.1029/2007GL031447

Zhang, X., Wang, J., Gao, F., Liu, Y., Schaaf, C., Friedl, M., Yu, Y., Jayavelu, S., Gray, J., Liu, L., Yan, D., Henebry, G.M., 2017. Exploration of scaling effects on coarse resolution land surface phenology. Remote Sens. Environ. 190, 318–330. https://doi.org/10.1016/j.rse.2017.01.001

Zhang, X., Wang, J., Henebry, G.M., Gao, F., 2020. Development and evaluation of a new algorithm for detecting 30 m land surface phenology from VIIRS and HLS time series. ISPRS J. Photogramm. Remote Sens. 161, 37–51. https://doi.org/10.1016/j.isprsjprs.2020.01.012

CHAPTER 2: Impacts of Wildfires on Interannual Trends in Land Surface Phenology: An Investigation of the Hayman Fire

The content of this chapter was published: Wang, J., Zhang, X., 2017. Impacts of wildfires on interannual trends in land surface phenology: an investigation of the Hayman Fire. Environ. Res. Lett. 12, 054008. https://doi.org/10.1088/1748-9326/aa6ad9.

Abstract

Land surface phenology (LSP) derived from satellite data has been widely associated with recent global climate change. However, LSP is frequently influenced by land disturbances, which significantly limits our understanding of the phenological trends driven by climate change. Because wildfire is one of the most significant disturbance agents, we investigated the influences of wildfire on the start of growing season (SOS) and the interannual trends of SOS in the Hayman Fire area occurred in 2002 in Colorado using time series of daily MODIS data (2001-2014). Results show that the Hayman Fire advanced the area-integrated SOS by 15.2 days and converted SOS from a delaying trend of 3.9 days/decade to an advancing trend of -1.9 days/decade during 2001-2014. The fire impacts on SOS increased from low burn severity to high burn severity. Moreover, the rate of increase of annual maximum and minimum EVI2 from 2003-2014 reflects that vegetation greenness could recover to pre-fire status in 2022 and 2053, respectively, which suggests that the fire impacts on the satellite-derived SOS variability and the interannual trends should continue in the next few decades.

2.1. Introduction

Vegetation phenology, characterizing both physical changes (e.g., leaf development and abscission) in vegetation structure and the inherent seasonality of mass and energy flux, is considered to be a crucial regulator of ecosystem processes and feedbacks to climate (Gu et al., 2003; Richardson et al., 2012), as well as a sensitive bioindicator of monitoring climate change and carbon cycle (Richardson et al., 2013). In recent years, growing evidence has emerged that climate change is altering phenological

variation in terrestrial ecosystems across scales from individual species to landscapes (Angert et al., 2005; Richardson et al., 2013; Schwartz et al., 2006). As a result, vegetation phenology has been selected as one of the most effective and simplest indicators to track changes in the ecology of species in response to climate change (Pachauri et al., 2014) and is listed as one of the leading indicators of climate change identified by the United States (US) Global Change Research Program (http://www.globalchange.gov/) and US Environmental Protection Agency (EPA) (https://www.epa.gov/climate-indicators).

Satellite data have been widely recognized as a powerful tool in identifying spatially distributed phenological indicators of climate change. Specifically, the start of growing season (SOS) has been extensively derived from the Advanced Very High Resolution Radiometer (AVHRR) Normalized Difference Vegetation Index (NDVI) data, which have been available since 1981, based on various approaches and time periods (de Beurs and Henebry, 2005a; de Jong et al., 2011; Reed et al., 1994; White et al., 2009; Zhang et al., 2007; Zhou et al., 2001). The interannual SOS trend has been widely used to associate with regional or global climate change although the magnitude and direction of SOS trends varied greatly in different locations, time periods, spatial and temporal scales, and measuring methods (Jeong et al., 2011; Shen et al., 2014; Walther, 2004; Zhang et al., 2007; Zhou et al., 2001).

Unlike the field observations of species-specific phenology, land surface phenology (LSP) is commonly used to refer to the area-integrated phenology of vegetation communities detected from satellite remote sensing (de Beurs and Henebry, 2004). Within a satellite pixel, land surface components and plant species composite may

be strongly altered by land disturbances. This could lead to a great change of phenological timing within a satellite pixel and may in turn significantly modify the direction and magnitude of the interannual phenological trend. It is very likely that current detections of LSP indicators can be strongly influenced by land use, disturbance history, and human activity (Buyantuyev and Wu, 2012; de Beurs and Henebry, 2004; Romo-Leon et al., 2016; White et al., 2005). This issue severely limits our understanding of phenological variability and trends reflecting climate change across regional to global scales (White et al., 2005). Thus, it is necessary to separate the abrupt change caused by land disturbance from the gradual change associated with climate change (Verbesselt et al., 2010).

Wildfire is one of the most important drivers of land disturbances across the world. Because fire size, severity and frequency have been increasing in many parts of the world during past decades (Marlon et al., 2012; Pechony and Shindell, 2010; Westerling et al., 2006), the impacts of wildfires on the changes of land cover types and soil properties (such as nutrients and water availability) have likely increased (Miller et al., 2013). Although some studies demonstrated the post-fire LSP variation (Di-Mauro et al., 2014; Fernandez-Manso et al., 2016; Sankey et al., 2013; Storey et al., 2016; van Leeuwen, 2008; Van Leeuwen et al., 2010), however, the quantitative impact of wildfire on LSP and its interannual trend has been barely investigated and remains poorly understood.

This study aims to quantitatively explore the impact of wildfire on interannual LSP trend. Specifically, we detected LSP around the Hayman Fire in the central United States using a time series of daily Moderate-resolution Imaging Spectroradiometer

(MODIS) data from 2001-2014. We further quantified the difference between pre-fire and post-fire LSP for the areas with different levels of burn severity and calculated the LSP trends inside and outside the burn scar, with which the wildfire influence on LSP was explored.

2.2. Methodology

2.2.1. Burn severity and land cover data

The Hayman Fire, which started on June 8 and ended on July 18, 2002, in Colorado's Front Range (39°13'12.0"N, 105°17' 13.2"W; see Figure 2-1a), was the largest wildfire in the recorded history of Colorado with a burned area of 526 km^2. We obtained the burned area and burn severity levels from the Monitoring Trends in Burn Severity (MTBS; http://www.mtbs.gov) map. These data were generated by comparing the pre-fire and post-fire Normalized Burn Ratio (NBR) derived from Landsat data at a 30 m resolution (Eidenshink et al., 2007). Burn severity represents primarily the effect of fire on vegetation biomass levels, which is classified as the categories of unburned to low, low, moderate, high, and increased greenness. Areas affected by clouds, cloud shadows, and data gaps are labeled as non-processing. To match the LSP map (see subsection 2.2), the burn severity map was resampled to 240 m based on the majority of burn severity levels. The upscaled burn severity map contains 52.1% of high severity, 17.5% of moderate severity, 4.3% of low severity, 2.5% of unburned to low, 0.7% of non-processing, and no area of increased greenness (Figure 2-1b). The pixels with non-processing were excluded for further analyses because of limited coverage. To investigate the wildfire impact on LSP, we set up a buffer zone of 5 km outside the burn scar as a reference representing the area without disturbances.

National Land Cover Database (NLCD; can be found in http://www.mrlc.gov) data in 2001, 2006 and 2011 were acquired to analyze the change of land cover types, which were before (in 2001) and after (in 2006 and 2011) the fire occurrence. The NLCD maps were produced using Landsat data with a spatial resolution of 30 m (Fry et al., 2011; Homer et al., 2007, 2015). The NLCD land cover was reclassified into seven types that are forest, shrubland, grassland, developed land, cultivated land, barren, and water (Figure 2-1). NLCD 2011 was not shown here because the land cover type was almost the same as that in 2006 in our study region. Before the fire occurrence, forests were dominant, which mainly consisted of evergreen forests (mainly ponderosa pine-Douglas fir forest) with small proportions of deciduous and mixed forest (<2%) and a few shrub patches scattered. After the fire occurrence, the forests were mainly converted to shrublands with a small portion of grasslands around the burn perimeter, but some forests remained unchanged after the fire. The unchanged forests were mainly located in the areas with unburned/low and low burn severity, while the land cover conversions generally occurred in the areas with moderate and high burn severity. The proportion of 30-m land cover in each 240-m grid of the upscaled burn severity map was further calculated and averaged based on the burn severity levels to quantify the burn severity influence on land cover conversion.

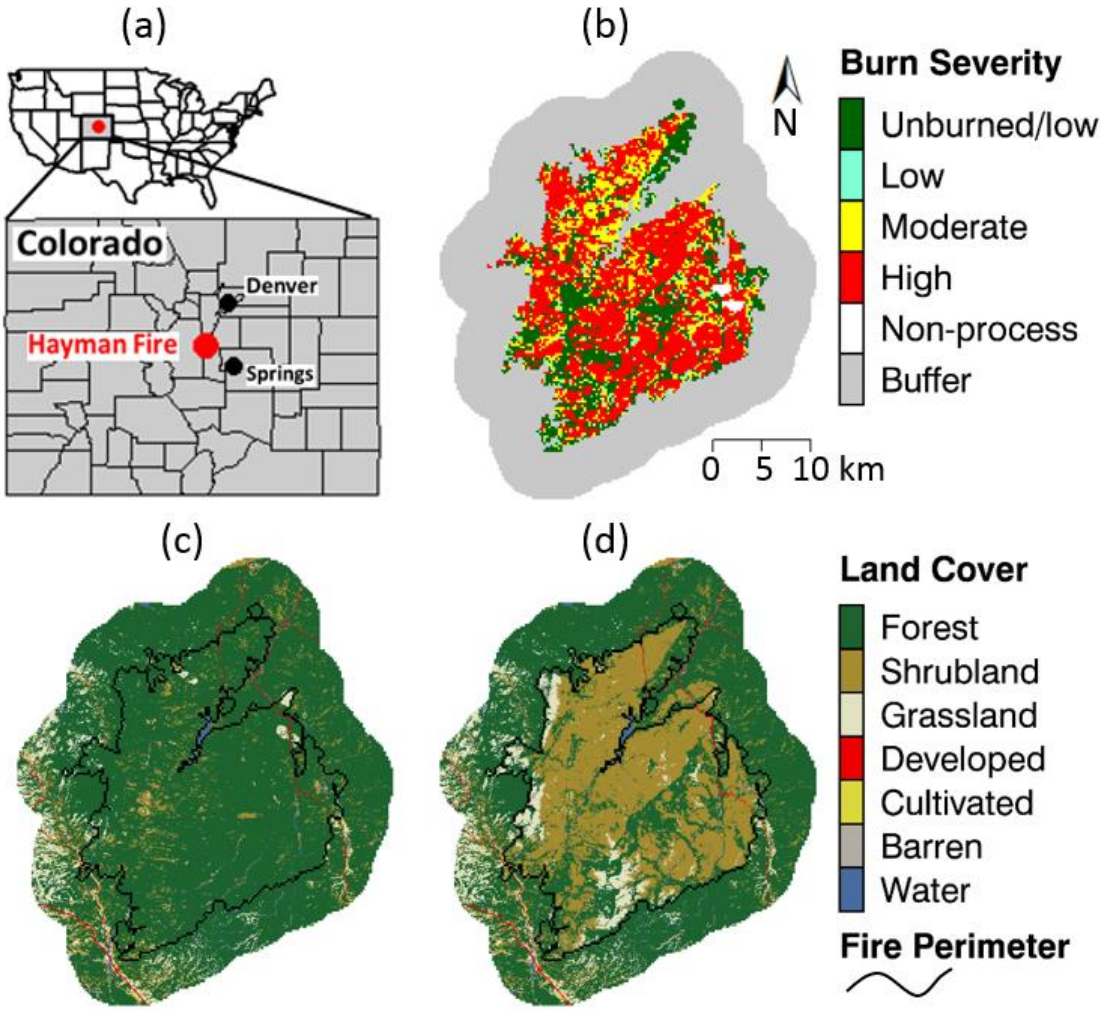

Figure 2-1. The location of the Hayman Fire (a), burn severity map (grey is the buffer zone with a width of 5 km used as an unburned reference) resampled to 240 m (b), and National Land Cover Database maps in 2001 (c) and 2006 (d) at 30-m resolution.

2.2.2. Phenology detection from satellite data

To detect LSP in the Hayman Fire area, we first collected daily MODIS surface reflectance products (MOD09GQ, V006) in tile H09V05 at a spatial resolution of 250 m from 2001-2014. Reflectances at red and near-infrared bands in MOD09GQ were used to calculate daily two-band enhanced vegetation index (EVI2), which is equivalent to EVI

(Jiang et al., 2008). Compared with NDVI which combines reflectances at near-infrared and red bands to reflect vegetation greenness, EVI is developed by adding the blue band and other adjustment coefficients so that it is less sensitive to soil background brightness and atmospheric scattering contamination and does not saturate over high densely-vegetated areas (Huete et al., 2002). After replacing the blue band (relatively low signal-to-noise ratio) using the correlative properties of surface reflectance between the red and blue bands, EVI is modified to EVI2 that remains the advantages over NDVI (Jiang et al., 2008). Further, MODIS land surface temperature (LST) products (MOD11A1, V005) and daily surface reflectance products (MOD09GA, V006) at a spatial resolution of 1 km were also collected for extracting LST and cloud and snow flags, respectively. The LST and cloud and snow flag data were simply downscaled to 250 m using a nearest neighbor approach. Because of missing MODIS data in early 2000 (1/1/2000-2/23/2000) and in June 2002, which severely impaired the accuracy of LSP detection, our study period was set to be 2001 (pre-fire) and 2003-2014 (post-fire), which was simply called as 2001-2014 hereafter.

The hybrid piecewise-logistic-model-based LSP detection algorithm (HPLM-LPSD) was applied to retrieve the LSP metrics from the time series of daily EVI2 (Zhang, 2015; Zhang et al., 2003). There were mainly five steps in implementing HPLM-LPSD to retrieve phenological metrics for a target year: (1) establishment of a three-day EVI2 time series composited by selecting good quality observations, (2) determination of background EVI2 by calculating the mean of the 10% largest EVI2 values with cloud- and snow-free observations during a winter period defined using LST<278K (during the dormancy phase), (3) smoothing of the EVI2 time series by removing the local sharp

peak or trough with a Savitzky-Golay filter and a running local median filter, (4) reconstruction of the EVI2 time series using the hybrid piecewise logistic functions, and (5) detection of the phenological transition dates by identifying the day of year (DOY) which shows the maximal or minimal rate of change in the curvature along the reconstructed EVI2 time series. The temporal EVI2 observations and phenology detection were illustrated in Figure 2-2.

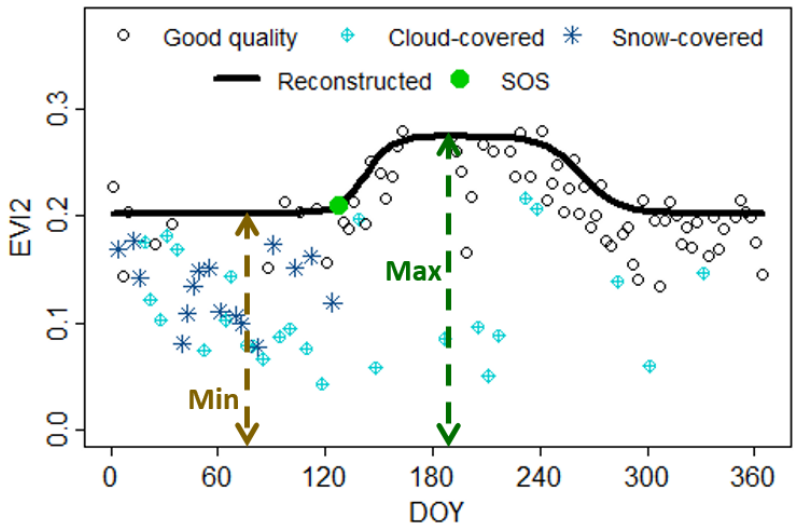

Figure 2-2. An example of reconstructing temporal vegetative EVI2 trajectory and detecting SOS, minimum EVI2 (Min), and maximum EVI2 (Max) using HPLM-LPSD. Note that fill values (invalid observation in MOD09GQ) are not presented. The irregular variation in good quality EVI2 is likely associated with the residual cloud contamination and bidirectional reflectance distribution function.

The confidence of phenology detections was quantified using the proportion of good quality (cloud- and snow-free) EVI2 (PGQ_{SOS}) around the SOS occurrence (Zhang,

2015; Zhang et al., 2009). To ensure the reliability of SOS detections, a filter of PGQ_{SOS} >40% was applied to select high confidence SOS pixels.

In addition, the annual maximum and minimum EVI2 were also derived from the EVI2 time series reconstructed based on the hybrid piecewise logistic model. The minimum EVI2 is usually the background EVI2 during a winter period determined in step 2 of HPLM-LPSD. The resultant metrics were then resampled to 240 m using the nearest neighbor method.

2.2.3. Investigation of wildfire impacts on SOS

The impact of wildfire on SOS was quantitatively analyzed using two parameters. First, spatial SOS anomaly was calculated by comparing the SOS values inside the burn scar with those in the buffer zone (as a reference) outside the burn scar for individual years.

$$SOS_{a,y} = SOS_{i,y} - SOS_{o,y} \quad (1)$$

where $SOS_{i,y}$ and $SOS_{o,y}$ are the area-integrated SOS (median of SOSs) inside the burn scar and in the buffer zone for year y, respectively, and $SOS_{a,y}$ is the spatial SOS anomaly in year y. As the pre-fire record is only available in 2001, $SOS_{a,2001}$ was used as the pre-fire measurement. The average spatial anomaly from 2003-2014 was used as the post-fire measurement. The spatial pattern of SOS anomalies in pre-fire and post-fire was further compared.

Second, SOS trends were examined and compared for overall areas inside the burn scar and in the buffer zone and for individual pixels, respectively. Overall trends were determined from the time series of SOS during 2001-2014 inside the burn scar ($SOS_{i,y}$) and in the buffer zone ($SOS_{o,y}$), separately. The trends for individual pixels were

also calculated with a simple linear regression to evaluate the detailed spatial variations. The significance of the trends was determined using the single tailed student's t-test. Note only the pixels (2,174 inside the burn scar and 2,317 in the buffer) with valid SOS detections (PGQ_{SOS}>40%) for the entire study period (2001-2014) were included for the trend analysis.

2.3. Results

2.3.1. Land cover change by wildfire and post-fire vegetation recovery

Figure 2-3 presents the comparisons of proportions of 30-m land cover in each 240-m pixel before and after the fire occurrence. This result, to some extent, indicated the land cover changes by wildfire burning with different severity levels. In the entire study area, natural vegetation (forests, shrublands and grasslands) accounted for more than 97% on average. In the buffer zone, the proportion of forests, shrublands, and grasslands was 80%, 9% and 8%, respectively, with little difference between pre-fire and post-fire periods. In the burn scar, the proportion of forests, shrublands, grasslands was 90%, 7%, and 2% in 2001 and 30%, 60%, and 8% in 2006 and 2011, respectively. While evergreen and deciduous shrubs were not separated in shrublands, the forests were mainly evergreen, among which deciduous and mixed forests only accounted for 1.61% in 2001 and 1.14% in 2006 and 2011. The forest proportion before the fire event was large in the regions with high burn severity while small in the low burn severity, indicating that the regions with more forests tended to be burned more severely. The forest proportion after fire occurrence decreased while the shrubland and grassland proportion increased with the burn severity level, indicating that higher burn severity caused more forests converted

to shrublands and grasslands. The land cover proportions in 2011 were almost the same as those in 2006.

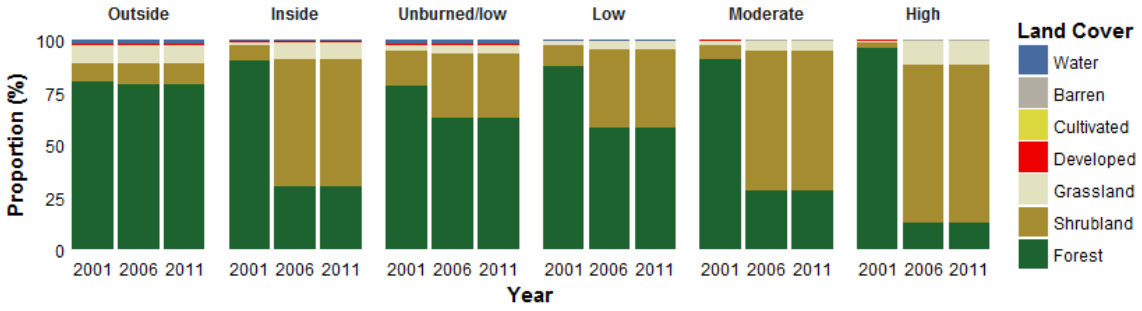

Figure 2-3. The proportion of 30-m land cover in each 240-m pixel in 2001, 2006, and 2011 at different burn severity levels derived from NLCD maps (Outside is the buffer zone, Inside is the entire burn scar, and Unburned/low, Low, Moderate, and High represent different levels of burn severity).

Figure 2-4 displays variations of annual maximum and minimum EVI2 values to demonstrate vegetation recovery through the post-fire period (2003-2014). The annual maximum EVI2 represented the overall vegetation growth in the Hayman Fire because almost all the plants reached their peaks during summer. In contrast, the annual minimum EVI2 revealed the recovery of evergreen plants because there were no green leaves on deciduous plants during winter. In 2001, the annual maximum and minimum EVI2 values inside the burn scar and in the buffer zone were very similar, demonstrating that their vegetation growing conditions were almost identical across the region before fire occurrence. The slight divergences appeared in the minimum EVI2, which might be caused by the variation in proportion of evergreen and deciduous plants. After the occurrence of the Hayman Fire in 2002, both maximum and minimum EVI2 values inside the burn scar dropped sharply but basically remained stable in the buffer zone. In the

post-fire period (2003-2014), the EVI2 inside the burn scar showed increasing trend, as the vegetation recovering and non-native plants invading. The rate of increase on average was 0.052 per decade in the maximum EVI2 and 0.029 per decade in the minimum EVI2. These rates reflected the recovery of total vegetation and evergreen trees, separately. The increase rate in EVI2s was similar across the areas with different levels of burn severity although the magnitude of EVI2 values varied. Based on the current recovery rates, the annual maximum and minimum EVI2 and would reach pre-fire status in 2025 and 2053, respectively.

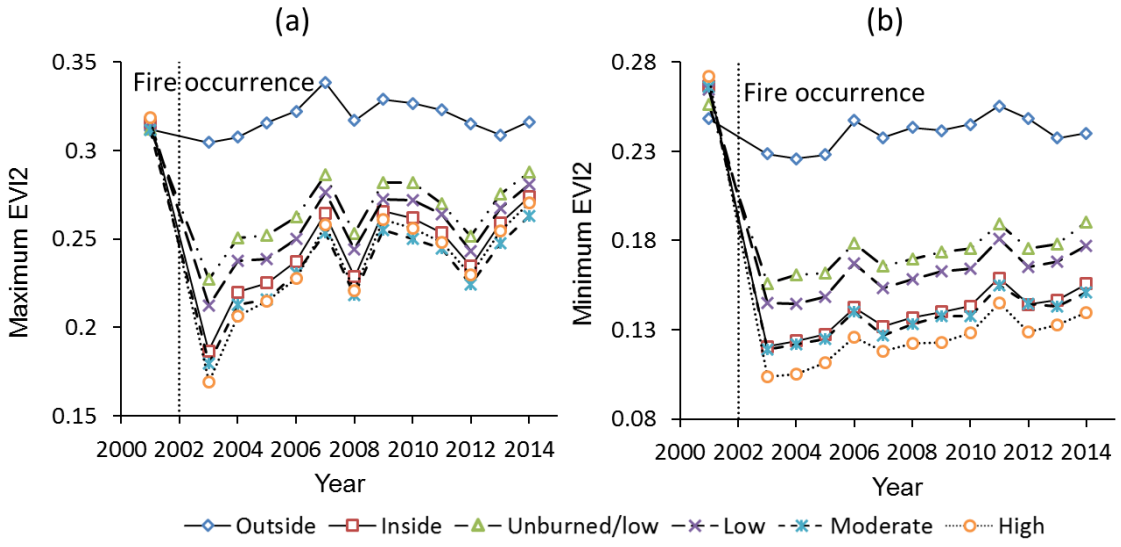

Figure 2-4. The spatially-averaged annual EVI2 time series with different burn severity levels from 2001 to 2014: annual maximum EVI2 (a) and annual minimum EVI2 (b) in the buffer zone (Outside) and inside the burn scar (Unburned/low, Low, Moderate, and High are the EVI2 with different burn severity levels and Inside is the EVI2 in the entire burn scar).

2.3.2. Impacts of fire on SOS in different levels of burn severity

Figure 2-5 displays the spatial distributions of SOS around the Hayman Fire in one year before (2001) and after (2003) the fire occurrence. For the proper comparison, the SOS dates only represent the pixels with high confidence, which varied spatially from 40 to 200 DOY. In both years, the southern and eastern regions tended to have later SOS dates, compared to the western and central parts. In the buffer zone, SOS was relatively stable from 2001 to 2003, although it was later in the west and east regions and earlier in the north and southeast. Inside the burn scar, SOS dates were generally advanced, except for small patches in the center where SOS was delayed.

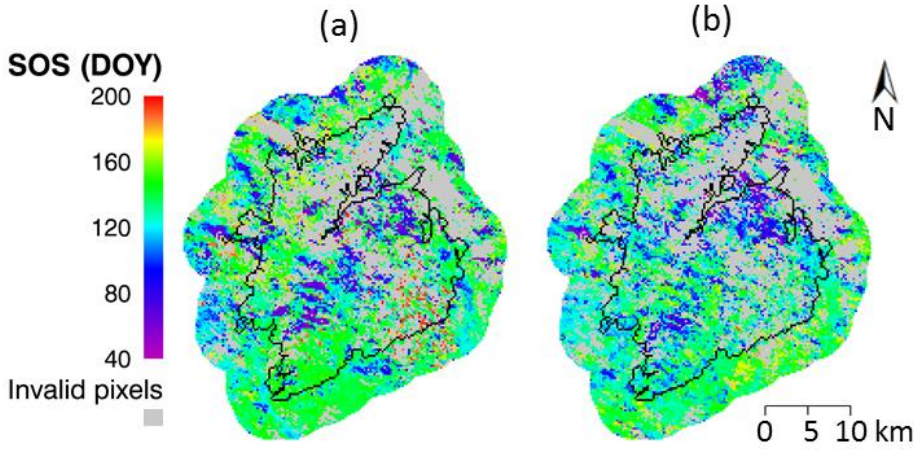

Figure 2-5. Spatial distributions of SOS (DOY) in 2001 (a) and 2003 (b).

The spatial SOS anomaly in pre-fire (2001) and post-fire (2003-2014) revealed the fire impacts on SOS (Figure 2-6 and Table 2-1). Before the fire occurrence, the anomaly was 0 for the areas of entire burn scar relative to the buffer zone although it varied from -1.0 to 3.0 days for different local areas. After the fire occurrence, the anomaly became highly variant, which showed considerably early SOS within the burn

scar. The SOS anomaly during post-fire was strongly dependent on burn severity. It varied from -9.1 days in unburned/low severity to -18.5 days in high severity, and was -15.2 days for the entire burn scar. The difference of spatial SOS anomaly between pre-fire and post-fire was -8.1 days in unburned/low severity and -18.5 days in high severity. It was -15.2 days for the entire burn scar.

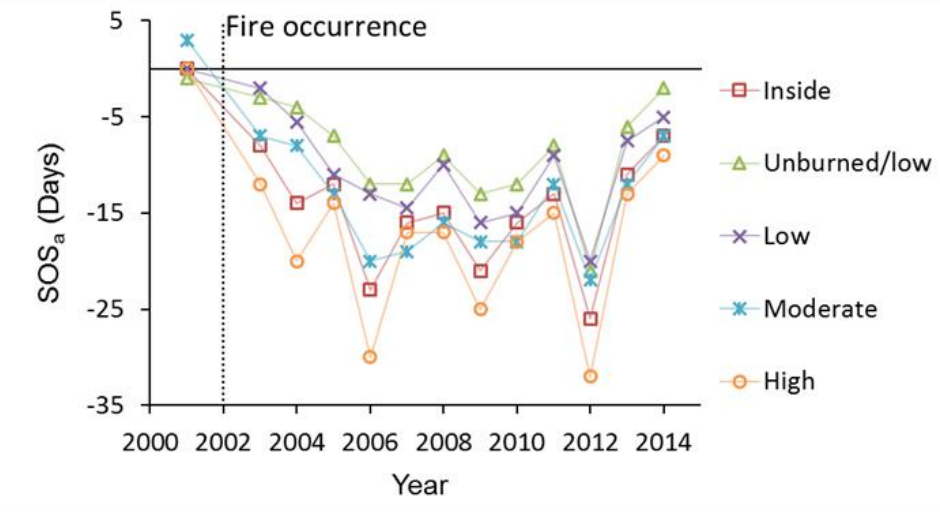

Figure 2-6. Interannual variation in the spatial SOS anomaly (SOSa) for different burn severity levels (Unburned/low, Low, Moderate, and High) and the entire burn scar (Inside).

Spatial SOS anomaly showed great variations interannually during the post-fire from 2003-2014 (Figure 2-6). The magnitude (absolute value) of SOS anomaly increased from 2003-2006, remained relatively stable from 2006-2011, and decreased from 2011-2014. During the period of post-fire (12 years), the large anomaly occurred in 2006, 2009, and 2012, with a value of over 21 days for the entire burn scar and as large as 32 days in the high burn severity, which represented three troughs. In 2013 and 2014, the

anomaly in the areas of unburned/low severity returned to the pre-fire status, which was -1.0 days in 2001 and -2.0 days in 2014.

Table 2-1. The spatial SOS anomalies (unit: days) in pre-fire (2001) and post-fire (2003-2014) and their differences for different burn severity levels (Unburned/low, Low, Moderate, and High) and the entire burn scar (Inside).

Burn Severity	Unburned/low	Low	Moderate	High	Inside
pre-fire	-1.0	0.0	3.0	0.0	0.0
post-fire	-9.1	-10.7	-14.3	-18.5	-15.2
Difference	-8.1	-10.7	-17.3	-18.5	-15.2

2.3.3. Impacts of fire on SOS trend in 2001-2014

Figure 2-7 shows the comparison of the interannual variation in area-integrated SOS inside the burn scar and in the buffer zone during 2001-2014. Overall, SOS shifted early inside the burn scar relative to that in the buffer zone. The interannual variation in these two regions was similar in most years, particularly after 2009. However, the SOS trends during the study period were contrary for the buffer zone and burned area. It was 3.9 days/decade in the buffer zone, while it was -1.9 days/decade inside the burn scar. The dramatic SOS advance occurred in 2012, in which SOS was 35 days and 21 days earlier than that in neighboring years inside burn scar and in the buffer zone, respectively.

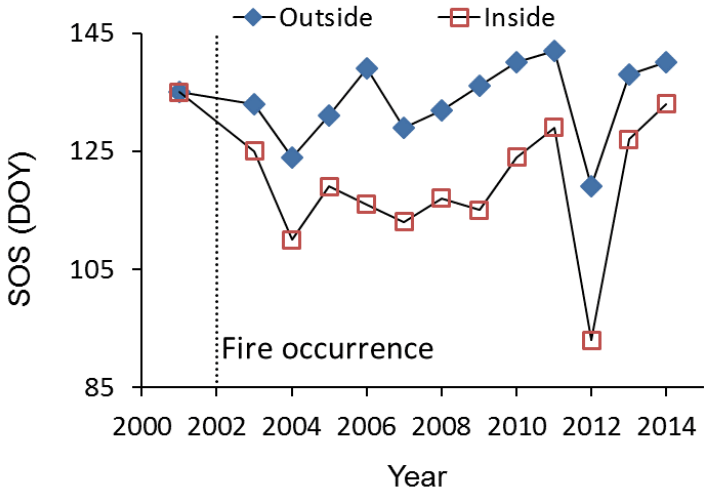

Figure 2-7. Interannual variation in area-integrated SOS inside the burn scar (Inside) and in the buffer zone (Outside) at the Hayman Fire area.

The SOS trend at the pixel scale was very complex. Figure 2-8 shows the pixel frequency with different trends inside the burn scar and in the buffer zone, respectively. In the buffer zone, SOS trend was positive in 55.4% of pixels (10.1% with $p<0.1$) and it was negative in 44.6% of pixels (7.0% with $p<0.1$). In contrast, the SOS trend inside the burn scar was positive in 41.4% of pixels (7.5% with $p<0.1$) and it was negative in 58.6% of pixels (10.0% with $p<0.1$).

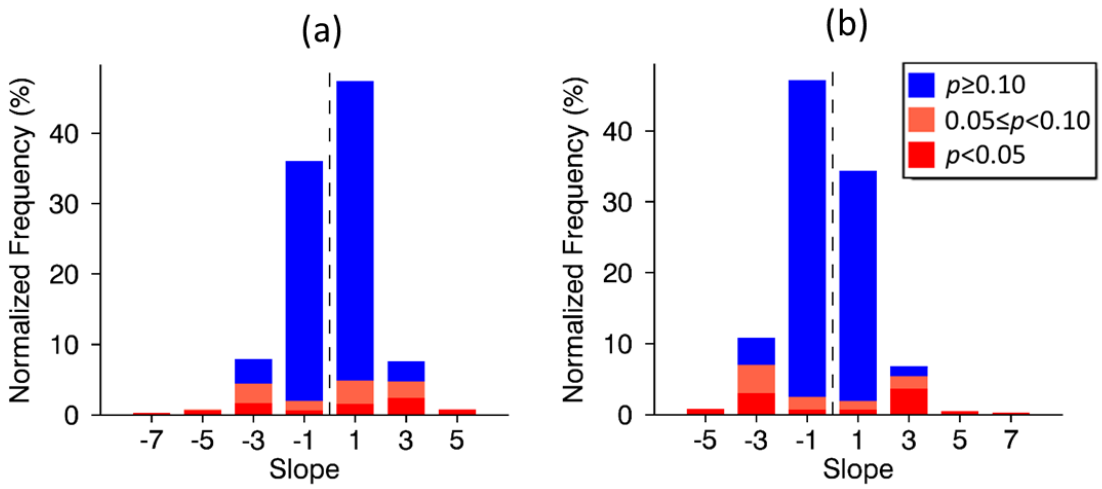

Figure 2-8. The pixel frequency of SOS trend (days/year) in the buffer zone (a) and inside the burn scar (b) during 2001-2014.

2.4. Discussion and conclusions

This study examined the wildfire impact on LSP SOS in the Hayman Fire. Evergreen forests were dominant across the regions before fire occurrence. However, the fire occurrence in 2002 disturbed land surface, which resulted in the conversion of forests to shrublands and grasslands according to the NLCD in 2001 and 2006 (Figures 2-1 and 2-3). As a result, LSP SOS inside the burn scar advanced dramatically, which was 15.2 days on average, compared with the undisturbed buffer zone outside the burn scar (as a reference). The SOS advance was mainly associated with the fact that shrubs, grasses, and young trees usually unfold their leaves earlier than mature trees (Badeck et al., 2004; Seiwa, 1999). The LSP SOS was also strongly influenced by burn severity, which was quantified using the spatial SOS anomaly. In the areas with unburned/low burn severity, the vegetation disturbance was light, so that the SOS anomaly was generally less than 10 days during the post-fire (2003-2014). However, it could be as high as 32 days in the high

burn severity. Note that the land cover conversion caused by wildfire could also change the local environment such as skin temperature because land surface energy balance varies among different vegetation types (Lee et al., 2011; Shen et al., 2015). The alteration of skin temperature could also have effects on vegetation phenology, which is worth investigating in the future but is beyond the scope of this study.

The interannual variation in EVI2 is likely to track well the gradual progresses of vegetation regeneration. The annual minimum EVI2, representing the greenness of evergreen trees (including evergreen forests and evergreen shrubs) during winter period when there were no green leaves on deciduous species, showed a relatively low and stable rate of recovery through 2003-2014. This trend agrees well with field observations indicating the slow progress of regeneration by tree seedlings after the Hayman Fire burning, particularly in the high severity burned areas (Chambers et al., 2016; Rhoades et al., 2011). On the other hand, the annual maximum EVI2, representing greenness from shrubs, grasses, and forests, showed two stages from 2003-2014. It recovered rapidly from 2003-2007, coinciding with the field observations that understory plant communities returned back to the cover of the pre-fire levels by 2007 (Fornwalt and Kaufmann, 2014). The lower maximum EVI2 inside the burn scar relative to the references in the buffer was the result of low abundance of evergreen trees after the fire. After 2007, the increasing rate of the maximum EVI2 slowed down and became comparable to that of the minimum EVI2. This indicates that the interannual trend in both minimum and maximum EVI2 represented gradual regeneration of evergreen trees after the completion of understory recovery. Overall, the annual maximum and minimum EVI2 trajectories from 2003-2014 suggest that vegetation greenness could recover to pre-

fire status in 2022 and 2053 at the current rates respectively. Of course, this projection is of high uncertainty because the influence of climate change and species interactions make the projection of forest recovery very complex (Miller et al., 2013). However, the recovery was not reflected in NLCD land cover maps in 2006 and 2011. This is mainly due to the NLCD classification system that defines forests as the areas dominated by trees generally higher than 5 m tall while young trees lower than 5 m are classified as shrubland (Homer et al., 2007). Tree growth is relatively slow in this area. For example, newly-established ponderosa pine in the Colorado Front Range takes more than 20 years to get 1-2 m tall (Huckaby et al., 2003) and 20-year old Douglas-fir in Northern Rocky Mountains is less than 2.4 m (Ferguson and Carlson, 2010). Moreover, land cover type is classified based on the entire pixel, which is unlikely to detect the subpixel variation of tree recovery.

The forest recovery could further be connected to LSP SOS trajectories. The magnitudes of spatial SOS anomalies continuously increased during 2003-2007, corresponding to the increase of understory species coverage (Fornwalt and Kaufmann, 2014). After 2007, the magnitudes of SOS anomalies showed decreasing trends, in response to the continuous regeneration of evergreen trees and relatively stable understory (Chambers et al., 2016; Rhoades et al., 2011). In particular, the magnitude of SOS anomalies became smaller after 2013, which is likely associated with the denser tree canopy causing less understory detected by satellites.

The magnitude and direction of the interannual trend of LSP SOS were also significantly altered by the Hayman Fire. The interannual trend was converted from 3.9 days/decade in the unburned buffer zone to -1.9 days/decade inside the burn scar during

2001-2014. It is likely that the fire impacts on LSP SOS will continue during the long recovery period. However, climate change may play a more and more important role in the interannual variation of SOS with the forest recovering.

The time series SOS further revealed that extreme weather and climate events had relatively less profound impacts on vegetation phenology than fire events did in a long-term period. In 2012, the contiguous United States experienced exceptionally warm spring and the most severe drought since 1930s (Wolf et al., 2016). The warmest spring greatly advanced the SOS across the region of the Hayman Fire, while the advanced days were much larger inside the burn scar than those in the buffer zone because of the difference in land cover types. On the other hand, severe droughts reduced the annual maximum EVI2 but had little impacts on the minimum EVI2 even in the following year. However, such dramatic impacts on vegetation phenology only appeared in the specific years (a short time period), and vegetation (including seasonal timing and magnitude) generally recovered quickly in the following few years.

The result from this study suggests that it should be cautious against simply viewing LSP trends as indicative of climate change. Although the interannual LSP detected from AVHRR and MODIS data has been widely associated with climate change in regional or global scales (de Beurs and Henebry, 2005a; de Jong et al., 2011; Zhang et al., 2007; Zhou et al., 2001), land disturbances caused by both natural processes (including insect outbreak, storm damage, flooding, drought, and wildfire) and human activities (including urbanization and deforestation) are likely to interrupt the trends reflecting climate change. This is due to the fact that disturbances can result in rapid conversions of the vegetated land surface, including profound changes in community

composition as a result of biotic invasions, either through native range expansion, introduced species, or outbreaks of pathogens (Bradley et al., 2010; Mack et al., 2000). Even though the disturbance could be identified using the change detection approaches if it occurred several years away from either the start or end of a long-term phenological time series (de Beurs and Henebry, 2005b; Verbesselt et al., 2010), the detection would be very challenging in this study in which the disturbance happened only one year later than the begin of the time series. As a result, reliable phenological trends associated with climate change could be obtained if the pixels with land disturbances were explicitly subtracted.

Finally, it should be aware that the impact of land disturbance on LSP is likely to act more widely. It is due to the fact that fire frequency and size have increased and the trend will continue (Westerling et al., 2006) and that human populations and their use of land have modified about one-third to one-half of the land surface and transformed another third or more of the terrestrial biosphere into rangelands and seminatural anthromes (Ellis, 2011; Vitousek et al., 1997). Thus, studies with longer temporal periods and larger spatial scales are still required to move forward.

Acknowledgements

This work was supported by NASA contracts NNX15AB96A and NNX14AQ18A. We obtained MTBS data from http://www.mtbs.gov, NLCD data from http://www.mrlc.gov, and MODIS products of MOD09GQ, MOD09GA, and MOD11A1 from https://lpdaac.usgs.gov/dataset_discovery/modis/modis_products_table.

References

Angert, A., Biraud, S., Bonfils, C., Henning, C.C., Buermann, W., Pinzon, J., Tucker,

C.J., Fung, I., 2005. Drier summers cancel out the CO2 uptake enhancement induced by warmer springs. Proc. Natl. Acad. Sci. U. S. A. 102, 10823–10827.

Badeck, F.-W.F., Bondeau, A., Böttcher, K., Doktor, D., Lucht, W., Schaber, J.J., Sitch, S., Bottcher, K., Doktor, D., Lucht, W., Schaber, J.J., Sitch, S., 2004. Responses of spring phenology to climate change. New Phytol. 162, 295–309. https://doi.org/10.1111/j.1469-8137.2004.01059.x

Bradley, B.A., Wilcove, D.S., Oppenheimer, M., 2010. Climate change increases risk of plant invasion in the Eastern United States. Biol. Invasions 12, 1855–1872.

Buyantuyev, A., Wu, J., 2012. Urbanization diversifies land surface phenology in arid environments: interactions among vegetation, climatic variation, and land use pattern in the Phoenix metropolitan region, USA. Landsc. Urban Plan. 105, 149–159.

Chambers, M.E., Fornwalt, P.J., Malone, S.L., Battaglia, M.A., 2016. Patterns of conifer regeneration following high severity wildfire in ponderosa pine-dominated forests of the Colorado Front Range. For. Ecol. Manage. 378, 57–67. https://doi.org/10.1016/j.foreco.2016.07.001

de Beurs, K. M, Henebry, G.M., 2005a. Land surface phenology and temperature variation in the International Geosphere-Biosphere Program high-latitude transects. Glob. Chang. Biol. 11, 779–790. https://doi.org/10.1111/j.1365-2486.2005.00949.x

de Beurs, K. M., Henebry, G.M., 2005b. A statistical framework for the analysis of long image time series. Int. J. Remote Sens. 26, 1551–1573. https://doi.org/10.1080/01431160512331326657

de Beurs, K.M., Henebry, G.M., 2004. Land surface phenology, climatic variation, and

institutional change: Analyzing agricultural land cover change in Kazakhstan. Remote Sens. Environ. 89, 497–509. https://doi.org/10.1016/j.rse.2003.11.006

de Jong, R., de Bruin, S., de Wit, A., Schaepman, M.E., Dent, D.L., 2011. Analysis of monotonic greening and browning trends from global NDVI time-series. Remote Sens. Environ. 115, 692–702.

Di-Mauro, B., Fava, F., Busetto, L., Crosta, G.F., Colombo, R., 2014. Post-fire resilience in the Alpine region estimated from MODIS satellite multispectral data. Int. J. Appl. Earth Obs. Geoinf. 32, 163–172. https://doi.org/10.1016/j.jag.2014.04.010

Eidenshink, J., Schwind, B., Brewer, K., Zhu, Z., Quayle, B., Howard, S., 2007. A Project for Monitoring Trends in Burn Severity. Fire Ecol. 3, 3–21. https://doi.org/10.4996/fireecology.0301003

Ellis, E.C., 2011. Anthropogenic transformation of the terrestrial biosphere. Philos. Trans. R. Soc. London A Math. Phys. Eng. Sci. 369, 1010–1035.

Ferguson, D.E., Carlson, C.E., 2010. Height-age relationships for regeneration-size trees in the northern Rocky Mountains, USA. USDA, Forest Service, Rocky Mountain Research Station, Fort Collins, CO.

Fernandez-Manso, A., Quintano, C., Roberts, D.A., 2016. Burn severity influence on post-fire vegetation cover resilience from Landsat MESMA fraction images time series in Mediterranean forest ecosystems. Remote Sens. Environ. 184, 112–123. https://doi.org/10.1016/j.rse.2016.06.015

Fornwalt, P.J., Kaufmann, M.R., 2014. Understorey plant community dynamics following a large, mixed severity wildfire in a Pinus ponderosa-Pseudotsuga menziesii forest, Colorado, USA. J. Veg. Sci. 25, 805–818.

https://doi.org/10.1111/jvs.12128

Fry, J.A., Xian, G., Jin, S., Dewitz, J.A., Homer, C.G., Limin, Y., Barnes, C.A., Herold, N.D., Wickham, J.D., 2011. Completion of the 2006 national land cover database for the conterminous United States. Photogramm. Eng. Remote Sensing 77, 858–864.

Gu, L., Post, W.M., Baldocchi, D., Black, T.A., Verma, S.B., Vesala, T., Wofsy, S.C., 2003. Phenology of vegetation photosynthesis, in: Phenology: An Integrative Environmental Science. Springer, pp. 467–485.

Homer, C., Dewitz, J., Fry, J., Coan, M., Hossain, N., Larson, C., Herold, N., McKerrow, A., VanDriel, J.N., Wickham, J., 2007. Completion of the 2001 national land cover database for the counterminous United States. Photogramm. Eng. Remote Sensing 73, 337.

Homer, C.G., Dewitz, J.A., Yang, L., Jin, S., Danielson, P., Xian, G., Coulston, J., Herold, N.D., Wickham, J.D., Megown, K., 2015. Completion of the 2011 National Land Cover Database for the conterminous United States-Representing a decade of land cover change information. Photogramm. Eng. Remote Sensing 81, 345–354.

Huckaby, L.S., Kaufmann, M.R., Fornwalt, P.J., Stoker, J.M., Dennis, C., 2003. Field guide to old ponderosa pines in the Colorado Front Range. USDA, Forest Service, Rocky Mountain Research Station, Fort Collins, CO.

Huete, A., Didan, K., Miura, T., Rodriguez, E.P., Gao, X., Ferreira, L.G., 2002. Overview of the radiometric and biophysical performance of the MODIS vegetation indices. Remote Sens. Environ. 83, 195–213. https://doi.org/http://dx.doi.org/10.1016/S0034-4257(02)00096-2

Jeong, S.J., Ho, C.H., Gim, H.J., Brown, M.E., 2011. Phenology shifts at start vs. end of

growing season in temperate vegetation over the Northern Hemisphere for the period 1982-2008. Glob. Chang. Biol. 17, 2385–2399. https://doi.org/10.1111/j.1365-2486.2011.02397.x

Jiang, Z., Huete, A.R., Didan, K., Miura, T., 2008. Development of a two-band enhanced vegetation index without a blue band. Remote Sens. Environ. 112, 3833–3845. https://doi.org/http://dx.doi.org/10.1016/j.rse.2008.06.006

Lee, X., Goulden, M.L., Hollinger, D.Y., Barr, A., Black, T.A., Bohrer, G., Bracho, R., Drake, B., Goldstein, A., Gu, L., 2011. Observed increase in local cooling effect of deforestation at higher latitudes. Nature 479, 384–387.

Mack, R.N., Simberloff, D., Mark Lonsdale, W., Evans, H., Clout, M., Bazzaz, F.A., 2000. Biotic invasions: causes, epidemiology, global consequences, and control. Ecol. Appl. 10, 689–710.

Marlon, J.R., Bartlein, P.J., Gavin, D.G., Long, C.J., Anderson, R.S., Briles, C.E., Brown, K.J., Colombaroli, D., Hallett, D.J., Power, M.J., Scharf, E.A., Walsh, M.K., 2012. Long-term perspective on wildfires in the western USA. Proc. Natl. Acad. Sci. U. S. A. 109, E535-43. https://doi.org/10.1073/pnas.1112839109

Miller, R.F., Chambers, J.C., Pyke, D. a, Pierson, F.B., Williams, C.J., Fred, B., Jason, C. a, 2013. A Review of Fire Effects on Vegetation and Soils in the Great Basin Region : Response and Ecological Site Characteristics, Gen. Tech. Rep. RMRS-GTR-308. Fort Collins, CO. https://doi.org/Gen Tech Rep RMRS--GTR-308

Pachauri, R.K., Allen, M.R., Barros, V.R., Broome, J., Cramer, W., Christ, R., Church, J.A., Clarke, L., Dahe, Q., Dasgupta, P., 2014. Climate change 2014: synthesis Report. Contribution of working groups I, II and III to the fifth assessment report of

the intergovernmental panel on climate change. IPCC.

Pechony, O., Shindell, D.T., 2010. Driving forces of global wildfires over the past millennium and the forthcoming century. Proc. Natl. Acad. Sci. U. S. A. 107, 19167–70. https://doi.org/10.1073/pnas.1003669107

Reed, B.C., Brown, J.F., VanderZee, D., Loveland, T.R., Merchant, J.W., Ohlen, D.O., 1994. Measuring phenological variability from satellite imagery. J. Veg. Sci. 5, 703–714. https://doi.org/10.2307/3235884

Rhoades, C.C., Entwistle, D., Butler, D., 2011. The influence of wildfire extent and severity on streamwater chemistry, sediment and temperature following the Hayman Fire, Colorado. Int. J. Wildl. Fire 20, 430–442. https://doi.org/10.1071/WF09086

Richardson, A.D., Anderson, R.S., Arain, M.A., Barr, A.G., Bohrer, G., Chen, G., Chen, J.M., Ciais, P., Davis, K.J., Desai, A.R., Dietze, M.C., Dragoni, D., Garrity, S.R., Gough, C.M., Grant, R., Hollinger, D.Y., Margolis, H. a., Mccaughey, H., Migliavacca, M., Monson, R.K., Munger, J.W., Poulter, B., Raczka, B.M., Ricciuto, D.M., Sahoo, A.K., Schaefer, K., Tian, H., Vargas, R., Verbeeck, H., Xiao, J., Xue, Y., 2012. Terrestrial biosphere models need better representation of vegetation phenology: Results from the North American Carbon Program Site Synthesis. Glob. Chang. Biol. 18, 566–584. https://doi.org/10.1111/j.1365-2486.2011.02562.x

Richardson, A.D., Keenan, T.F., Migliavacca, M., Ryu, Y., Sonnentag, O., Toomey, M., 2013. Climate change, phenology, and phenological control of vegetation feedbacks to the climate system. Agric. For. Meteorol. 169, 156–173. https://doi.org/10.1016/j.agrformet.2012.09.012

Romo-Leon, J.R., van Leeuwen, W.J.D., Castellanos-Villegas, A., 2016. Land Use and

Environmental Variability Impacts on the Phenology of Arid Agro-Ecosystems. Environ. Manage. 57, 283–297. https://doi.org/10.1007/s00267-015-0617-7

Sankey, J.B., Wallace, C.S.A., Ravi, S., 2013. Phenology-based, remote sensing of post-burn disturbance windows in rangelands. Ecol. Indic. 30, 35–44. https://doi.org/10.1016/j.ecolind.2013.02.004

Schwartz, M.D., Ahas, R., Aasa, A., 2006. Onset of spring starting earlier across the Northern Hemisphere. Glob. Chang. Biol. 12, 343–351. https://doi.org/10.1111/j.1365-2486.2005.01097.x

Seiwa, K., 1999. Changes in leaf phenology are dependent on tree height in Acer mono, a deciduous broad-leaved tree. Ann. Bot. 83, 355–361. https://doi.org/10.1006/anbo.1998.0831

Shen, M., Piao, S., Jeong, S.-J., Zhou, L., Zeng, Z., Ciais, P., Chen, D., Huang, M., Jin, C.-S., Li, L.Z.X., 2015. Evaporative cooling over the Tibetan Plateau induced by vegetation growth. Proc. Natl. Acad. Sci. 112, 9299–9304.

Shen, M., Zhang, G., Cong, N., Wang, S., Kong, W., Piao, S., 2014. Increasing altitudinal gradient of spring vegetation phenology during the last decade on the Qinghai–Tibetan Plateau. Agric. For. Meteorol. 189–190, 71–80. https://doi.org/http://dx.doi.org/10.1016/j.agrformet.2014.01.003

Storey, E.A., Stow, D.A., O'Leary, J.F., 2016. Assessing postfire recovery of chamise chaparral using multi-temporal spectral vegetation index trajectories derived from Landsat imagery. Remote Sens. Environ. 183, 53–64. https://doi.org/10.1016/j.rse.2016.05.018

van Leeuwen, W.J.D., 2008. Monitoring the Effects of Forest Restoration Treatments on

Post-Fire Vegetation Recovery with MODIS Multitemporal Data. Sensors 8, 2017–2042. https://doi.org/10.3390/s8032017

Van Leeuwen, W.J.D., Casady, G.M., Neary, D.G., Bautista, S., Alloza, J.A., Carmel, Y., Wittenberg, L., Malkinson, D., Orr, B.J., 2010. Monitoring post-wildfire vegetation response with remotely sensed time-series data in Spain, USA and Israel. Int. J. Wildl. Fire 19, 75–93. https://doi.org/10.1071/WF08078

Verbesselt, J., Hyndman, R., Zeileis, A., Culvenor, D., 2010. Phenological change detection while accounting for abrupt and gradual trends in satellite image time series. Remote Sens. Environ. 114, 2970–2980. https://doi.org/10.1016/j.rse.2010.08.003

Vitousek, P.M., Aber, J.D., Howarth, R.W., Likens, G.E., Matson, P.A., Schindler, D.W., Schlesinger, W.H., Tilman, D.G., 1997. Human alteration of the global nitrogen cycle: sources and consequences. Ecol. Appl. 7, 737–750.

Walther, G., 2004. Plants in a warmer world. Perspect. Plant Ecol. Evol. Syst. 6, 169–185. https://doi.org/10.1078/1433-8319-00076

Westerling, a. L., Hidalgo, H.G., Cayan, D.R., Swetnam, T.W., 2006. Warming and earlier spring increase western U.S. forest wildfire activity. Science 313, 940–3. https://doi.org/10.1126/science.1128834

White, M.A., De Beurs, K.M., Didan, K., Inouye, D.W., Richardson, A.D., Jensen, O.P., O'keefe, J., Zhang, G., Nemani, R.R., Van Leeuwen, W.J.D., Brown, J.F., De Wit, A., Schaepman, M., Lin, X., Dettinger, M., Bailey, A.S., Kimball, J., Schwartz, M.D., Baldocchi, D.D., Lee, J.T., Lauenroth, W.K., 2009. Intercomparison, interpretation, and assessment of spring phenology in North America estimated from

remote sensing for 1982-2006. Glob. Chang. Biol. 15, 2335–2359. https://doi.org/10.1111/j.1365-2486.2009.01910.x

White, M.A., Hoffman, F., Hargrove, W.W., Nemani, R.R., 2005. A global framework for monitoring phenological responses to climate change. Geophys. Res. Lett. 32, L04705.

Wolf, S., Keenan, T.F., Fisher, J.B., Baldocchi, D.D., Desai, A.R., Richardson, A.D., Scott, R.L., Law, B.E., Litvak, M.E., Brunsell, N.A., 2016. Warm spring reduced carbon cycle impact of the 2012 US summer drought. Proc. Natl. Acad. Sci. 113, 5880–5885.

Zhang, X., 2015. Reconstruction of a complete global time series of daily vegetation index trajectory from long-term AVHRR data. Remote Sens. Environ. 156, 457–472. https://doi.org/10.1016/j.rse.2014.10.012

Zhang, X., Friedl, M.A., Schaaf, C.B., 2009. Sensitivity of vegetation phenology detection to the temporal resolution of satellite data. Int. J. Remote Sens. 30, 2061–2074. https://doi.org/10.1080/01431160802549237

Zhang, X., Friedl, M.A., Schaaf, C.B., Strahler, A.H., Hodges, J.C.F.F., Gao, F., Reed, B.C., Huete, A., 2003. Monitoring vegetation phenology using MODIS. Remote Sens. Environ. 84, 471–475. https://doi.org/10.1016/S0034-4257(02)00135-9

Zhang, X., Tarpley, D., Sullivan, J.T., 2007. Diverse responses of vegetation phenology to a warming climate. Geophys. Res. Lett. 34, 1–5. https://doi.org/10.1029/2007GL031447

Zhou, L., Tucker, C.J., Kaufmann, R.K., Slayback, D., Shabanov, N. V, Myneni, R.B., 2001. Variations in northern vegetation activity inferred from satellite data of

vegetation index during 1981 to 1999. J. Geophys. Res. Atmos. 106, 20069–20083.

CHAPTER 3: Investigation of Wildfire Impacts on Land Surface Phenology from MODIS Time Series in the Western US Forests

The content of this chapter was published: Wang, J., Zhang, X., 2020. Investigation of wildfire impacts on land surface phenology from MODIS time series in the western US forests. ISPRS J. Photogramm. Remote Sens. 159, 281–295. https://doi.org/10.1016/j.isprsjprs.2019.11.027.

Abstract

Land surface phenology (LSP) characterizes the timing and greenness of seasonal vegetation growth in satellite pixels and it has been widely used to associate with climate change. However, wildfire, causing considerable land surface changes, exerts abrupt changes on the LSP magnitudes and great influences on the LSP long-term trends, which are poorly investigated. This study for the first time conducted a systematic analysis of the wildfire impacts on LSP by investigating 838 forest wildfires occurred from 2002-2014 across the western United States. Specifically, we derived three LSP timing metrics that are the start (SOS), end (EOS), and length (LOS) of growing season and two LSP greenness metrics that are seasonal greenness maximum (GMax) and minimum (GMin) from daily time series of 250-m MODIS two-band enhanced vegetation index (EVI2) during 2001-2015. Burned area and burn severity were obtained from the Monitoring Trends in Burn Severity project. The results showed GMax and GMin were decreased at an extent of 0.063 and 0.074 EVI2, respectively. LSP timings presented diverse responses to wildfire occurrences. Absolute abrupt shift of > 2 days in SOS appeared in 73% of burned areas with 40% advances and 33% delays, the shift in EOS occurred in 80% of burned areas with 33% advances and 47% delays, and the shift in LOS occurred in 85% of the burned areas with 36% shortening and 49% lengthening. Moreover, the LSP changes were significantly influenced by burn severity with the largest impact on LSP timing at the moderate burn severity and on LSP greenness at the high burn severity. Finally, the phenological trends from 2001-2015 differed significantly between burned and unburned reference areas and the trend difference varied with the wildfire occurrence year. Overall, this study demonstrated that wildfires exert complex and diverse impacts

on LSP timing and greenness metrics and significantly influence LSP trends associating with climate change. The approach developed in this study provides a prototype to investigate LSP responses to other land disturbances associated with natural processes and human activities on the landscape.

3.1. Introduction

Land surface phenology (LSP) quantifies the seasonal dynamics of vegetated land surfaces from satellite data in terms of both timing and magnitude of vegetation greenness development (Zhang, 2018). LSP timing represents key transition dates in the annual cycle of vegetation growth and LSP greenness quantifies the magnitude of vegetation growth at a certain phenological stage. The most important phenological metrics during a vegetation-growing season are the LSP timing metrics of start (SOS), end (EOS), and length (LOS) of growing season and the LSP greenness metrics of greenness maximum (GMax) and greenness minimum (GMin). These metrics are calculated from the reconstructed temporal satellite greenness after removing abiotic noises (Wang et al., 2019; Yuan et al., 2018; Zhang, 2015; Zhang et al., 2003). Because vegetation phenology is a sensitive indicator of biological responses to climate change (Cleland et al., 2012; Ivits et al., 2012; Morisette et al., 2009), LSP provides an ideal basis for developing a climate indicator related to temporally consistent and spatially exhaustive measurements required for national-scale assessments (Morisette et al., 2009). Long-term records of vegetation phenology have greatly contributed to the understanding of the biological responses to climate change at regional to continental scales (Cleland et al., 2007; Körner and Basler, 2010; Parmesan and Yohe, 2003; Richardson et al., 2013; Walther, 2010). Indeed, interannual variations in LSP timing and greenness have been

widely revealed from long-term satellite data (Alcaraz-Segura et al., 2010; de Jong et al., 2012; Jeong et al., 2011; Liu et al., 2017; Wang et al., 2016; Zhang et al., 2014), which show trends of advanced SOS, delayed EOS, lengthened LOS, and increased greenness because of regional or global warming climate (Richardson et al., 2013; Zhou et al., 2003; Zhu et al., 2016).

Current LSP-based climate indicators detected from satellite data can be strongly influenced by land disturbance including land cover and land use changes and human activities (Buyantuyev and Wu, 2012; de Beurs and Henebry, 2004; Romo-Leon et al., 2016; White et al., 2005). This influence severely limits our understanding of the phenological variability and trends reflecting climate change across regional to global scales (Romo-Leon et al., 2016; White et al., 2005). The impact of land disturbance on the effectiveness of LSP as a climate indicator is due to the fact that LSP in a satellite pixel reflects the seasonal dynamics of a vegetation community with complex species. Changes in species compositions and abundances within a pixel can greatly alter remotely sensed LSP. As a result, changes in species compositions and abundances can interrupt the long-term phenological trends that are commonly considered to be driven by climate change at a regional scale (Zhang et al., 2019).

Wildfire is one of the most important land disturbance agents across the world although variation of vegetation species compositions in a satellite pixel can be caused by other factors including climate extremes and agricultural and forestry management practices. Wildfire is particularly important with the increases in aspects of size, severity, and frequency in many parts of the world during past decades (Marlon et al., 2012; Pechony and Shindell, 2010; Westerling et al., 2006). Wildfire impacts on LSP have been

found in a few case studies by investigating both LSP timing and greenness metrics in forests with an abrupt burning and a gradual post-fire succession (Di-Mauro et al., 2014; Wang and Zhang, 2017). After a wildfire burning, LSP greenness decreases abruptly with the consumption of green vegetation and the extent of decrease usually increases with burn severity (Keeley, 2009; Lentile et al., 2007; Montorio Llovería et al., 2016). In contrast, the change of LSP timing metrics in post-fire years is very complex, which is a function of surface conditions, burn severity, and phenological characteristics between the early successional species (usually grasses and shrubs) recolonizing the burned area and pre-fire trees. Unlike the unanimous decrease in greenness, wildfire-caused diverse changes in LSP timing were revealed in a few existing studies. Specifically, analyzing Moderate Resolution Imaging Spectroradiometer (MODIS) time series shows that SOS in burned areas compared to unburned areas was delayed in Northern Italy alpine forests (Di-Mauro et al., 2014) and Mt Carmel, Israel (Van Leeuwen et al., 2010) but advanced in Colorado evergreen forests (Wang and Zhang, 2017).

Wildfires also have great influences on long-term interannual trends in both LSP timing and greenness. The abrupt LSP changes by biomass burning and the post-fire recovery processes could alter the long-term LSP time series (Di-Mauro et al., 2014; Lhermitte et al., 2011; Meng et al., 2015; Wang and Zhang, 2017). However, many studies on LSP trends have not paid attention to the potential interruption of wildfire or other land disturbances (Julien and Sobrino, 2009; Li et al., 2019; Piao et al., 2014; Zeng et al., 2011; Zhang et al., 2007), while some analyzed the LSP by excluding the disturbed areas (Jönsson et al., 2018; Melaas et al., 2016). We still know little about how large impacts that disturbances such as wildfires could impose on LSP trends, despite that

only a few studies targeted on it. For example, Wang and Zhang (2017) found that the 2002 Hayman Fire resulted in more pixels showing an advancing trend of SOS in the burned areas than in the unburned areas based on long-term MODIS data. Sulla-Menashe et al. (2018) revealed that wildfire disturbance is the most common and important source that impacts the trend of annual-maximum Landsat Normalized Difference Vegetation Index (NDVI) time series in Canadian boreal forests. However, such studies are very limited and more insights are required to reveal the wildfire influences on LSP trends.

Overall, three major shortages exist in current studies on the wildfire impacts on forest LSP. First, a few individual wildfire events were investigated with inconsistent results (Di-Mauro et al., 2014; Serbin et al., 2009; Van Leeuwen et al., 2010; Wang and Zhang, 2017), which impede our understanding of wildfire impacts on LSP timing metrics at a regional scale. Second, most of current studies focused on a single LSP metric without discussing the phenological responses described by both LSP timing and greenness metrics to wildfires. Third, while current studies simply presented the long-term LSP in the burned and reference areas, there is a lack of efforts to quantify the wildfire impacts on the short-term abrupt LSP change and long-term LSP trends.

To better understand the impacts of land disturbance on LSP, which could have significant interruptions to climate-driven LSP trends, this study conducts the first systematic analysis of forest wildfire impacts on LSP metrics of both timing (SOS, EOS, and LOS) and greenness (GMax and GMin) that are derived from MODIS data from 2001-2015 across the western United States (US). The main goals of this study are (1) to characterize the wildfire impacts on the abrupt changes of LSP magnitudes at a regional

scale, (2) to investigate the LSP change with burn severity, and (3) to examine the wildfire impacts on long-term interannual LSP trends.

3.2. Materials and methods

3.2.1. Study area and wildfires

The study area covers the western US where forests are mainly distributed in Western Cordillera and Upper Gila Mountains. The major forest type consists of Douglas-fir, ponderosa pine, and lodgepole pine along the altitudinal zonation (Zhu and Evans, 1994). Climate change in the western US is evidenced by the warming temperatures and frequent droughts, which has led to increases in extent and intensity of wildfires since the mid-1980s (Dale et al., 2001; Westerling et al., 2006). The trend is believed to be going to continue for decades.

To analyze wildfire impacts on forest LSP from 2001-2015, we obtained burned areas, burn severity, and unburned references from Monitoring Trends in Burn Severity (MTBS) for the period of 2002-2014 (Eidenshink et al., 2007). Note that wildfires in 2001 and 2015 were excluded because (1) the wildfire impacts on LSP were quantified based on both pre-fire and post-fire LSP but there were no pre-fire LSP for wildfires in 2001 and no post-fire LSP for wildfires in 2015 (see Section 2.3.2), and (2) LSP metrics were not retrieved in the burned area for the wildfire occurrence year (see Section 2.2). As a wildfire event can burn different land cover types, forest pixels were selected from the National Land Cover Database (NLCD) maps in 2001, 2006, and 2011 (Fry et al., 2011; Homer et al., 2007, 2015). Both MTBS and NLCD are derived from Landsat imagery at a spatial resolution of 30 m and stored in Albers equal-area conic projection. MTBS, through comparing the pre-fire and post-fire normalized burn ratio,

generates consistently burned area and burn severity (unburned/low, low, moderate, high, and increased greenness). NLCD provides 16-class land cover maps based primarily on a decision-tree classification. To be aligned with the MODIS data (see Section 2.2), MTBS maps were resampled to 240 m based on the majority of burn severity, and NLCD maps were aggregated to 240 m by calculating the proportions of different 30-m land cover types.

We selected the burned and reference areas based on MTBS for each wildfire event following the five steps. (1) Performed the segmentation over the burned pixels and label each segment as an individual wildfire event. (2) Set up a 5-km buffer zone (unburned in the wildfire occurrence year) surrounding the burned area for each wildfire event. (3) Excluded the pixels burned more than once during 2002-2014 from the burned areas and the pixels burned in other years (not the given wildfire occurrence year) from the buffer areas (Figure 3-1). Pixels with burn severity of increased greenness and non-processing in the burned areas were further excluded because of limited coverage (<3%). (4) Selected the pure forest pixels in the burned and buffer areas for each wildfire event based on the NLCD maps. The pure forest pixel at 240 m was defined as that with ≥80% 30-m forest pixels. For a burned area, the NLCD map closely prior to wildfire occurrence was used. In the buffer area, pixels classified as forest in all years of 2001, 2006, and 2011 were selected as reference pixels. (5) Calculated the areas of the burned and reference forest pixels for each wildfire event and excluded the wildfire events with a burned or reference forest area less than 10 km^2 to minimize the edge effect.

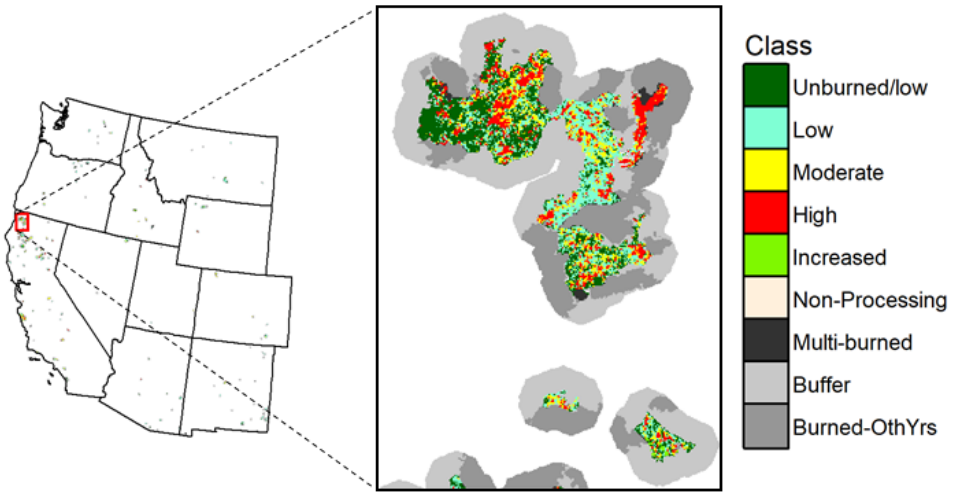

Figure 3-1. Illustration of selecting burned and reference pixels. Multi-burned denotes the pixels burned more than once during 2002-2014 and Burned-OthYrs denotes the pixels burned in other years than the wildfire occurrence year.

Finally, we obtained 838 wildfire events during 2002-2014 for further analysis (Figure 3-2). In all the burned and reference areas, 95.3% of pixels are evergreen forests, 2.2% are deciduous forests, and 2.5% are mixed forests.

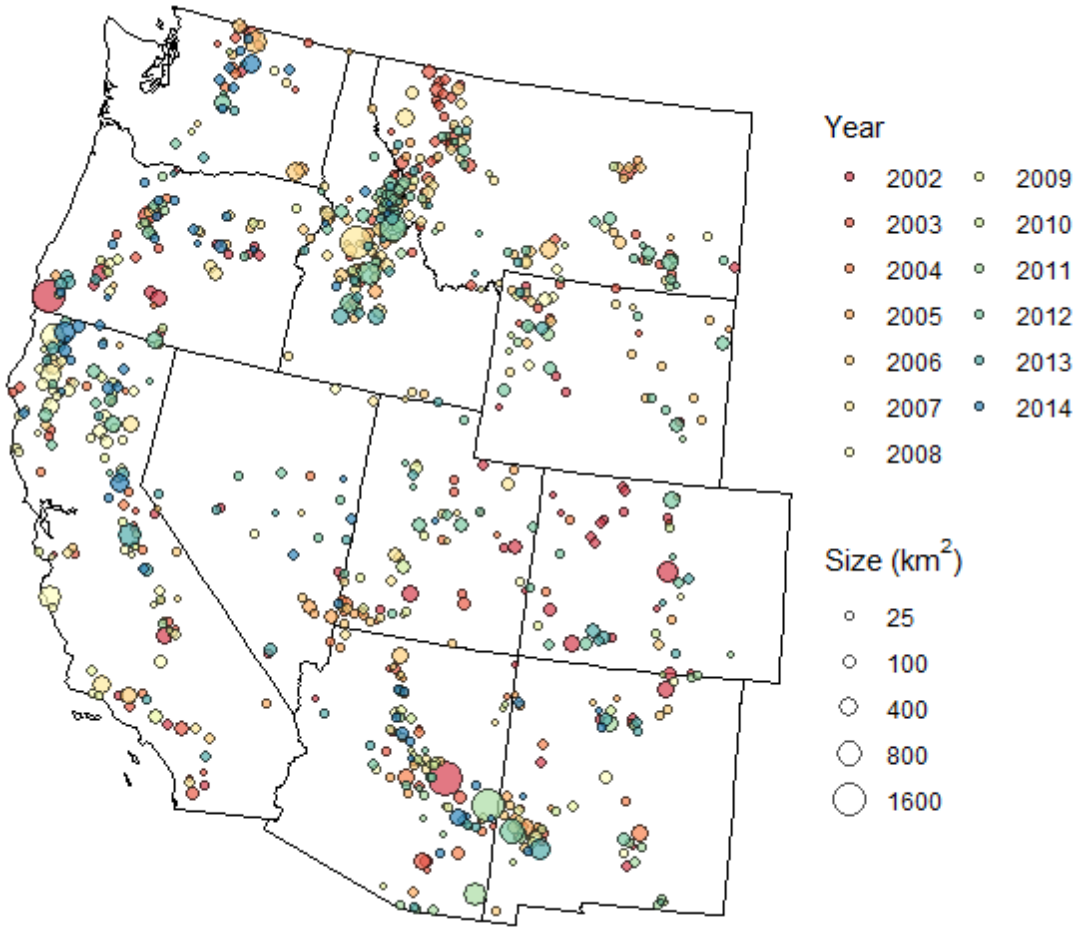

Figure 3-2. Selected forest fires occurring during 2002-2014. Wildfire size was calculated based on the forest pixels burned in each wildfire event. The color indicates the year of wildfire occurrence and the circle size varies continuously in representing the change of burned areas with five marks provided.

3.2.2. LSP detection

We used the hybrid piecewise-logistic-model-based LSP detection algorithm (HPLM-LPSD) to detect the five LSP metrics (SOS, EOS, LOS, GMax, and GMin) from daily 250-m MODIS surface reflectance (the actual pixel size in 250-m MODIS products

is 231.66 m) time series (Zhang, 2015; Zhang et al., 2003). The HPLM-LPSD algorithm fits the time series of vegetation index with piecewise logistic models and identifies the phenological transition dates using the maximal or minimal rate of change in the curvature along the reconstructed time series. Compared to various phenology detection methods (Jönsson and Eklundh, 2004; White et al., 1997; Yu et al., 2010), the HPLM-LPSD algorithm has several advantages (Beck et al., 2006; Zhang, 2018): providing a simple, bounded, continuous function for modeling vegetation growth and decay processes, assigning each parameter to a biophysical meaning related to vegetation growth or senescence, performing superiorly to both Fourier-based and asymmetric Gaussian functions for fitting remote-sensing-based phenology development, being capable of describing either symmetric or asymmetric vegetation greenness development, simulating multiple cycles of vegetation growths flexibly, and providing no predefined thresholds in the identification of phenological transition dates. Therefore, we processed the phenology detections using the HPLM-LSPD with the detail described as follows (Figures 3-3 and 3-4).

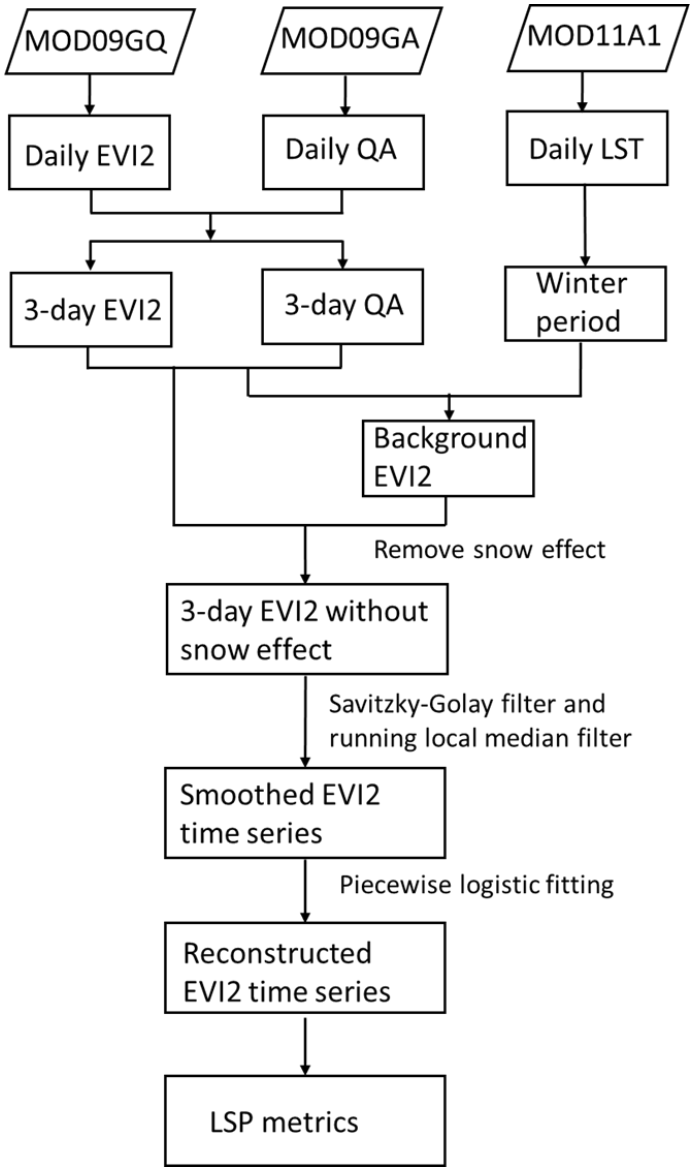

Figure 3-3. Flowchart of land surface phenology detection using HPLM-LPSD.

(1) A daily time series of two-band enhanced vegetation index (EVI2) with quality assessment (QA) was generated. EVI2 was used in this study because, compared to NDVI, it is less sensitive to soil background brightness and atmospheric scattering contamination and does not saturate over high densely-vegetated areas although both indices are based on reflectances at red and near-infrared bands (Huete et al., 2002; Jiang

et al., 2008; Rocha and Shaver, 2009). Moreover, EVI2 provides better phenology detections than NDVI when compared with the PhenoCam phenology (Rocha and Shaver, 2009), ground observed phenology from both national phenology network and AmeriFlux (Peng et al., 2017), and flux tower observations (Karkauskaite et al., 2017). In practice, a daily 250-m EVI2 time series was first calculated (Jiang et al., 2008) from MOD09GQ during 2001-2015. Then, the QA flags (including cloud and snow flags) for the daily EVI2 time series were derived from daily 1-km surface reflectance products (MOD09GA, V006), which were downscaled to 250 m using a nearest neighbor approach.

(2) To reduce the uncertainties and data volumes and improve the processing speed of LSP detection while to still remain the fine temporal resolution, the daily EVI2 time series was aggregated to three-day composites by selecting the EVI2 value with the best quality within a three-day period using QA flags (Zhang et al., 2018). If there were more than one EVI2 value with the best quality in a three-day period, the maximum value was used. It is assumed that forest changes within a three-day period are negligible and three-day composites would not reduce the accuracy of phenology detection (Zhang et al., 2009).

(3) To remove the effect of snow in the EVI2 data, a background EVI2 was determined and used to replace the snow-contaminated values. Specifically, the background EVI2 for each year was calculated as the mean of the 10% largest EVI2 values with cloud- and snow-free observations during winter periods. The winter period was defined using daytime land surface temperature (LST $\leq$278 K) that was obtained from daily MODIS LST products (MOD11A1, V006). Although the vegetation growth

could happen at daily mean air temperature below 278 K (Shen et al., 2012), the daytime LST threshold was only used to identify the time period when snow effect could take place, rather than to determine an exact winter period by date (Zhang et al., 2018). The EVI2 values less than the background EVI2 during the winter periods were considered as snow or cloud contaminated values and replaced by the background EVI2.

(4) To reduce the noise (particularly local sharp peaks or troughs) impacts on phenology detection, EVI2 time series were smoothed using a Savitzky-Golay filter (Chen et al., 2004) and a running local median filter.

(5) To reconstruct the EVI2 time series, the hybrid piecewise logistic functions were used to fit the time series (Zhang, 2015):

$$EVI2(t) = \begin{cases} \frac{c_1}{1+e^{a_1+b_1 t}} + EVI2_b & \text{Favorable growth condition} \\ \frac{c_2+dt}{1+e^{a_1+b_1 t}} + EVI2_b & \text{Vegetation stress condition} \end{cases} \quad (1)$$

where t is the time in day of year (DOY), $EVI2_b$ is the background EVI2, and a, b, c, and d are the coefficients to be retrieved by fitting the logistic functions. The time series fit to the two functions in the equation (1) was compared with an agreement index to determine whether the plant suffers from stress or not (Zhang et al., 2018).

(6) Based on the reconstructed EVI2 time series, the LSP dates were identified as the days with the maximal or minimal rate of change in the curvature. GMax and GMin were retrieved as the annual maximum and minimum values, respectively, in the reconstructed EVI2 time series. Thus, GMax represents the greenness from a vegetation community (all vegetation types) within a pixel while GMin indicates the evergreen vegetation without deciduous species. For SOS and EOS, the confidence of detections

was quantified using the proportion of good quality (cloud- and snow-free) EVI2 (PGQ) around the DOY of SOS and EOS, respectively (Zhang, 2015; Zhang et al., 2009). To ensure the reliability of LSP detections, a filter of PGQ >40% for both SOS and EOS was applied to select the high confidence pixels, for which the LOS is calculated as the difference between EOS and SOS.

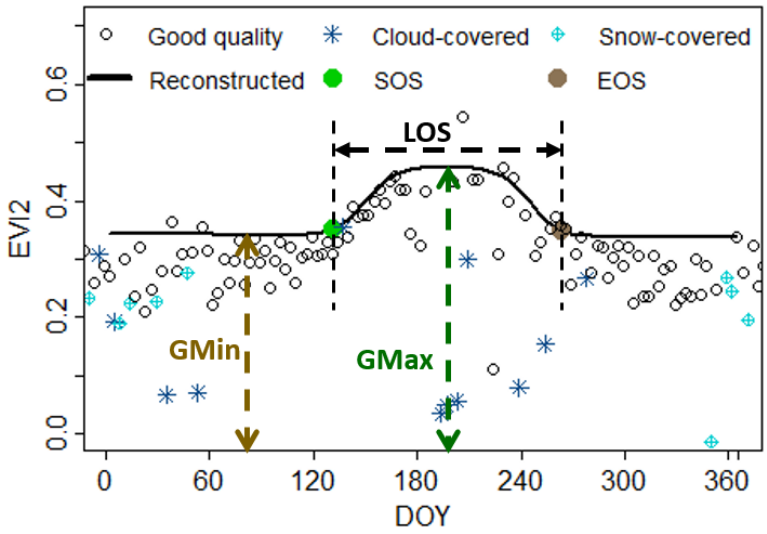

Figure 3-4. Illustration of retrieving LSP timing (SOS, EOS, and LOS) and greenness (GMax and GMin) metrics of an evergreen forest pixel (33°50'0'' N, 107°28'10.8'' W).

The resultant 250-m LSP metrics were reprojected to Albers equal-area conic projection and resampled using the nearest neighbor method to match 240-m burned areas and land cover types. LSP metrics were then spatially aggregated, respectively, for burned and reference forest pixels for each wildfire event using the median of the high confidence pixels. Similarly, the spatial aggregation was also performed with different burn severity levels. As a result, the aggregated LSP metrics in each wildfire event were stratified into six groups: the entire burned area, burn severity levels of unburned/low,

low, moderate, and high, and the reference area. Only the groups that contained more than 50 pixels with high confidence LSP detections were considered valid and used in the following analysis.

Note that LSP metrics were not retrieved in a burned area for the year of wildfire occurrence. It was because wildfires severely interrupted the regular temporal EVI2 development and increased uncertainties in phenology detections.

3.2.3. Investigation of wildfire impacts

3.2.3.1. Abrupt wildfire impacts on LSP magnitude

The wildfire impacts on the post-fire LSP magnitudes (or abrupt LSP change) were quantified by comparing the LSP in a burned area with that in the corresponding reference. This comparison could reduce the effects of landscape variation with different climate and other environmental factors across the western US forests. A reference was previously obtained from the burned area during pre-fires (Meng et al., 2015) or the surrounding unburned buffer during post-fires (Cuevas-gonzález et al., 2009; Fernandez-Manso et al., 2016; Sulla-Menashe et al., 2018; Wang and Zhang, 2017; Yang et al., 2017). The potential bias of LSP reference could be caused from the interannual variation in climate for the first method and from the inherent difference (of climate and topography) between the burned and unburned areas for the second method.

In this study, we quantified the wildfire impacts on LSP magnitudes using both references obtained from the post-fire unburned buffer and the pre-fire burned area. Specifically, for each burned area (wildfire event occurred during 2002-2014), the spatial anomaly was first calculated as the LSP difference between a burned area and its reference area (Equation 2), which was calculated for the entire study period. The spatial

anomaly before the fire occurrence was averaged (Equation 3) to quantify the inherent difference (of climate and topography) between the burned and unburned areas, which should be zero for a homogeneous area. The wildfire-caused spatial anomaly was then calculated by removing the inherent difference (Equation 4). Finally, the abrupt LSP change impacted by a wildfire was calculated by averaging the spatial anomaly during the first three post-fire years (Equation 5), which was to minimize the uncertainties from LSP detections and other factors.

$$LSP_{anom}(y) = LSP_{burn}(y) - LSP_{ref}(y) \quad (2)$$

$$LSP_{anom,pre} = \frac{\sum_{y<yf} LSP_{anom}(y)}{n_{pre}} \quad (3)$$

$$LSP_{fire}(y) = LSP_{anom}(y) - LSP_{anom,pre} \quad (4)$$

$$\overline{LSP_{fire}} = \frac{\sum_{yf+1}^{yf+3} LSP_{fire}(y)}{3} \quad (5)$$

In Equations 2-5, LSP represents an individual phenological metric of SOS, EOS, LOS, GMax, or GMin; $LSP_{anom}(y)$ is the spatial anomaly in year *y* for a fire event; $LSP_{burn}(y)$ is the area-aggregated (median value) LSP metrics in either the entire burned area or the area burned at a specific level of burn severity (see Section 2.2); $LSP_{ref}(y)$ is the area-aggregated LSP metrics within its reference area in year y; yf is the wildfire occurrence year; $y < yf$ is the pre-fire years; n_{pre} is the number of years in the pre-fire period; $LSP_{fire}(y)$ is the adjusted spatial anomaly in year *y*; and $\overline{LSP_{fire}}$ is the mean of $LSP_{fire}(y)$ during the three years after wildfire occurrence, representing the abrupt LSP change caused by a wildfire.

LSP data during at least three pre-fire and three post-fire years were required to ensure the reliability of calculating the abrupt wildfire impacts. Thus, the abrupt LSP change was only quantified for the wildfires (and different severity levels) occurred from 2004-2012, in which 511 wildfire events with valid LSP detections were selected from a total of 533 wildfire events.

3.2.3.2. Wildfire impacts on interannual LSP trends.

The wildfire impacts on interannual trends of four LSP metrics (SOS, EOS, GMax, and GMin) were explored in two different ways. First, we compared the LSP trends between the burned and reference areas during the period of 2001-2015 for each wildfire event occurred during 2002-2014. This analysis was to quantify the extent of wildfires (land disturbances) impacts on LSP trends in a time series and to explore the difference of LSP trends with and without wildfire interruptions. The LSP trend in a reference area mainly represents the actual response of vegetation communities to climate change, which could be taken as a climate indicator. However, LSP trends in the burned areas represent the response of vegetation communities to the interaction of climate changes and wildfire impacts (abrupt changes and post-fire recovery). The LSP trends were calculated using data during the period of 2001-2015 because the trends could be affected by wildfires no matter which year the fire occurred. The wildfire events occurred in 2001 and 2015 were not included because the LSP was not detected for the year of wildfire occurrence (see Section 2.2). In that case, the LSP trends for 2001 and 2015 wildfires only represent post-fire and pre-fire phenology variation, respectively.

Specifically, the LSP trend was calculated using a non-parametric Sen's slope and Mann-Kendall (MK) trend test, as LSP time series was not strictly met all the statistical

premises of linear regression such as the linearity and independence of observations (de Beurs and Henebry, 2004). Further, the interannual trend was only determined for the wildfire events where valid LSP detections were more than 10 years during 2001-2015. As a result, 786 out of 838 wildfire events occurred during 2002-2014 were selected to investigate the wildfire impacts on LSP trends. As a result, two sets (786 burned and 786 reference areas) of LSP trends were compared using boxplots and the Student's *t*-test. Moreover, because the year of wildfire occurrence in a given time series could have impacts on the interannual LSP trends, we analyzed the LSP trends by grouping wildfires based on the wildfire occurrence year. To increase wildfire samples with significant LSP trends for statistical analyses, wildfires occurred during 2002-2014 were stratified into five groups, *i.e.*, 2002-2003, 2004-2006, 2007-2009, 2010-2012, and 2013-2014. Note that different numbers of years were assigned in these groups because the 13 wildfire years from 2002-2014 cannot be evenly divided into multiple groups. In each group, the LSP trends from 2001-2015 were compared between the burned and reference areas.

Second, we compared the post-fire LSP trends in the burned and reference areas for the wildfire events occurred at the beginning (2002-2005) of the study period. This comparison was used to quantify the impacts of post-fire recovery process on LSP trends. The pre-fire LSP trends were not investigated because they could be well represented by the trends in unburned reference areas. The LSP trends during the post-fire periods were also determined using the Sen's slope and MK trend test for the wildfire events with valid LSP detections for more than 10 years. As a result, 235 wildfire events occurred during 2002-2005 were selected to compare LSP trends.

3.3. Results

3.3.1. Abrupt changes of LSP magnitudes

Figure 3-5 presents the abrupt changes of LSP magnitudes in SOS, EOS, LOS, GMax, and GMin for 511 wildfires occurred during 2004-2012 in the western US forests. SOS, EOS, and LOS were all altered by wildfires although the shift direction could be either earlier (shorter LOS) or later (longer LOS). The wildfire-caused SOS advance was mainly located in north California, southwest Montana, Wyoming, west Colorado, and New Mexico, where EOS delay and LOS lengthening mainly presented. In Idaho and south California, many wildfires caused a later SOS and EOS (Figures 3-5a, b). Specifically, 73% of burned areas showed an absolute shift of > 2 days in SOS (Figure 3-6) with 40% advances and 33% delays. Among these, there were 58%, 11%, and 3% of burned areas caused an absolute SOS shift of 2-10 days, 10-20 days, and >20 days, respectively. In contrast, 80% of burned areas showed absolute shifts of > 2 days in EOS (Figure 3-6) with 33% advances and 47% delays. There were 52%, 18%, and 10% of wildfires caused an absolute EOS shift of 2-10 days, 10-20 days, and >20 days, respectively. As a result, 85% of burned areas showed an absolute change of >2 days in LOS with 36% shortening and 49% lengthening. Among them, absolute LOS change of 2-10 days, 10-20 days, and >20 days appeared in 47%, 23%, and 14% of wildfires, respectively.

As expected, the vast majority of wildfires caused reductions in GMax (97% wildfires) and GMin (99% wildfires). On average, wildfires caused significant reductions ($p \ll 0.001$ based on a paired Student's *t*-test) in GMax (-0.063±0.040 EVI2) and GMin

(-0.074±0.038 EVI2). The reduction was the largest in northern California, followed by that in the northwest and southeast regions (Figures 3-5d, e).

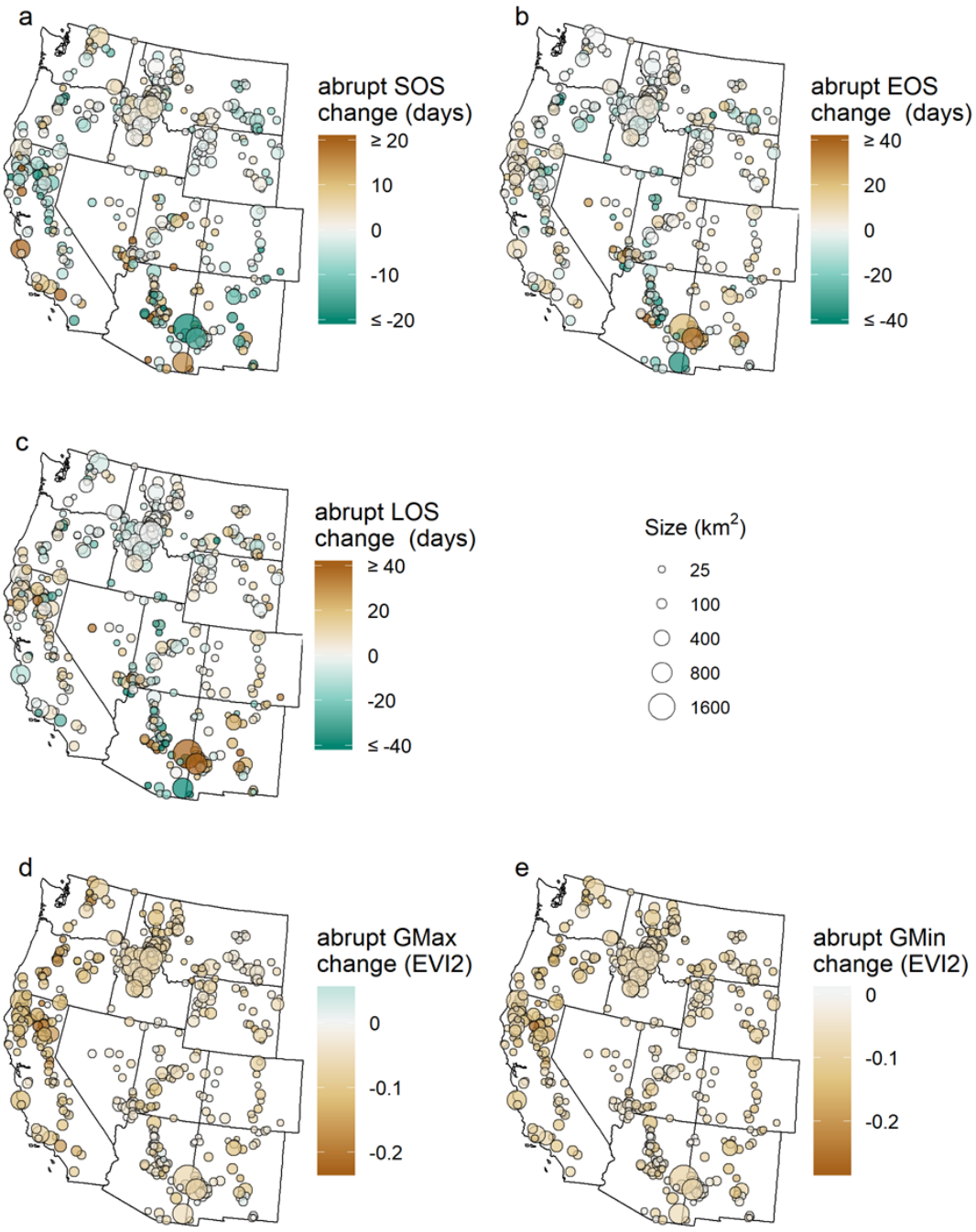

Figure 3-5. Spatial distributions of abrupt changes of LSP magnitude caused by wildfires based on the data in the first three post-fire years. (a) SOS, (b) EOS, (c) LOS, (d) GMax, and (e) GMin.

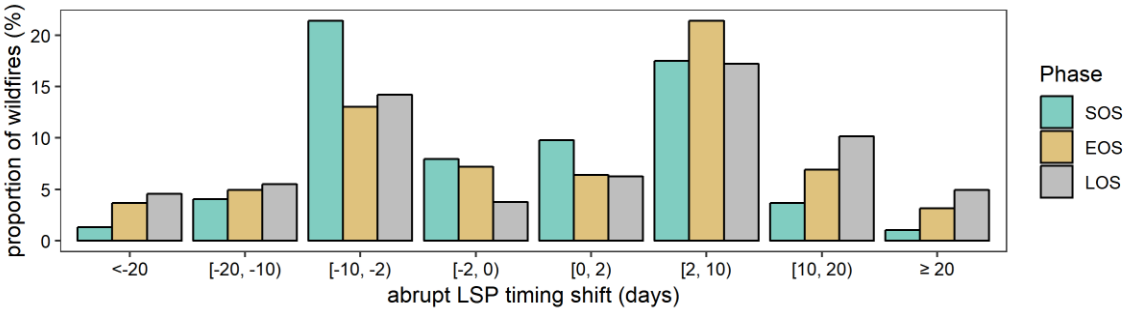

Figure 3-6. Histogram of abrupt LSP timing shifts.

3.3.2. Abrupt LSP change with burn severity

Figure 3-7 shows the abrupt LSP change varying with the level of burn severity. As wildfire-caused shifts of SOS, EOS, and LOS were divergent in the advancing/shortening and delaying/lengthening directions (Figure 3-5), analyzing all the wildfire events together would make the two directions cancel each other. Thus, wildfire events with LSP timing shifts in the two opposite directions were separately analyzed. For wildfires causing SOS advances, the absolute value of SOS shift increased with burn severity, reached the maximum (~6 days) in the moderate burn severity, and then decreased in the high burn severity (Figure 3-7a). For wildfires causing SOS delays, SOS shift kept increasing with the burn severity, which was about 7 days at high burn severity (Figure 3-7b). On the other hand, for wildfires with EOS either advances or delays, the absolute value of EOS shift reached the maximum (~8 days) in moderate and became smaller either towards high or unburned/low severity (Figures 3-7c, d). A similar pattern was found for LOS change. The absolute LOS change increased with the burn severity and reached 10 days at high burn severity for the shortening LOS events (Figure 3-7e) and it reached the maximum (~10 days) in the moderate burn severity for the lengthening LOS events (Figure 3-7f).

The influence of burn severity on LSP greenness was straightforward. As the vast majority of wildfires caused reductions in GMax and GMin, the abrupt greenness change averaged from all the fires was presented (Figures 3-7g, h). The extent of abrupt greenness decreases in both GMax and GMin increased with burn severity.

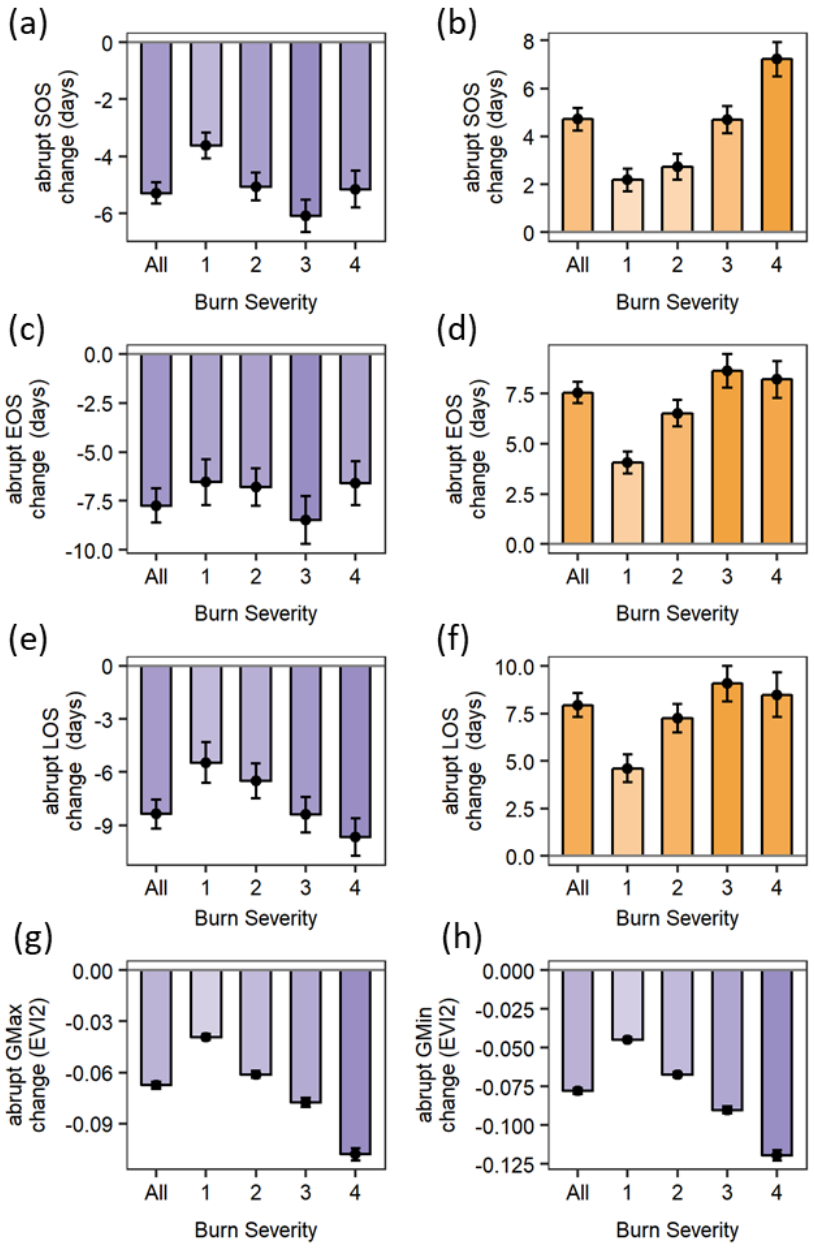

Figure 3-7. Wildfire impacts on LSP magnitude during the first three post-fire years against burn severity. SOS shifts averaged from wildfires causing SOS (a) advances and (b) delays; EOS shifts averaged from wildfires causing EOS (c) advances and (d) delays; LOS changes averaged from wildfires causing LOS (c) shortening and (d) lengthening; (g) abrupt GMax change from all wildfires; and (h) abrupt GMin change from all wildfires. X-axis represents the level of burn severity, where all, 1, 2, 3, and 4 represent the entire burned area and areas burned in unburned/low, low, moderate, and high severity, respectively. Error bar represents the standard error of mean.

3.3.3. Wildfire impacts on interannual LSP trends in 2001-2015

Table 3-1 presents the LSP trends from 2001-2015 in the burned and reference areas for all the 786 wildfires burned in 2002-2014 to reveal the wildfire impacts on LSP and Figure 3-8 compares the trends in the burned and reference areas using boxplots. The two-sided Student's *t*-test revealed that the trends of four LSP metrics (SOS, EOS, GMax, and GMin) in the burned areas were significantly different from those in the reference areas. Specifically, the significant trends in the burned areas were lower than those in the reference areas for all but GMax (Table 3-1 and Figure 3-8). Moreover, it shows that trends in the burned areas presented a wider range than those in the reference areas for all the LSP metrics (Table 3-1 and Figure 3-8).

Table 3-1. Summary of significant ($p<0.05$) trends of SOS, EOS, GMax, and GMin in the burned (B) and reference (R) areas for 786 wildfires. The unit of trend is days/year for SOS and EOS and EVI2/year for GMax and GMin. Wildfires_sig indicates the wildfires with significant LSP trends, among which wildfires+ and wildfires- indicate the wildfire events with significantly positive and negative trends, respectively. Numbers in parentheses are the proportion (%) of wildfire events, which are the proportion of wildfire_sig to all the 786 wildfires and the proportions of wildfire+ and wildfires- to relative to wildfires with wildfire_sig.

	SOS		**EOS**		**GMax**		**GMin**	
	B	R	B	R	B	R	B	R
	Frequency and proportion (%) of wildfire events							
Wildfires_sig	20 (2.54)	15 (1.91)	115 (14.63)	98 (12.47)	161 (20.48)	229 (29.13)	198 (25.19)	336 (42.75)
Wildfires+	(35.00)	(66.67)	(5.22)	(1.02)	(75.16)	(89.08)	(36.36)	(65.77)
Wildfires-	(65.00)	(33.33)	(94.78)	(98.98)	(24.84)	(10.92)	(63.64)	(34.23)
	Mean trends (days/year for SOS and EOS and EVI2/year for GMax and GMin)							
Wildfires_sig	-0.96	0.63	-1.97	-1.54	0.0042	0.0024	-0.0011	0.0008
Wildfires+	1.73	1.80	1.57	1.62	0.0071	0.0030	0.0061	0.0023
Wildfires-	-2.41	-1.70	-2.16	-1.57	-0.0048	-0.0025	-0.0053	-0.0021
	Trend at percentiles for wildfires_sig							
5^{th} percentile	-3.6	-1.9	-6.7	-4.1	-0.0059	-0.0021	-0.0081	-0.0030
95^{th} percentile	2.3	2.5	-0.1	-0.7	0.0137	0.0060	0.0110	0.0037
5^{th}-95^{th} range	5.9	4.4	6.6	3.4	0.0196	0.0081	0.0191	0.0067
	Difference of trends							
	-1.59*		-0.43*		0.0018**		-0.0019***	

*The difference of trends between the burned and reference areas was tested by a two-sided Student's t-test. ***: $p<0.001$; **: $p<0.01$; and *$p<0.05$.*

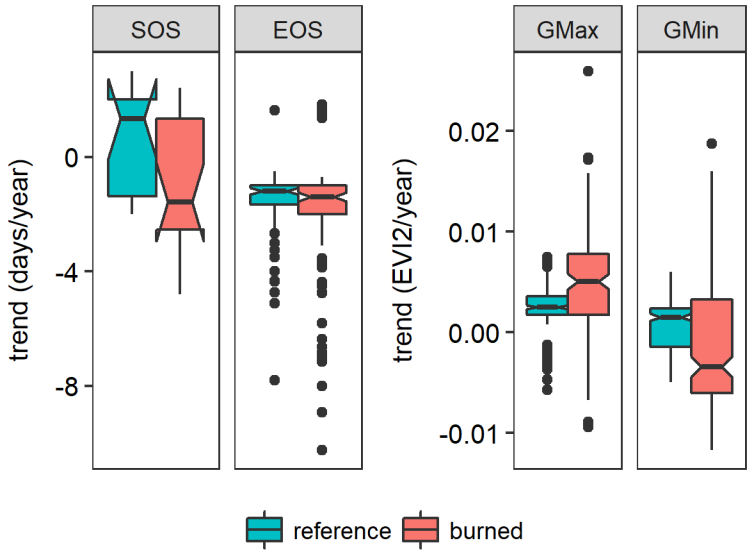

Figure 3-8. Boxplot for significant ($p<0.05$) trends of SOS, EOS, GMax, and GMin in the burned and reference areas.

For SOS, significant ($p<0.05$) trends were only found in 2.54% of the 786 burned areas and 1.91% of the 786 reference areas with the corresponding average trend of -0.96 days/year and 0.63 days/year, respectively (Table 3-1). Among the areas with significant SOS trends, advancing trends occurred in 65.00% burned areas but only in 33.33% reference areas; delaying trends showed the opposite proportions (Table 3-1). The burned areas with advancing SOS trends were mainly distributed in the west region of the western US (Figure 3-9a), while the reference areas with delaying SOS trends were mainly located in the east region (Figure 3-9b).

Relative to SOS, more fire events showed significant EOS trends that were 14.63% in the burned areas and 12.47% in the reference areas (Table 3-1 and Figures 3-

9c, d). Among the burned and reference areas with significant trends, the vast majority showed advancing trends (94.78% and 98.98% for burned and reference areas, respectively). However, the averaged trends in the burned areas were significantly reduced by 0.43 days/year ($p<0.05$) than those in the reference areas.

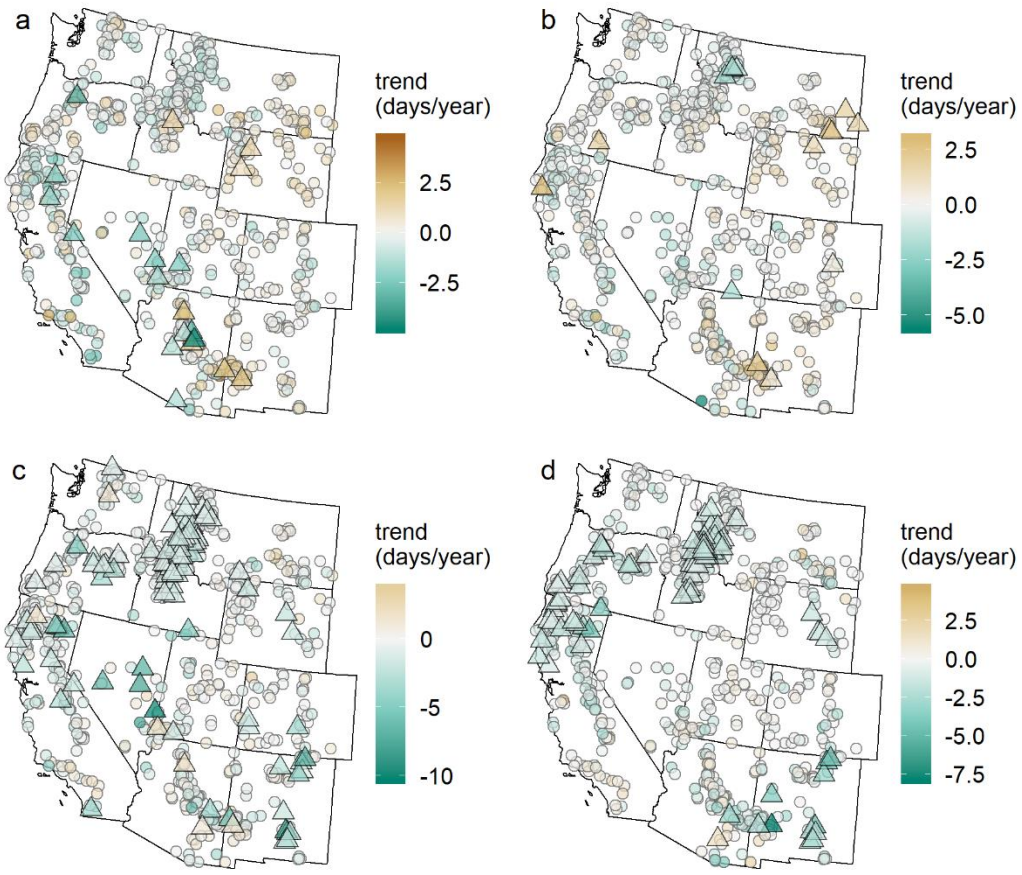

Figure 3-9. Spatial distribution of SOS and EOS trends from 2001-2015 in the burned and reference areas. (a) SOS trends in burned areas, (b) SOS trends in reference areas, (c) EOS trends in burned areas, and (d) EOS trends in reference areas. Triangles are trends with a $p<0.05$.

Over the reference areas with significant ($p<0.05$) trends (29.13% areas for GMax and 42.76% areas for GMin), GMax and GMin showed greening trends at a rate of

0.0024 and 0.0008 EVI2/year, respectively (Table 3-1). Specifically, 89.08% of significant GMax trends were greening trends while 10.92% browning; and 65.77% of significant GMin trends were greening trends while 34.23% browning. In burned areas, however, GMax trends increased by 0.0018 EVI2/year ($p<0.01$) compared to those in reference areas, while GMin trends decreased by 0.0019 EVI2/year ($p<0.001$). The burned areas with significant trends were reduced to 20.48% and 25.19% for GMax and GMin, respectively. Moreover, the burned areas with significant greening trends were reduced to 75.16% and 36.36% for GMax and GMin, respectively.

Figure 3-10 presents the spatial distribution of LSP greenness trends in burned and reference areas. The comparison between the burned and reference areas shows that the greening trends of GMax and GMin were interrupted by wildfires, which resulted in browning trends (both GMax and GMin) occurring in a large amount of the burned areas, such as Northwestern Great Plains (western Montana and Wyoming), Klamath Mountains and Sierra Nevada in northern California, and Idaho Batholith. Although more reference areas showed browning trends in GMin than GMax, the pattern was greatly enhanced in the burned areas, particularly Middle Rockies (the junction of Montana, Wyoming, and Idaho), Idaho Batholith, Wasatch and Uinta Mountains (Utah), and New Mexico Mountains.

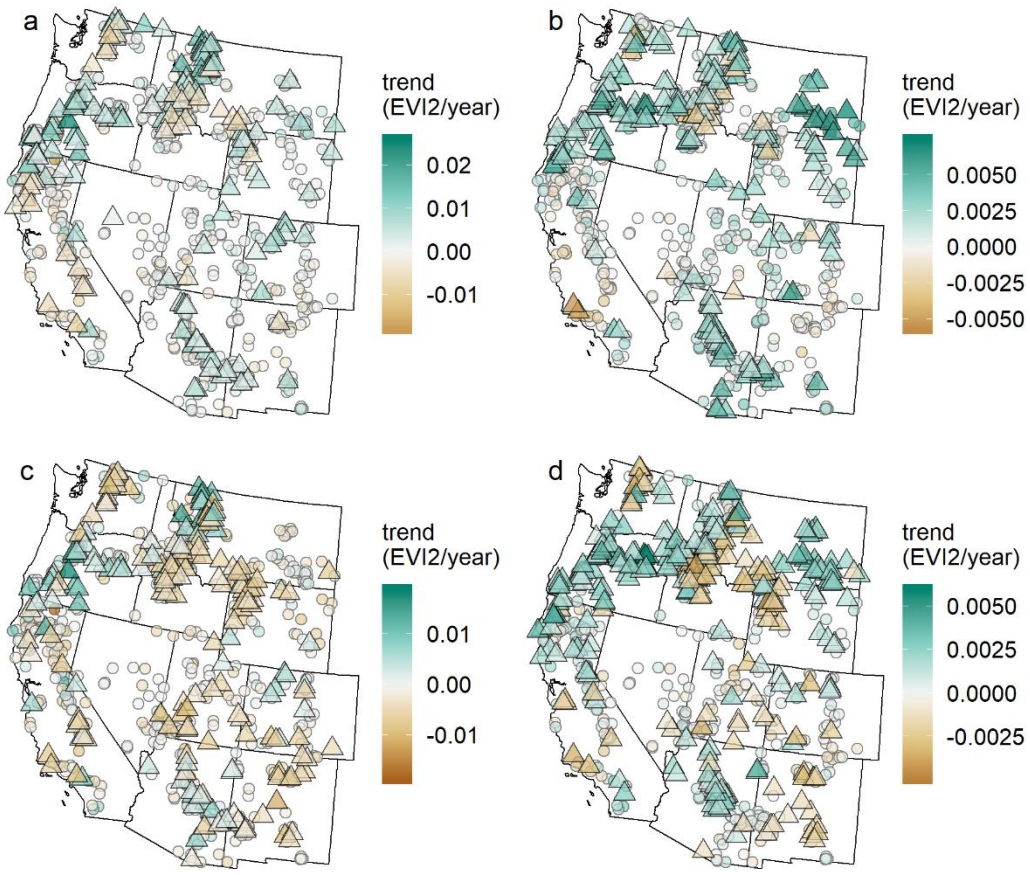

Figure 3-10. Spatial distributions of GMax and GMin trends from 2001-2015 in the burned and reference areas. (a) GMax in burned areas, (b) GMax in reference areas, (c) GMin in burned areas, and (d) GMin in reference areas. Triangles are trends with a $p<0.05$.

Figure 3-11 shows that the magnitude and direction of wildfire impacts on phenological trends were a function of wildfire occurrence year. Note that SOS was excluded from this analysis as the limited number of burned areas with significant SOS trends (Table 3-1). As expected, unlike in the reference areas, the LSP (EOS, GMax, and GMin) trends in the burned areas were strongly influenced by the wildfire occurrence year. Specifically, EOS trends in burned areas reduced (absolute value) with the wildfire

occurrence year (Figure 3-11a). In other words, the rate of advancing EOS during the study period became smaller if the fire occurrence year became later. Compared to the reference areas, the burned areas had significantly larger advancing EOS trends due to wildfires occurred during 2002-2003 and smaller EOS trends due to wildfires during 2013-2014.

GMax and GMin trends in the burned areas varied with the wildfire occurrence year in a convex shape (Figure 3-11b, c) while the trends in the reference areas were relatively stable with a slight greenness increase. Specifically, both GMax and GMin showed the largest trend of greenness increase for the burned areas where wildfires occurred during the early years. The greening trends reduced and converted to browning trends when wildfire occurrence became later. In contrast, the largest browning trends (negative GMax and GMin) appeared around 2009. For the burned areas with fire occurrence in late years, the GMax and GMin returned from negative (browning) to positive (greening) trends.

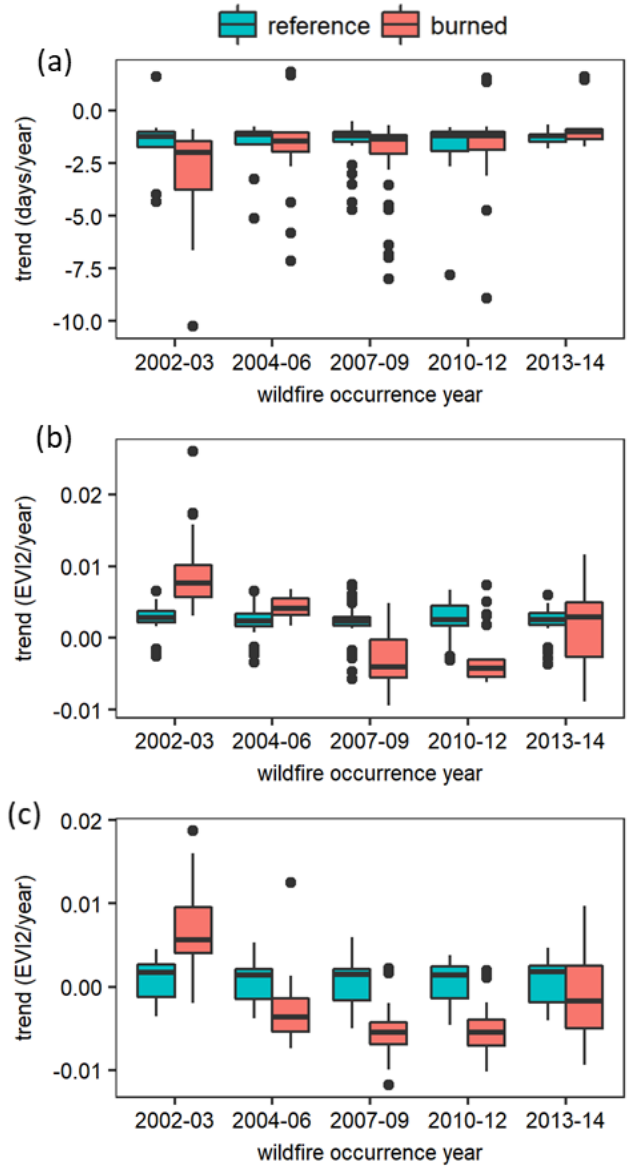

Figure 3-11. Interannual trends against wildfire occurrence year. (a) EOS, (b) GMax, and (c) GMin.

3.3.4. Wildfire impacts on post-fire LSP trends

Figure 3-12 shows the comparisons between the post-fire LSP trends in the burned and reference areas for the wildfire events occurred in 2002-2005. Again, SOS was excluded from this analysis as only seven burned areas and five reference areas with

significant SOS trends. The significant (p<0.05) post-fire EOS trends in the burned areas were slightly lower than those in the reference areas, although the difference is not statistically significant (p>0.1). EOS was delayed by 7.3 days on average based on those burned areas with significant post-fire EOS trends. In contrast, the significant post-fire trends of GMax and GMin were larger (p<0.05) than those in the reference areas.

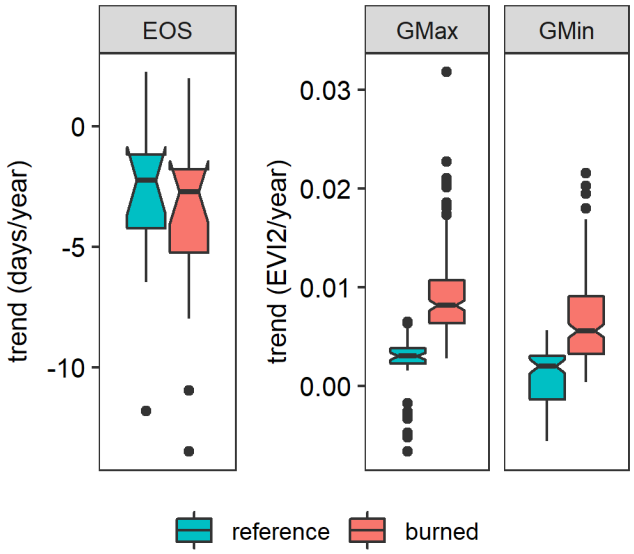

Figure 3-12. Boxplot for significant (p<0.05) trends of EOS, GMax, and GMin during the post-fire years in the burned and reference areas for the wildfire events occurred in 2002-2005.

3.4. . Discussion

This study for the first time explored the wildfire impacts on the magnitudes and trends of both LSP greenness and timing metrics at a regional scale. There are several new approaches and important findings. First, a new approach was developed to quantify wildfire impacts on LSP. Previous studies used a reference based on either the pre-fire burned area or the post-fire unburned buffer to quantify the wildfire impacts on

LSP magnitudes (Cuevas-gonzález et al., 2009; Fernandez-Manso et al., 2016; Meng et al., 2015; Sulla-Menashe et al., 2018; Wang and Zhang, 2017; Yang et al., 2017), which would cause bias from either the interannual variation in climate or from the inherent spatial difference (of climate and topography). In contrast, this study quantified the reference by combining both the pre-fire burned area and the post-fire buffer area, which reduced the bias that existed in the single reference. This approach provides a prototype to investigate LSP responses to other land disturbances, such as direct human activities on the landscape (agricultural, forestry, grazing practices, and urbanization). Second, the combination of LSP timing and greenness could provide a comprehensive set of metrics to trace post-fire LSP development and recovery of understory and evergreen tree canopy, separately, which is impossible in previous studies that only use maximum satellite greenness (Chen et al., 2011; Cuevas-gonzález et al., 2009; Goetz et al., 2006; Veraverbeke et al., 2012; Yang et al., 2017). Third, the systematic analyses of 838 forest wildfires over the western US revealed that wildfire impacts on LSP and its trends are complex and profound. Fourth, moderate burn severity could have the strongest influence on LSP timing although LSP greenness reduced largest in high burn severity. Fifth, wildfires mostly advanced SOS, delayed EOS, and lengthened LOS although the patterns were diverse. Sixth, LSP trends in a given time period were significantly altered by wildfires and the magnitude and direction of wildfire impacts on LSP trends were a function of wildfire occurrence year.

3.4.1. Abrupt wildfire impacts on LSP magnitude

Two LSP greenness metrics of GMax and GMin during a growing season represent the green vegetation cover from all vegetation (a mixture of both herbaceous and evergreen woody plants) and evergreen vegetation, respectively. Not surprisingly, both LSP greenness metrics of GMax (-0.063±0.040 EVI2) and GMin (-0.074±0.038 EVI2) experienced an abrupt decrease with the consumption of biomass. A smaller abrupt decrease of GMax than GMin (Figure 3-7) was because the quick recolonization of forbs and herbs contributed more to GMax increase in the three years following fires. This indicates that GMin is a more effective indicator to reflect the wildfire impacts on evergreen forests.

The abrupt changes in LSP timing caused by wildfires are divergent in the western US forests, which aligns well with the findings of wildfire-caused LSP shifts in many local studies (Di-Mauro et al., 2014; Serbin et al., 2009; Wang and Zhang, 2017). The diverse responses of LSP timing are mainly associated with the wildfire-caused changes in vegetation species and soil conditions (Cooper et al., 2017), which all vary among individual wildfire events. Particularly, the early successional species (usually understory species) recolonize the burned area after wildfires, which have different phenological characteristics from the pre-fire trees. As a result, LSP timing shifts after wildfire occurrences. An early successional species with earlier SOS and later EOS than the pre-fire trees would cause an advanced SOS, delayed EOS, and lengthened LOS, and vice versa. As phenological characteristics in early successional species vary greatly among individual wildfires across different ecosystems and locations, the LSP timing

shows divergent directions with spatial variability. Overall, this study revealed that more wildfires caused an earlier SOS, later EOS, and longer LOS (Figure 3-6).

Further, burn severity, determining the degree of the post-fire soil degradation, has different effects on the diverse abrupt LSP changes in timing and greenness metrics. The amplitudes of LSP greenness (GMax and GMin) reduction increased monotonously with the level of burn severity (Figures 3-7g, h) because more vegetation biomass was consumed at a higher burn severity (Montorio Llovería et al., 2016). However, wildfire-caused LSP timing shifts (except for SOS delays in Figure 3-7b and LOS shortening in Figure 3-7e) showed a convex relationship with burn severity and the maximum absolute phenological shift occurred in the moderate burn severity. This is likely associated with the following facts. Higher levels of burn severity caused more forest loss with more understory species colonization as shown in the NLCD maps (the results of NLCD changes were not shown here), which was expected to cause larger LSP shifts. However, higher levels of burn severity would cause more soil damage (a loss of organic matter and an increase of water repellency) (Lewis et al., 2006), which impairs the plant growth and impedes the re-colonization of early-successional plants (Lentile et al., 2007). Thus, a trade-off between forest loss with understory species colonization and soil damage results in the occurrence of the maximum absolute LSP shift at the moderate burn severity. Such a convex relationship is supported by a similar pattern that the species-specific post-fire forest recovery rate varies with the burn severity (Meng et al., 2018).

Moreover, individual wildfires influence different timing metrics in varying extents. Generally, the impacts were higher in EOS than SOS as the absolute shift >10 days appeared in 15% of burned areas for SOS but in 28% of burned areas for EOS. This

suggests that vegetation species during post-fire years are diverse showing distinguishable EOS, which is supported by some other studies. For example, Hill et al. (2010) found that the largest phenological difference among various tree species appears on imagery acquired in autumn by analyzing time series Landsat data. Similarly, Pasquarella et al. (2018) found autumn offset is capable of distinguishing different hardwood communities. The large abrupt change in LOS (>10 days in 37% of burned areas) was the result of SOS and EOS shift. It suggests that SOS and EOS were usually changed in opposite directions for individual wildfires which amplified the LOS changes.

3.4.2. Wildfire impacts on interannual LSP trends.

Long-term LSP trends, which are commonly used to indicate climate change, are expected to be interrupted by both the wildfire-caused abrupt change and gradual post-fire recovery. This interruption was revealed by comparing the interannual LSP trends between the burned and reference areas, where the trends in the reference areas were considered as the actual response of western US forests to regional climate change.

In this study, the LSP trends were determined based on a non-parametric Sen's slope and MK trend test. Although the change detection methods, including Breaks For Additive Seasonal and Trend (Verbesselt et al., 2010), Detecting Breakpoints and Estimating Segments in Trend (Jamali et al., 2015), and LandTrendr (Kennedy et al., 2010), can also be used to detect disturbance-related vegetation dynamic trends, they were not used in this study due to three reasons. First, the three change detection methods detect where or if breakpoints occurred without knowledge of impact factors. However, we, in this study, focus on how wildfire impacts on LSP magnitude and LSP trends because we know well the time and area of fire occurrences based on MTBS data.

Second, these methods are not able to manifest the impacts of wildfires on the LSP trend in an entire time series, as they only detect piece-wise trends (Jamali et al., 2015; Kennedy et al., 2010; Verbesselt et al., 2010). Third, the methods use parametric linear regression to determine the trends. Compared with the Sen's slope and MK trend test used in this study, the parametric linear regression is less suitable to LSP time series which was not strictly met all the statistical premises of linear regression such as the linearity and independence of observations (de Beurs and Henebry, 2004).

The impacts of post-fire recovery on LSP trends were evidently revealed from the trends in the post-fire years based on the wildfires occurred in 2002-2005 (Figure 3-12). In post-fire periods, the LSP metrics in the burned areas changed towards the pre-fire status, which is opposite to the direction of wildfire-caused abrupt changes. Specifically, as wildfires abruptly decreased the LSP greenness (GMax and GMin), the post-fire trends of LSP greenness were much larger in the burned areas than the reference areas. On the contrary, while EOS was overall delayed abruptly by the wildfires, the post-fire EOS trends in the long-term were advanced. This trend pattern is associated with the recovery process that the pre-fire tree species, which was substituted by understory species causing abrupt changes, would re-dominate gradually during post-fire under preferable climate conditions (Davis et al., 2019).

The LSP trends in the entire study period (2001-2015) with wildfires occurred in 2002-2014 revealed the impacts of integral wildfire impacts from both wildfire-caused abrupt change and post-fire recovery. The comparison of LSP trends in the entire study period between the burned and reference areas demonstrates that simply taking LSP trends as climate indicators could cause large uncertainties. This suggests that it should

be cautious to use the results from most current studies that associated the LSP trends to climate changes without excluding the land disturbance impacts (such as fires) (Julien and Sobrino, 2009; Li et al., 2019; Piao et al., 2014; Zeng et al., 2011; Zhang et al., 2007),.

The LSP trends were also greatly impacted by the wildfire occurrence year in a time series (Figure 3-11). For wildfires occurred at the beginning (2002-2003) of the time period (2001-2015), the trends were larger in the burned areas than the reference areas for GMax and GMin and smaller for EOS. It is because the LSP in post-fire years contributed largely to the LSP trends. With the wildfire occurrence becoming later, the contribution of LSP in post-fire years to LSP trends decreased while the abrupt LSP change plays a significant role. Usually, an abrupt change in the middle or late years in the time series is more likely to cause a trend towards the direction of the abrupt change (opposite to the direction of post-fire recovery), which is a browning trend for GMax and GMin and a delaying trend for EOS. For the wildfire occurred at the very end of the given period (2013-2014), the fire impact on LSP trend was relatively milder because the majority of the years (2001-2012) for trend calculation were pre-fire. The pattern of trends of GMax and GMin in the burned areas is similar to the greenness trends in Canadian boreal forests where the wildfire occurrence year caused variation in greening and browning trends (Sulla-Menashe et al., 2018).

Integrating all the wildfires occurred during the study period (2002-2014), LSP trends in the burned areas showed significant differences from those in reference areas according to the two-sided Student's *t*-test. Compared to reference areas, wildfires converted the direction of trends for SOS (from a delaying 0.63 to an advancing -0.96

days/year) and GMin (from a greening 0.0008 to browning -0.0011 EVI2/year); and wildfires enhanced the trends for EOS (from an advancing -1.54 to -1.97 days/year) and GMax (from a greening 0.0024 to 0.0042 EVI2/year). It should be noted that the trend values were averaged from all significant trends with wildfires occurred in different years in order to illustrate the wildfire impacts. The different wildfire impacts on the trends of GMax and GMin are likely due to two reasons. First, the recovery rate is larger for GMax than GMin because of the quick recolonization of forbs and herbs in the post-fire years. Second, compared with GMin, GMax showed more significant trends in burned areas with wildfires occurred at the beginning (2002-2003) and less in the middle (2007-2009) of the study period. Because greenness trends were larger in the burned areas than in the reference areas for wildfires occurred at the beginning and smaller for wildfires occurred in the middle, the averaged trends were increased for GMax while decreased for GMin.

The wildfire impacts on LSP trends in 2001-2015 are also reflected in the other two aspects. First, the proportion of burned areas with significant trends of both LSP greenness and timing differed from those in reference areas. It is because the wildfire-caused abrupt LSP change and the following recovery can either break, enhance, and impair an existing climate-driven trend, or form a new trend in a time series that originally showed no trend as reflected in the corresponding reference area. Second, trends of SOS, EOS, GMax, and GMin presented a wider range in the burned areas than those in the reference areas (Table 3-1 and Figure 3-8). This is likely due to the fact that wildfires caused large abrupt changes in an LSP time series and resulted in steeper trends (*i.e.* regression slopes).

3.4.3. Implications and limitations

The systematic analysis of 838 wildfires occurred in 2002-2014 in the western US forests implies that wildfires might have significant influences on regional phenological trends. The wildfire-caused changes in trends of both the entire time series from 2001-2015 and post-fire time series indicate that the wildfires occurred either during or before a given study period can influence the interannual trends. As a result, historical fires could have considerable impacts on LSP trends at a regional scale. Although the area influenced by wildfire in a single year is on average only 0.7% of total lands based on the MTBS data from 1984-2014, the total burned area during this period accounts for 12.3% forest area. Moreover, the wildfire impacts on LSP are likely widespread in the near future because the wildfire frequency and size in the western US is expected to increase in the future decades. Indeed, explicit understanding of wildfire impacts on LSP is critical for the investigation of actual LSP trends associating with climate change (Jeganathan et al., 2014; Zhang et al., 2019).

More importantly, similar to wildfires, other land disturbance should be considered when using satellite-derived phenological trends to interpret global climate change. The impact of land disturbance on phenological trend could be more profound because land cover and land use change could be caused by natural processes (such as climate extremes and disturbances), direct human activities on the landscape (such as agricultural, forestry, grazing management practices, and urbanization), and indirect human activities affecting the landscape (such as modifications to hydrological routing and flow and soil quality). The impacts could be very significant because direct human activities have modified one-third to one-half of the planetary land surface and

transformed at least another one-third of the terrestrial biosphere into rangelands and seminatural anthromes (Ellis, 2011; Vitousek et al., 1997). This impact has also demonstrated in agricultural area (Zhang et al., 2019), where crop type change contributes two-thirds of long-term phenological trends in central USA.

We acknowledge there are still a few limitations in this study. First, more investigation is needed to obtain a clear understanding of the factors determining the wildfire-caused abrupt changes in LSP, particularly timing metrics. Although this study investigated the effect of burn severity on abrupt LSP changes, other factors such as fire type can also have an influence. Specifically, in the western US forests, crown fires cause more tree mortalities and expose more understory vegetation while surface fires mainly burn surface litter, duff, and understory vegetation. As a result, different fire types cause different changes in vegetation species, soil conditions, and surface temperature, which in turn influence the abrupt LSP changes. Second, the wildfire impacts on LSP could vary with different forest types. This study only discussed the wildfire impacts in evergreen forests because the limited number of wildfires, burning deciduous and mixed forests in the western US in 2004-2012, impeded a statistically meaningful analysis. Indeed, it is needed in future to investigate the impacts of different forest wildfires on LSP. Third, the LSP trends in the burned areas are a result of other factors that include climate, topography, and burn severity. Although the direct influence of climate and topography on LSP variation is largely removed using references, their interactions with wildfire impacts could still influence LSP variation. Specifically, vegetation growth and phenology are influenced by post-fire climatic factors such as maximum surface

temperature and soil moisture (Davis et al., 2019) and burn severity that are dependent on topography (Alexander et al., 2006).

Finally, validation of satellite-derived trends is critical but it is currently infeasible although a large number of articles have investigated satellite-derived phenological trends. To appropriately validate a phenological trend, the satellite pixel should spatially and temporally match well with field observations during a long time period. This kind of field observations is currently unavailable. Even though it should be cautious to interpret satellite-derived trends, the basic results from this study are reliable. It is due to the fact that the HPLM-LPSD has been extensively evaluated using observations from long-term ecological research, plots of the forest stands, network flux tower, PhenoCam, national phenology network, time series of Landsat data, and landscape phenology indices (Ganguly et al., 2010; Liang et al., 2011; Moon et al., 2019; Peng et al., 2017; Soudani et al., 2008; Zhang et al., 2006; Zhang, 2015; Zhang et al., 2018), that the interannual variation of post-fire LSP detected using HPLM-LPSD agreed well with field observations (Wang and Zhang, 2017), and that the divergent wildfire impacts on LSP timing metrics from this study are aligned with many local studies (Di-Mauro et al., 2014; Serbin et al., 2009; Wang and Zhang, 2017). However, to sufficiently evaluate the accuracy of phenological trends, direct validations are still needed in future although it is very challenging for a large area such as the western US.

3.5. Conclusions

This study for the first time investigated the wildfire impacts on both magnitudes and trends of LSP greenness and timing metrics based on 838 forest fires occurred from 2002-2014 over the western US. Wildfire impacts on the magnitude of LSP metrics were

quantified using the average during the first three post-fire years, which reduced the data uncertainty for a single year. Analyses of abrupt LSP change indicated that LSP greenness metrics were decreased significantly (-0.063 EVI2 for GMax and -0.074 EVI2 for GMin) and the decreasing extents increased with burn severity, where GMin and GMax represented the change for evergreen forests and overall vegetation greenness, respectively. Further, LSP timing metrics showed diverse responses to wildfire impacts because land surface properties and burn severity after wildfires varied greatly among individual burned areas. As a result, the absolute abrupt change was larger than 2 days in 73% of burned areas for SOS, 80% for EOS, and 85% for LOS, which was larger than 10 days in 15%, 28%, and 37% of burned areas for SOS, EOS, and LOS, respectively. Moreover, abrupt changes in LSP timing present a convex relationship with burn severity and the maximum shift of LSP timing appeared in the moderate burn severity. Finally, long-term trends of LSP metrics differed significantly between burned areas and unburned reference areas, particularly for SOS and GMin of which the trend directions were converted. Specifically, the unburned reference areas showed a delaying SOS trend (0.63 days/year) and greening GMin trend (0.0008 EVI2/year), while the burned areas showed an advancing SOS trend (-0.96 days/year) and a browning GMin trend (-0.0011 EVI2/year). The trends from the burned areas were strongly dependent on the year of wildfire occurrence in a long time series. This suggests that wildfire impacts should be explicitly considered for taking LSP trends as an indicator of climate change and this study provides a prototype for investigating the impacts of land disturbances caused by natural process and human activities on LSP trends across various regional scales.

Acknowledgments

This work was supported by NASA contract 80NSSC18K0626. Authors also thank the data providers: MTBS data was obtained from www.mtbs.gov; NLCD data was obtained from www.mrlc.gov; and MODIS products (MOD09GQ, MOD09GA, and MOD11A1) were obtained from https://lpdaac.usgs.gov/dataset_discovery/modis/modis_products_table.

References

Alcaraz-Segura, D., Chuvieco, E., Epstein, H.E., Kasischke, E.S., Trishchenko, A., 2010. Debating the greening vs. browning of the North American boreal forest: Differences between satellite datasets. Glob. Chang. Biol. 16, 760–770. doi:10.1111/j.1365-2486.2009.01956.x

Alexander, J.D., Seavy, N.E., Ralph, C.J., Hogoboom, B., 2006. Vegetation and topographical correlates of fire severity from two fires in the Klamath-Siskiyou region of Oregon and California. Int. J. Wildl. Fire 15, 237–245.

Beck, P.S.A., Atzberger, C., Høgda, K.A., Johansen, B., Skidmore, A.K., 2006. Improved monitoring of vegetation dynamics at very high latitudes: A new method using MODIS NDVI. Remote Sens. Environ. 100, 321–334.

Buyantuyev, A., Wu, J., 2012. Urbanization diversifies land surface phenology in arid environments: interactions among vegetation, climatic variation, and land use pattern in the Phoenix metropolitan region, USA. Landsc. Urban Plan. 105, 149–159.

Chen, J., Jönsson, P., Tamura, M., Gu, Z., Matsushita, B., Eklundh, L., 2004. A simple

method for reconstructing a high-quality NDVI time-series data set based on the Savitzky-Golay filter. Remote Sens. Environ. 91, 332–344. doi:10.1016/j.rse.2004.03.014

Chen, X., Vogelmann, J.E., Rollins, M., Ohlen, D., Key, C.H., Yang, L., Huang, C., Shi, H., 2011. Detecting post-fire burn severity and vegetation recovery using multitemporal remote sensing spectral indices and field-collected composite burn index data in a ponderosa pine forest. Int. J. Remote Sens. 32, 7905–7927.

Cleland, E.E., Allen, J.M., Crimmins, T.M., Dunne, J.A., Pau, S., Travers, S.E., Zavaleta, E.S., Wolkovich, E.M., 2012. Phenological tracking enables positive species responses to climate change. Ecology 93, 1765–1771. doi:10.1890/11-1912.1

Cleland, E.E., Chuine, I., Menzel, A., Mooney, H.A., Schwartz, M.D., 2007. Shifting plant phenology in response to global change. Trends Ecol. Evol. 22, 357–365. doi:https://doi.org/10.1016/j.tree.2007.04.003

Cooper, L.A., Ballantyne, A.P., Holden, Z.A., Landguth, E.L., 2017. Disturbance impacts on land surface temperature and gross primary productivity in the western United States. J. Geophys. Res. Biogeosciences 122, 930–946. doi:10.1002/2016JG003622

Crawley, M.J., 1996. Life history and environment, in: Crawley, M.J. (Ed.), Plant Ecology. Wiley Online Library, pp. 73–131. doi:doi.org/10.1002/9781444313642.ch4

Cuevas-gonzález, M., Gerard, F., Balzter, H., Riano, D., Riaño, D., 2009. Analysing forest recovery after wildfire disturbance in boreal Siberia using remotely sensed vegetation indices. Glob. Chang. Biol. 15, 561–577. doi:10.1111/j.1365-2486.2008.01784.x

Dale, V.H., Joyce, L.A., McNulty, S., Neilson, R.P., Ayres, M.P., Flannigan, M.D., Hanson, P.J., Irland, L.C., Lugo, A.E., Peterson, C.J., Simberloff, D., Swanson, F.J., Stocks, B.J., Wotton, B.M., 2001. Climate change and forest disturbances. Bioscience 51, 723. doi:10.1641/0006-3568(2001)051[0723:CCAFD]2.0.CO;2

Davis, K.T., Dobrowski, S.Z., Higuera, P.E., Holden, Z.A., Veblen, T.T., Rother, M.T., Parks, S.A., Sala, A., Maneta, M.P., 2019. Wildfires and climate change push low-elevation forests across a critical climate threshold for tree regeneration. Proc. Natl. Acad. Sci. 116, 6193 LP – 6198. doi:10.1073/pnas.1815107116

de Beurs, K.M., Henebry, G.M., 2004. Trend analysis of the pathfinder AVHRR land (PAL) NDVI data for the deserts of central Asia. IEEE Geosci. Remote Sens. Lett. 1, 282–286. doi:10.1109/LGRS.2004.834805

de Jong, R., Verbesselt, J., Schaepman, M.E., de Bruin, S., 2012. Trend changes in global greening and browning: Contribution of short-term trends to longer-term change. Glob. Chang. Biol. 18, 642–655. doi:10.1111/j.1365-2486.2011.02578.x

Di-Mauro, B., Fava, F., Busetto, L., Crosta, G.F., Colombo, R., 2014. Post-fire resilience in the Alpine region estimated from MODIS satellite multispectral data. Int. J. Appl. Earth Obs. Geoinf. 32, 163–172. doi:10.1016/j.jag.2014.04.010

Eidenshink, J., Schwind, B., Brewer, K., Zhu, Z., Quayle, B., Howard, S., 2007. A Project for Monitoring Trends in Burn Severity. Fire Ecol. 3, 3–21. doi:10.4996/fireecology.0301003

Ellis, E.C., 2011. Anthropogenic transformation of the terrestrial biosphere. Philos. Trans. R. Soc. London A Math. Phys. Eng. Sci. 369, 1010–1035.

Fernandez-Manso, A., Quintano, C., Roberts, D.A., 2016. Burn severity influence on

post-fire vegetation cover resilience from Landsat MESMA fraction images time series in Mediterranean forest ecosystems. Remote Sens. Environ. 184, 112–123. doi:10.1016/j.rse.2016.06.015

Fry, J.A., Xian, G., Jin, S., Dewitz, J.A., Homer, C.G., Limin, Y., Barnes, C.A., Herold, N.D., Wickham, J.D., 2011. Completion of the 2006 national land cover database for the conterminous United States. Photogramm. Eng. Remote Sensing 77, 858–864.

Ganguly, S., Friedl, M.A., Tan, B., Zhang, X., Verma, M., 2010. Land surface phenology from MODIS: Characterization of the Collection 5 global land cover dynamics product. Remote Sens. Environ. 114, 1805–1816. doi:10.1016/j.rse.2010.04.005

Goetz, S.J., Fiske, G.J., Bunn, A.G., 2006. Using satellite time-series data sets to analyze fire disturbance and forest recovery across Canada. Remote Sens. Environ. 101, 352–365. doi:10.1016/j.rse.2006.01.011

Hill, R.A., Wilson, A.K., George, M., Hinsley, S.A., 2010. Mapping tree species in temperate deciduous woodland using time-series multi-spectral data. Appl. Veg. Sci. 13, 86–99. doi:10.1111/j.1654-109X.2009.01053.x

Homer, C., Dewitz, J., Fry, J., Coan, M., Hossain, N., Larson, C., Herold, N., McKerrow, A., VanDriel, J.N., Wickham, J., 2007. Completion of the 2001 national land cover database for the counterminous United States. Photogramm. Eng. Remote Sensing 73, 337.

Homer, C.G., Dewitz, J.A., Yang, L., Jin, S., Danielson, P., Xian, G., Coulston, J., Herold, N.D., Wickham, J.D., Megown, K., 2015. Completion of the 2011 National Land Cover Database for the conterminous United States-Representing a decade of land cover change information. Photogramm. Eng. Remote Sensing 81, 345–354.

Huete, A., Didan, K., Miura, T., Rodriguez, E.P., Gao, X., Ferreira, L.G., 2002. Overview of the radiometric and biophysical performance of the MODIS vegetation indices. Remote Sens. Environ. 83, 195–213. doi:http://dx.doi.org/10.1016/S0034-4257(02)00096-2

Ivits, E., Cherlet, M., Tóth, G., Sommer, S., Mehl, W., Vogt, J., Micale, F., 2012. Combining satellite derived phenology with climate data for climate change impact assessment. Glob. Planet. Change 88, 85–97.

Jamali, S., Jönsson, P., Eklundh, L., Ardö, J., Seaquist, J., 2015. Detecting changes in vegetation trends using time series segmentation. Remote Sens. Environ. 156, 182–195. doi:10.1016/j.rse.2014.09.010

Jeganathan, C., Dash, J., Atkinson, P.M., 2014. Remotely sensed trends in the phenology of northern high latitude terrestrial vegetation, controlling for land cover change and vegetation type. Remote Sens. Environ. 143, 154–170. doi:10.1016/j.rse.2013.11.020

Jeong, S.J., Ho, C.H., Gim, H.J., Brown, M.E., 2011. Phenology shifts at start vs. end of growing season in temperate vegetation over the Northern Hemisphere for the period 1982-2008. Glob. Chang. Biol. 17, 2385–2399. doi:10.1111/j.1365-2486.2011.02397.x

Jiang, Z., Huete, A.R., Didan, K., Miura, T., 2008. Development of a two-band enhanced vegetation index without a blue band. Remote Sens. Environ. 112, 3833–3845. doi:http://dx.doi.org/10.1016/j.rse.2008.06.006

Jönsson, P., Cai, Z., Melaas, E., Friedl, M.A., Eklundh, L., 2018. A method for robust estimation of vegetation seasonality from Landsat and Sentinel-2 time series data.

Remote Sens. 10. doi:10.3390/rs10040635

Jönsson, P., Eklundh, L., 2004. TIMESAT—a program for analyzing time-series of satellite sensor data. Comput. Geosci. 30, 833–845.

Julien, Y., Sobrino, J.A., 2009. Global land surface phenology trends from GIMMS database. Int. J. Remote Sens. 30, 3495–3513. doi:10.1080/01431160802562255

Karkauskaite, P., Tagesson, T., Fensholt, R., 2017. Evaluation of the plant phenology index (PPI), NDVI and EVI for start-of-season trend analysis of the Northern Hemisphere boreal zone. Remote Sens. 9, 485.

Keeley, J.E., 2009. Fire intensity, fire severity and burn severity: A brief review and suggested usage. Int. J. Wildl. Fire 18, 116–126. doi:10.1071/WF07049

Kennedy, R.E., Yang, Z., Cohen, W.B., 2010. Detecting trends in forest disturbance and recovery using yearly Landsat time series: 1. LandTrendr - Temporal segmentation algorithms. Remote Sens. Environ. 114, 2897–2910. doi:10.1016/j.rse.2010.07.008

Körner, C., Basler, D., 2010. Phenology Under Global Warming. Science (80-.). 327, 1461 LP – 1462. doi:10.1126/science.1186473

Lentile, L.B., Morgan, P., Hudak, A.T., Bobbitt, M.J., Lewis, S. a., Smith, A.M.S., Robichaud, P.R., 2007. Post-Fire Burn Severity and Vegetaion Response Following Eight Large Wildfires Across the Western United States. Fire Ecol. Spec. Issue 3, 91–108. doi:10.4996/fireecology.0301091

Lewis, S.A., Wu, J.Q., Robichaud, P.R., 2006. Assessing burn severity and comparing soil water repellency, Hayman Fire, Colorado. Hydrol. Process. 20, 1–16. doi:10.1002/hyp.5880

Lhermitte, S., Verbesselt, J., Verstraeten, W.W., Veraverbeke, S., Coppin, P., 2011.

Assessing intra-annual vegetation regrowth after fire using the pixel based regeneration index. ISPRS J. Photogramm. Remote Sens. 66, 17–27. doi:https://doi.org/10.1016/j.isprsjprs.2010.08.004

Li, Y., Zhang, Y., Gu, F., Liu, S., 2019. Discrepancies in vegetation phenology trends and shift patterns in different climatic zones in middle and eastern Eurasia between 1982 and 2015. Ecol. Evol. 9, 8664–8675. doi:10.1002/ece3.5408

Liang, L., Schwartz, M.D., Fei, S., 2011. Validating satellite phenology through intensive ground observation and landscape scaling in a mixed seasonal forest. Remote Sens. Environ. 115, 143–157. doi:10.1016/j.rse.2010.08.013

Liu, Z., Wu, C., Liu, Y., Wang, X., Fang, B., Yuan, W., Ge, Q., 2017. Spring green-up date derived from GIMMS3g and SPOT-VGT NDVI of winter wheat cropland in the North China Plain. ISPRS J. Photogramm. Remote Sens. 130, 81–91. doi:https://doi.org/10.1016/j.isprsjprs.2017.05.015

Marlon, J.R., Bartlein, P.J., Gavin, D.G., Long, C.J., Anderson, R.S., Briles, C.E., Brown, K.J., Colombaroli, D., Hallett, D.J., Power, M.J., Scharf, E.A., Walsh, M.K., 2012. Long-term perspective on wildfires in the western USA. Proc. Natl. Acad. Sci. U. S. A. 109, E535-43. doi:10.1073/pnas.1112839109

Melaas, E.K., Sulla-Menashe, D., Gray, J.M., Black, T.A., Morin, T.H., Richardson, A.D., Friedl, M.A., 2016. Multisite analysis of land surface phenology in North American temperate and boreal deciduous forests from Landsat. Remote Sens. Environ. 186, 452–464. doi:10.1016/j.rse.2016.09.014

Meng, R., Dennison, P.E., Huang, C., Moritz, M.A., D'Antonio, C., 2015. Effects of fire severity and post-fire climate on short-term vegetation recovery of mixed-conifer

and red fir forests in the Sierra Nevada Mountains of California. Remote Sens. Environ. 171, 311–325. doi:10.1016/j.rse.2015.10.024

Meng, R., Wu, J., Zhao, F., Cook, B.D., Hanavan, R.P., Serbin, S.P., 2018. Measuring short-term post-fire forest recovery across a burn severity gradient in a mixed pine-oak forest using multi-sensor remote sensing techniques. Remote Sens. Environ. 210, 282–296. doi:10.1016/j.rse.2018.03.019

Montorio Llovería, R., Pérez-Cabello, F., García-Martín, A., 2016. Assessing post-fire ground cover in Mediterranean shrublands with field spectrometry and digital photography. ISPRS J. Photogramm. Remote Sens. 119, 187–197. doi:https://doi.org/10.1016/j.isprsjprs.2016.06.002

Moon, M., Zhang, X., Henebry, G.M., Liu, L., Gray, J.M., Melaas, E.K., Friedl, M.A., 2019. Long-term continuity in land surface phenology measurements: A comparative assessment of the MODIS land cover dynamics and VIIRS land surface phenology products. Remote Sens. Environ. 226, 74–92.

Morisette, J.T., Richardson, A.D., Knapp, A.K., Fisher, J.I., Graham, E.A., Abatzoglou, J., Wilson, B.E., Breshears, D.D., Henebry, G.M., Hanes, J.M., 2009. Tracking the rhythm of the seasons in the face of global change: phenological research in the 21st century. Front. Ecol. Environ. 7, 253–260.

Muller, R.N., 1978. The phenology, growth and ecosystem dynamics of Erythronium americanum in the northern hardwood forest. Ecol. Monogr. 48, 1–20.

Parmesan, C., Yohe, G., 2003. A globally coherent fingerprint of climate change impacts across natural systems. Nature 421, 37.

Pasquarella, V.J., Holden, C.E., Woodcock, C.E., 2018. Improved mapping of forest type

using spectral-temporal Landsat features. Remote Sens. Environ. 210, 193–207. doi:10.1016/j.rse.2018.02.064

Pechony, O., Shindell, D.T., 2010. Driving forces of global wildfires over the past millennium and the forthcoming century. Proc. Natl. Acad. Sci. U. S. A. 107, 19167–70. doi:10.1073/pnas.1003669107

Peng, D., Zhang, X., Wu, C., Huang, W., Gonsamo, A., Huete, A.R., Didan, K., Tan, B., Liu, X., Zhang, B., 2017. Intercomparison and evaluation of spring phenology products using National Phenology Network and AmeriFlux observations in the contiguous United States. Agric. For. Meteorol. 242, 33–46.

Piao, S., Nan, H., Huntingford, C., Ciais, P., Friedlingstein, P., Sitch, S., Peng, S., Ahlström, A., Canadell, J.G., Cong, N., Levis, S., Levy, P.E., Liu, L., Lomas, M.R., Mao, J., Myneni, R.B., Peylin, P., Poulter, B., Shi, X., Yin, G., Viovy, N., Wang, T., Wang, X., Zaehle, S., Zeng, N., Zeng, Z., Chen, A., 2014. Evidence for a weakening relationship between interannual temperature variability and northern vegetation activity. Nat. Commun. 5, 1–7. doi:10.1038/ncomms6018

Richardson, A.D., Keenan, T.F., Migliavacca, M., Ryu, Y., Sonnentag, O., Toomey, M., 2013. Climate change, phenology, and phenological control of vegetation feedbacks to the climate system. Agric. For. Meteorol. 169, 156–173. doi:10.1016/j.agrformet.2012.09.012

Richardson, A.D., O'Keefe, J., 2009. Phenological Differences Between Understory and Overstory: A Case Study Using the Long-Term Harvard Forest Records, in: Noormets, A. (Ed.), Phenology of Ecosystem Processes. Springer, New York, NY, USA, pp. 87–117. doi:10.1007/978-1-4419-0026-5

Rocha, A. V, Shaver, G.R., 2009. Advantages of a two band EVI calculated from solar and photosynthetically active radiation fluxes. Agric. For. Meteorol. 149, 1560–1563. doi:https://doi.org/10.1016/j.agrformet.2009.03.016

Romo-Leon, J.R., van Leeuwen, W.J.D., Castellanos-Villegas, A., 2016. Land Use and Environmental Variability Impacts on the Phenology of Arid Agro-Ecosystems. Environ. Manage. 57, 283–297. doi:10.1007/s00267-015-0617-7

Serbin, S.P., Gower, S.T., Ahl, D.E., 2009. Canopy dynamics and phenology of a boreal black spruce wildfire chronosequence. Agric. For. Meteorol. 149, 187–204. doi:10.1016/j.agrformet.2008.08.001

Shen, M., Tang, Y., Chen, J., Yang, W., 2012. Specification of thermal growing season in temperate China from 1960 to 2009. Clim. Change 114, 783–798. doi:10.1007/s10584-012-0434-4

Singh, K.K., Chen, Y.-H., Smart, L., Gray, J., Meentemeyer, R.K., 2018. Intra-annual phenology for detecting understory plant invasion in urban forests. ISPRS J. Photogramm. Remote Sens. 142, 151–161. doi:https://doi.org/10.1016/j.isprsjprs.2018.05.023

Soudani, K., Le Maire, G., Dufrêne, E., François, C., Delpierre, N., Ulrich, E., Cecchini, S., 2008. Evaluation of the onset of green-up in temperate deciduous broadleaf forests derived from Moderate Resolution Imaging Spectroradiometer (MODIS) data. Remote Sens. Environ. 112, 2643–2655.

Sulla-Menashe, D., Woodcock, C.E., Friedl, M.A., 2018. Canadian boreal forest greening and browning trends: an analysis of biogeographic patterns and the relative roles of disturbance versus climate drivers. Environ. Res. Lett. 13, 14007.

Van Leeuwen, W.J.D., Casady, G.M., Neary, D.G., Bautista, S., Alloza, J.A., Carmel, Y., Wittenberg, L., Malkinson, D., Orr, B.J., 2010. Monitoring post-wildfire vegetation response with remotely sensed time-series data in Spain, USA and Israel. Int. J. Wildl. Fire 19, 75–93. doi:10.1071/WF08078

Veraverbeke, S., Gitas, I., Katagis, T., Polychronaki, A., Somers, B., Goossens, R., 2012. Assessing post-fire vegetation recovery using red–near infrared vegetation indices: accounting for background and vegetation variability. ISPRS J. Photogramm. Remote Sens. 68, 28–39.

Verbesselt, J., Hyndman, R., Newnham, G., Culvenor, D., 2010. Detecting trend and seasonal changes in satellite image time series. Remote Sens. Environ. 114, 106–115. doi:10.1016/j.rse.2009.08.014

Vitousek, P.M., Aber, J.D., Howarth, R.W., Likens, G.E., Matson, P.A., Schindler, D.W., Schlesinger, W.H., Tilman, D.G., 1997. Human alteration of the global nitrogen cycle: sources and consequences. Ecol. Appl. 7, 737–750.

Walther, G.-R., 2010. Community and ecosystem responses to recent climate change. Philos. Trans. R. Soc. B Biol. Sci. 365, 2019–2024.

Wang, J., Wu, C., Wang, X., Zhang, X., 2019. A new algorithm for the estimation of leaf unfolding date using MODIS data over China's terrestrial ecosystems. ISPRS J. Photogramm. Remote Sens. 149, 77–90. doi:https://doi.org/10.1016/j.isprsjprs.2019.01.017

Wang, J., Zhang, X., 2017. Impacts of wildfires on interannual trends in land surface phenology: an investigation of the Hayman Fire. Environ. Res. Lett. 12, 054008. doi:10.1088/1748-9326/aa6ad9

Wang, S., Yang, B., Yang, Q., Lu, L., Wang, X., Peng, Y., 2016. Temporal trends and spatial variability of vegetation phenology over the Northern Hemisphere during 1982-2012. PLoS One 11, 1–21. doi:10.1371/journal.pone.0157134

Westerling, a. L., Hidalgo, H.G., Cayan, D.R., Swetnam, T.W., 2006. Warming and earlier spring increase western U.S. forest wildfire activity. Science 313, 940–3. doi:10.1126/science.1128834

White, M.A., Hoffman, F., Hargrove, W.W., Nemani, R.R., 2005. A global framework for monitoring phenological responses to climate change. Geophys. Res. Lett. 32, L04705.

White, M.A., Thornton, P.E., Running, S.W., 1997. A continental phenology model for monitoring vegetation responses to interannual climatic variability. Global Biogeochem. Cycles 11, 217–234. doi:10.1029/97GB00330

Yang, J., Pan, S., Dangal, S., Zhang, B., Wang, S., Tian, H., 2017. Continental-scale quantification of post-fire vegetation greenness recovery in temperate and boreal North America. Remote Sens. Environ. 199, 277–290. doi:10.1016/j.rse.2017.07.022

Yu, H., Luedeling, E., Xu, J., 2010. Winter and spring warming result in delayed spring phenology on the Tibetan Plateau. Proc. Natl. Acad. Sci. 107, 22151–22156.

Yuan, H., Wu, C., Lu, L., Wang, X., 2018. A new algorithm predicting the end of growth at five evergreen conifer forests based on nighttime temperature and the enhanced vegetation index. ISPRS J. Photogramm. Remote Sens. 144, 390–399. doi:https://doi.org/10.1016/j.isprsjprs.2018.08.013

Zeng, H., Jia, G., Epstein, H., 2011. Recent changes in phenology over the northern high

latitudes detected from multi-satellite data. Environ. Res. Lett. 6, 045508. doi:10.1088/1748-9326/6/4/045508

Zhang, X., 2018. Land Surface Phenology: Climate Data Record and Real-Time Monitoring, in: Liang, S. (Ed.), Reference Module in Earth Systems and Environmental Sciences-Comprehensive Remote Sensing. Elsevier, Oxford, pp. 35–52.

Zhang, X., 2015. Reconstruction of a complete global time series of daily vegetation index trajectory from long-term AVHRR data. Remote Sens. Environ. 156, 457–472. doi:10.1016/j.rse.2014.10.012

Zhang, X., Friedl, M. a., Schaaf, C.B., 2006. Global vegetation phenology from Moderate Resolution Imaging Spectroradiometer (MODIS): Evaluation of global patterns and comparison with in situ measurements. J. Geophys. Res. Biogeosciences 111, 1–14. doi:10.1029/2006JG000217

Zhang, X., Friedl, M.A., Schaaf, C.B., 2009. Sensitivity of vegetation phenology detection to the temporal resolution of satellite data. Int. J. Remote Sens. 30, 2061–2074. doi:10.1080/01431160802549237

Zhang, X., Friedl, M.A., Schaaf, C.B., Strahler, A.H., Hodges, J.C.F.F., Gao, F., Reed, B.C., Huete, A., 2003. Monitoring vegetation phenology using MODIS. Remote Sens. Environ. 84, 471–475. doi:10.1016/S0034-4257(02)00135-9

Zhang, X., Liu, L., Henebry, G., 2019. Impacts of land cover and land use change on long-term trend of land surface phenology: a case study in agricultural ecosystems. Environ. Res. Lett. 14, 044020.

Zhang, X., Liu, L., Liu, Y., Jayavelu, S., Wang, J., Moon, M., Henebry, G.M., Friedl,

M.A., Schaaf, C.B., 2018. Generation and evaluation of the VIIRS land surface phenology product. Remote Sens. Environ. 216, 212–229. doi:10.1016/j.rse.2018.06.047

Zhang, X., Tan, B., Yu, Y., 2014. Interannual variations and trends in global land surface phenology derived from enhanced vegetation index during 1982-2010. Int. J. Biometeorol. 58, 547–564. doi:10.1007/s00484-014-0802-z

Zhang, X., Tarpley, D., Sullivan, J.T., 2007. Diverse responses of vegetation phenology to a warming climate. Geophys. Res. Lett. 34, 1–5. doi:10.1029/2007GL031447

Zhou, L., Kaufmann, R.K., Tian, 1 Y, Myneni, R.B., Tucker, C.J., 2003. Relation between interannual variations in satellite measures of northern forest greenness and climate between 1982 and 1999. J. Geophys. Res. Atmos. 108, ACL-3. doi:10.1029/2002JD002510

Zhu, Z., Evans, D.L., 1994. US forest types and predicted percent forest cover from AVHRR data. PE RS- Photogramm. Eng. Remote Sens. 60, 525–531.

Zhu, Z., Piao, S., Myneni, R.B., Huang, M., Zeng, Z., Canadell, J.G., Ciais, P., Sitch, S., Friedlingstein, P., Arneth, A., Liu, R., Mao, J., Pan, Y., Peng, S., Peñuelas, J., Poulter, B., Cao, C., Cheng, L., Kato, E., Koven, C., Li, Y., Lian, X., Liu, Y., Liu, R., Mao, J., Pan, Y., Peng, S., Peuelas, J., Poulter, B., Pugh, T.A.M., Stocker, B.D., Viovy, N., Wang, X., Wang, Y., Xiao, Z., Yang, H., Zaehle, S., Zeng, N., 2016. Greening of the Earth and its drivers. Nat. Clim. Chang. 6, early online. doi:10.1038/NCLIMATE3004

CHAPTER 4: Exploring the Contribution of Land Cover Composition to Spatial and Interannual Variations of Land Surface Phenology in a Recently Burned Landscape Using Machine Learning

The content of this chapter was prepared in a manuscript and submitted to *Remote Sensing of Environment* for review:

Wang, J., Zhang, X., Rodman, K. C., Exploring the Contribution of Land Cover Composition to Spatial and Interannual Variations of Land Surface Phenology in a Recently Burned Landscape Using Machine Learning. *Remote Sensing of Environment*

Abstract

Land surface phenology (LSP) characterizes the seasonal dynamics of vegetation communities that compose individual satellite pixels. Although increasing evidence showed an effect of land cover composition within a pixel on LSP, it remains unclear to what extent land cover composition compares to and interacts with other drivers of phenology. To fill this gap, this study used a machine learning approach of the Boosted Regression Tree (BRT) to quantitatively assess the contributions of two land cover composition metrics, i.e., vegetation fractional coverage (VFC) and tree proportion to vegetation (TPV), and other factors mainly including climate and topography on the spatial and interannual variation in LSP throughout the 2002 Ponil Complex Fire in New Mexico, USA. Start (SOS) and end (EOS) of growing season were derived from 500-m MODIS data from 2001-2018 and 30-m Harmonized Landsat Sentinel-2 (HLS) data in 2018. Land cover composition was derived from PlanetScope and National Agriculture Imagery Program imagery in 2018 and MODIS growing season greenness from 2001-2018. BRT models of spatial variation in LSP showed that TPV was the most important predictor of SOS and EOS derived from both MODIS and HLS data in 2018. Further, the drivers of spatial variation in LSP are scale-dependent, indicating a greater role of topographic drivers at the finer scale (30-m HLS) than the coarser scale (500-m MODIS). BRT models for interannual LSP from MODIS in 2001-2018 indicated that the growing degree days (GDD) and the first freeze date (FFD) were the most important predictors of SOS and EOS, respectively. However, VFC was also a helpful predictor of interannual variation in both SOS and EOS. BRTs for both spatial and interannual variation in LSP also revealed that land cover composition exhibited a stronger effect on EOS than SOS.

This study demonstrates the utility of machine learning in modeling phenology and highlights the essential role of land cover composition in understanding the spatial and interannual variations of LSP. Our findings suggest that within-pixel changes in land cover composition should not be overlooked when investigating the change of land surface phenology.

4.1. . Introduction

Vegetation phenology is the science of studying periodic events in the life cycles of plant organisms (e.g., bud-burst, flowering, and abscission). As a crucial regulator of ecosystem processes and a sensitive bio-indicator of climate change, vegetation phenology has been studied extensively during the last few decades using various data sources including ground observations (Betancourt et al., 2005; Geng et al., 2020; Park and Mazer, 2018) and remote sensing measurements (Cao et al., 2015; Melaas et al., 2016; Zhang et al., 2020, 2003). While ground observations provide a long-term first-hand record of species-specific phenology, satellite remote sensing detects the area-integrated phenology of vegetation communities within a pixel that is usually referred to as land surface phenology (LSP) (de Beurs and Henebry, 2004). The record of both ground phenology and LSP has revealed a general trend of earlier spring and later autumn phenological events in response to a warming climate (Morin et al., 2010; White et al., 2009; Wu et al., 2016), but inverse trends of later spring and earlier autumn phenological events have also been observed (Fu et al., 2014; Jeong et al., 2011; Zhang et al., 2007). The direction and magnitude of recent phenological trends vary greatly among locations, periods, and plant species (Chmielewski and Rötzer, 2001; Piao et al., 2006; Primack et al., 2009).

The complex pattern of phenological variation is associated with various environmental factors that influence plant life cycles. Although temperature is generally regarded as the primary control, phenology is codetermined by other environmental factors such as photoperiod (Liu et al., 2018), precipitation (Jolly and Running, 2004; Shen et al., 2011), extreme weather events (Qiu et al., 2020; Van Wijk et al., 2003), and nutrient and water availability (Estiarte and Peñuelas, 2015; Fay et al., 2012). The seasonality of snow and freeze also influences vegetation phenology at mid- and high-latitudes and high elevations (Rodriguez-Galiano et al., 2016; Xie et al., 2017). Moreover, topographic properties (e.g., elevation and aspect) control the spatial pattern of vegetation phenology at a local to landscape scales (An et al., 2018; Misra et al., 2018; Xie et al., 2017).

Besides the aforementioned common factors controlling vegetation phenology development, satellite-based LSP is also influenced by variation in land cover composition within pixels (Chen et al., 2018; Melaas et al., 2015; Misra et al., 2018; Wang and Zhang, 2017). Satellite pixels at moderate (10-250 m m) and coarse (>250 m) spatial resolutions (Thomas et al., 2020) usually consist of a mixture of land cover types and vegetation species with different phenological responses to environmental factors (Augspurger et al., 2005; Zhang et al., 2017). Thus, changes in sub-pixel land cover composition, which could be caused by natural processes (e.g., disturbances, climate extremes, and species invasion) and human activities (e.g., urbanization, deforestation, and crop rotation) (Zhang et al., 2019), can alter LSP values and trends. Indeed, increasing evidence has revealed the effect of land cover composition on LSP in the past few years. For example, Misra et al. (2018) found the end of growing season (EOS) was

spatially linked to the sub-pixel percentage of broadleaf forests. Wang and Zhang (2020) found wildfire-caused land cover change triggered abrupt shifts in both start of growing season (SOS) and EOS in the western United States (US) forests relative to the LSP in surrounding unburned areas. LSP variation associated with land cover change could have significant influences on LSP trends (Wang and Zhang, 2017; Zhang et al., 2019), which limits the effectiveness of phenological trend monitoring climate change. Although this impact has been noted in recent studies (Chen et al., 2018; Cho et al., 2017; Misra et al., 2018; Wang and Zhang, 2020), we still lack quantitative analyses to reveal the contribution of land cover composition change to the LSP variation spatially and interannually compared to other drivers including climate and topography.

Current approaches to modeling the effects of individual drivers on vegetation phenology typically involve conventional statistical methods based on linear regression (Luedeling and Gassner, 2012; Misra et al., 2018; Shen et al., 2015). However, it has been demonstrated that the response of phenology to environmental factors such as temperature and precipitation is often nonlinear (Cober et al., 2014; Sparks et al., 2000), which limits the efficacy of the conventional methods in modeling phenology. In contrast, non-parametric machine learning methods are particularly suitable in handling the nonlinearities in phenology modeling because they make few assumptions about the relationship between response and predictors. Moreover, machine learning methods outperform the conventional statistical methods in handling the complex interactions among a large number of related predictors. With these advantages, machine learning has been attracting increasing attention in ecological modeling and prediction (Bond-

Lamberty et al., 2014; De'ath, 2007). However, its application in phenological modeling is still rare (Czernecki et al., 2018; Dai et al., 2019; Rodriguez-Galiano et al., 2016).

Using machine learning techniques, this study aims to quantitatively assess the relative contribution of land cover composition change on the spatial and interannual variation in LSP compared with other drivers mainly including climate and topography. To accomplish this objective, we performed a case study of LSP throughout the 2002 Ponil Complex Fire, located in mountainous forests in New Mexico, USA. Within the fire area, climate, topography, burn severity, and post-fire succession vary widely, providing a useful opportunity to investigate the spatial and interannual dynamics of land cover composition on LSP (Laughlin et al., 2004; Wang and Zhang, 2017). Specifically, SOS and EOS were detected using the 500-m Moderate Resolution Imaging Spectroradiometer (MODIS) data for 2001-2018 and the 30-m NASA Harmonized Landsat and Sentinel-2 (HLS) product in 2018, separately. The land cover composition in 2018 was derived from high-resolution imagery. By integrating land cover composition and other drivers in a machine learning model, we were able to assess the contribution of land cover composition change to the spatial and interannual variations of SOS and EOS when compared with other drivers.

4.2. Study area

The Ponil Complex Fire, which occurred in June 2002, is located at the mountainous forests of northeast New Mexico, USA (36°40'55.2"N, 105°02' 149.2"W; Figure 4-1a). The burn area covers 360 km^2 that is primarily within the boundaries of the Carson National Forest and the Philmont Scout Ranch. A portion of the Ponil Complex Fire was re-burned in the 2018 Ute Park Fire, and this area (denoted in grey color in

Figure 4-1b) was excluded from our study. Based on the Monitoring Trends in Burn Severity (MTBS) map (see Section 3.1.3), the remaining burned area consists of 26.5% of unburned/low severity, 14.7% of low severity, 20.1% of moderate severity, 32.5% of high severity, 0.4% of increased-greenness (i.e., post-fire vegetation that exceeded pre-fire cover), and 5.7% that was masked due to data gaps (i.e., non-processing; Figure 4-1b). Areas with increased-greenness and data gaps were further excluded from our analyses.

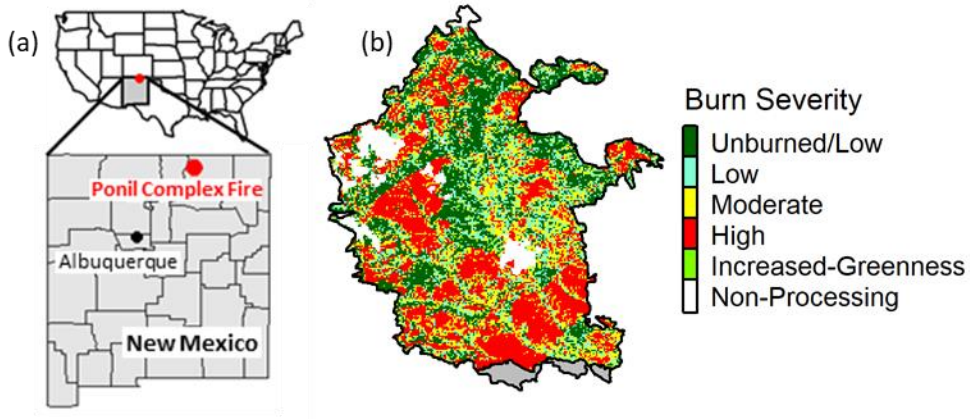

Figure 4-1. The location of the Ponil Complex Fire (a) and the Monitoring Trends in Burn Severity (MTBS) map (the grey area was removed from the study area because of overlapping with the Ute Park Fire) at 30 m (b).

In the study area, elevation ranges from 2,018 to 2,835 m; monthly average temperature varies from -3.0 ℃ in January to 17.5 ℃ in July; and average annual precipitation is 471 mm with a peak in July (71 mm) and August (77 mm) (averaged from 1980 to 2018 using Daymet data; see Section 3.3). The pre-fire vegetation was dominated by evergreen tree species (mostly ponderosa pine - *Pinus ponderosa* and Douglas-fir - *Pseudotsuga menziesii*) (Rodman et al., 2019). After the fire occurrence, understory

species including grasses and shrubs (mostly Gambel Oak – *Quercus gambelii*, a deciduous shrub species) quickly recolonized the burned area, followed by gradual but limited recovery of Ponderosa pine and Douglas-fir (Rodman et al., 2019). Because of the different adaptations of understory species and trees to fire and post-fire environmental conditions, vegetation species and land cover composition are widely variable throughout the burned area and changed throughout the study period.

4.3. Materials and methods

Data processing and modeling are described broadly in Figure 4-2. Briefly, after LSP was detected from MODIS and HLS data, the contribution of land cover composition to the spatial and interannual phenological variation was investigated using machine learning models. The spatial variation of LSP from MODIS and HLS in 2018 was modeled using predictors of land cover composition, climate, topography, and burn severity. The interannual variation in LSP from MODIS in 2001-2018 was modeled using land cover composition and climatic predictors after all the variables were interannually normalized (i.e., scaled to z-scores using pixel-specific means and standard deviations) to attenuate the spatial variations (Rodriguez-Galiano et al., 2016). Details are described in the following sections.

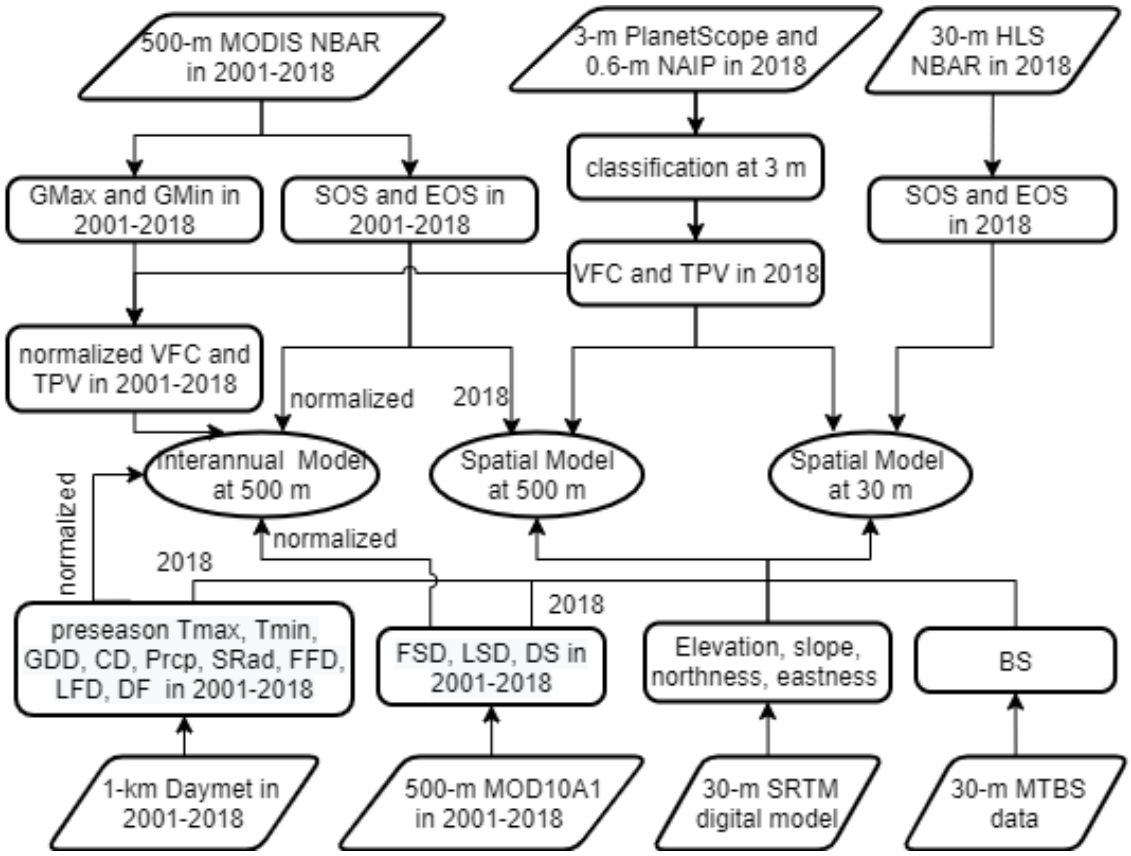

Figure 4-2. Flowchart of modeling the spatial and interannual variations of LSP from MODIS and HLS. The "2018" alongside the arrows indicates the variables in 2018 for the spatial models, while the "normalized" represents that the variables were interannually normalized during 2001-2018 for the interannual models (see Section 3.5).

4.3.1. Datasets

4.3.1.1. MODIS and HLS NBAR products.

The MODIS Nadir Bidirectional Reflectance Distribution Function (BRDF) - Adjusted Reflectances (NBAR) product (MCD43A4, V006) provides daily surface reflectance corrected to a common nadir view geometry at the local solar noon zenith angle at a 500-m resolution (the actual pixel size is 463.32 m) in the sinusoidal projection

(Wang et al., 2018). The daily NBAR values are calculated by inverting multi-date, multi-angle, cloud-free, atmospherically-corrected surface reflectance observations acquired by MODIS instruments aboard both the Terra and Aqua satellites over a 16-day period with a kernel-driven semi-empirical BRDF model (Schaaf et al., 2002). The corresponding quality assurance (QA) flag including the retrieval quality (full inversion, magnitude inversion, and filled value) and the retrieval strategy (snow-covered and snow-free) is provided in the MODIS NBAR/Albedo Quality product (MCD43A2, V006). We obtained the daily MODIS products for a single tile (h09v05) covering the study area from 2001-2018 from NASA (https://lpdaac.usgs.gov/dataset_discovery/modis/).

The HLS project at NASA generates spatially co-registered surface reflectance products using observations from Operational Land Imager (OLI) aboard Landsat 8 (launched in 2013) and Multi-Spectral Instrument (MSI) aboard Sentinel-2A (launched in 2015) and Sentinel-2B (launched in 2017) satellites (Claverie et al., 2018). The seamless HLS surface reflectance products are based on a set of algorithms including atmospheric correction, cloud and cloud-shadow masking, spatial co-registration and common gridding, BRDF normalization, and spectral bandpass adjustment. As a result, the HLS provides NBAR and QA at 30 m for OLI and MSI separately. The QA indicates whether the NBAR is contaminated by snow/ice, aerosol, cloud shadow, cloud, adjacent cloud, and cirrus clouds. Since 2017, HLS data provide a nominal global median average revisit interval of 2.9 days by combining Landsat-8, Sentinel-2A, and Sentinel-2B (Li and Roy, 2017). In this study, we obtained HLS surface reflectance data for tile 13SDA in a Universal Transverse Mercator (UTM) projection covering the study area in 2018 from NASA (https://hls.gsfc.nasa.gov/data/v1.4/).

4.3.1.2. The National Agriculture Imagery Program (NAIP) and PlanetScope imageries

To compute the land cover composition within 500-m and 30-m pixels, we developed a 3-m land cover map using multi-temporal high-resolution imagery from the National Agriculture Imagery Program (NAIP) and PlanetScope (Table 4-1). NAIP, administered by the US Department of Agriculture's Farm Service Agency (USDA - FSA), provides digital orthophotography with a spatial resolution of 0.5-2 m and an acquisition interval of two-five years in three-four bands – red (R), green (G), blue (B), and (in more recent collections) near-infrared (NIR) - in the continental US for free or low cost (USDA, 2015). In the study area, NAIP provides four-band imagery since 2011. PlanetScope is a CubeSat constellation in sun-synchronous orbits operated by Planet Labs providing daily observations across the Earth's surface (Planet Labs Inc, 2020). The Planet Ortho Scene Product (Level 3B) provides the surface reflectance in R, G, B, and NIR at a spatial resolution of 3 m. In the study area, the PlanetScope record started in 2016 with very limited acquisitions and became largely available since 2017. Because images from different seasons effectively distinguish different vegetation types (Persson et al., 2018; Tarantino et al., 2019), we used images in 2018 when NAIP was available and PlanetScope acquisitions were abundant for accurate classification. Specifically, we obtained the 0.6-m NAIP images covering the study area in June 2018 via Google Earth Engine (GEE) (https://developers.google.com/earth-engine/datasets/). For PlanetScope imagery, we surveyed all available data in 2018 and obtained five imagery collections (the acquisition interval in each collection is <8 days) covering the study area with

minimal cloud and snow contaminations from April to October in 2018 (https://www.planet.com/).

Table 4-1. High-resolution image collections used in the land cover classification.

Platform	Imagery acquisition date	Spatial resolution	Bands
PlanetScope	4/2/2018 - 4/9/2018	3 m	R,G,B, and NIR
PlanetScope	4/18/2018 - 4/19/2018	3 m	R,G,B, and NIR
PlanetScope	5/13/2018	3 m	R,G,B, and NIR
NAIP	6/20/2018 - 6/22/2018	0.6 m	R,G,B, and NIR
PlanetScope	6/25/2018 - 6/26/2018	3 m	R,G,B, and NIR
PlanetScope	10/3/2018	3 m	R,G,B, and NIR

4.3.1.3. Other datasets

We obtained data describing burn severity (BS) from the Monitoring Trends in Burn Severity (MTBS) program (www.mtbs.gov; Figure 4-1b). MTBS maps the location and severity of all large wildfires (> 200 ha in the eastern states and > 400 ha in the western states) that have occurred in the US since 1984 by comparing the pre-fire and post-fire Normalized Burn Ratio derived from Landsat data at a 30-m resolution (Eidenshink et al., 2007). In MTBS, thematic burn severity is represented using five discrete classes: unburned/low, low, moderate, high, and increased greenness; the areas without detections due to clouds, cloud shadows, and data gaps are denoted as non-processing (Eidenshink et al., 2007).

The Daymet meteorological data provide gridded estimates of daily weather parameters including minimum temperature (TMin), maximum temperature (TMax), precipitation (Prcp), and shortwave radiation (SRad) in North America at a resolution of 1 km since 1980 using terrain-aided interpolation of observations from weather stations (Thornton et al., 2017). The MODIS snow cover product (MOD10A1) provides daily snow cover, derived using the normalized difference snow index, at 500-m spatial resolution (Hall et al., 2002). The Shuttle Radar Topography Mission (SRTM) offers a worldwide digital elevation model (DEM) at 1 arc-second (30 m) resolution (Farr et al., 2007). We obtained Daymet records 2001-2018, MOD10A1 in 2001-2018, and SRTM data through GEE (https://developers.google.com/earth-engine/datasets/).

4.3.2. Detection of LSP timing and greenness metrics of from MODIS and HLS

LSP timing (SOS and EOS) and greenness (GMax and GMin) metrics were detected using a time series of the two-band enhanced vegetation index (EVI2) from MODIS in 2001-2018 and HLS in 2018. First, we computed a daily time series of EVI2 (Huete et al., 2002; Jiang et al., 2008), as well as normalized difference vegetation index (NDVI) and normalized difference water index (NDWI) (Delbart et al., 2005; Gao, 1996), from MODIS in 2001-2018 and HLS in 2018. We used NDVI and NDWI to reduce noise in the daily EVI2 time series (Zhang et al., 2020). Specifically, EVI2 values greater than 90% of NDVI (anomalously high) or smaller than NDWI (contaminated by land surface moisture such as snow and cloud) were excluded from the time series. Moreover, the quality of the remaining EVI2 values was labeled into “high quality”, “snow covered”, and “other quality” using the QA flags in MODIS and HLS products

(Zhang et al., 2018). Finally, the daily EVI2 time series were aggregated to three-day composites by selecting the maximum value with the best quality in the remaining EVI2.

Second, the hybrid piecewise logistic model – land surface phenology detection (HPLM-LSPD) algorithm was applied on the three-day EVI2 composites (Zhang, 2015; Zhang et al., 2003), because this algorithm has been demonstrated to be effective in various ecosystems (Liang et al., 2011; Richardson et al., 2006; Wang and Zhang, 2017). The implementation of HPLM-LSPD on the three-day EVI2 composites included four steps. (1) A background EVI2 value for a given year was calculated for each pixel as the mean of the 10% lowest "high quality" EVI2 values within a two-year period including the preceding half-year, the given year, and the following half-year. EVI2 values lower than the background EVI2 value were primarily due to cloud contamination and were excluded from the following processes. (2) The time series were gap-filled using linear interpolation and smoothed using a Savitzky-Golay filter (Chen et al., 2004) and a running local median filter. (3) The smoothed EVI2 time series was fitted using the hybrid piecewise logistic function. (4) SOS and EOS were identified as the day of year (DOY) with the maximal and minimal rate of change in the curvature in the spring and autumn, respectively; and GMax and GMin were retrieved as the annual maximum and minimum values, respectively, in the HPLM fitted EVI2 time series.

To evaluate the consistency of HPLM-LSPD performance on MODIS and HLS, we compared the retrieved SOS and EOS from these two datasets. We aggregated the 30-m HLS LSP to the 500-m MODIS scale using the percentile aggregation, which uses the timing with a specific percentile from the cumulative HLS SOS or EOS frequency distribution within a MODIS pixel (Zhang et al., 2017). The aggregated LSP from this

approach represents the date at which vegetation greenup or senescence has occurred in the specified percentage of the HLS pixels. We determined the percentile by selecting the one which generates the smallest difference between the aggregated HLS and MODIS LSP from a series of candidates (10%-90% with an interval of 5%). The difference was measured by using the mean absolute deviation and the mean deviation.

4.3.3. Computation of land cover composition

Based on the multi-temporal high-resolution images collected in 2018 (Table 4-1), we generated a 3-m land cover map using an unsupervised learning algorithm in GEE (Gorelick et al., 2017). The land cover was separated into three classes: tree, shrub/grass, and soil. Prior to classification, each of the six image collections in Table 4-1 was mosaicked and stacked into a multi-band composite spanning the entire study area. First, the NAIP image mosaic was resampled to 3 m to match PlanetScope. Next, we calculated brightness as the average of visible bands (RGB) and NDVI using the red and NIR bands from each image. Then, we merged these bands within each collection to create a six-band image consisting of the following: reflectance in R, G, B, and NIR, brightness, and NDVI. Finally, we stacked the six images to develop a composite with a total of 36 bands at a resolution of 3 m, as no apparent horizontal shifts were shown among different images. The observations in the 36-band composite were partitioned into 40 clusters using the k-means clustering method which minimizes within-cluster variances (Arthur and Vassilvitskii, 2006). From this, the 3-m land cover map in 2018 was generated by re-assigning each cluster to one of the three land cover classes: tree, shrub/grass, and soil. The classification accuracy was also evaluated with 1,000 validation samples that were randomly distributed in the study area by visually interpreting the 0.6-m NAIP imagery.

Two metrics of land cover composition [vegetation fractional coverage (VFC) and tree proportion to vegetation (TPV)] were computed at 500 m and 30 m by aggregating the 3-m land cover types in 2018. Specifically, VFC was calculated as the proportion of 3-m vegetated (tree and shrub/grass) pixels within a coarser-resolution pixel (500 m or 30 m); and TPV was calculated as the ratio of tree fractional coverage (similar to VFC but for trees only) to VFC in a coarser-resolution pixel. The computed VFC and TPV in 2018 were used in modeling the spatial variation in LSP from MODIS and HLS.

The interannual variation of VFC and TPV during 2001-2018 was required to assess the contribution of land cover composition to interannual LSP variations during the study period. As restricted by the limited availability of high-resolution imagery spanning multiple seasons, we were not able to directly retrieve the land cover composition for other years except 2018. In this study area, the dominant tree species (mostly Ponderosa and Douglas fir) are evergreen and shrub/grass species (mostly Gambel Oak) are deciduous. Considering there are no green leaves on deciduous shrubs and grasses during the winter period, the variation of GMin (the annual minimum of EVI2) is mainly caused by the evergreen trees in the study area; meanwhile, the variation of GMax (the annual maximum of EVI2) is caused by the entire (both evergreen and deciduous) vegetation. Thus, we assumed there were linear relationships between GMax and VFC as well as between GRatio (the ratio of GMin to GMax) and TPV. This assumption was based on the accordance of post-fire trajectories of GMin and GMax with the field-observed tree seedling and vegetation regeneration in a burned ponderosa pine – Douglas fir forest in Colorado (Wang and Zhang, 2017). In this study, the linear relationships were quantitatively verified using the GMax, GRatio, VFC, and TPV in

2018 (see Section 4.2). Thus, interannual variation in VFC and TPV was quantified using GMax and GRatio derived from MODIS during 2001-2018. We note that coefficients of the linear relationships between land cover composition and greenness metrics could vary spatially among pixels. However, the normalization process (see Section 3.5) should minimize the spatial variation in the coefficients. Therefore, we were able to directly use the normalized GMax and GRatio as surrogates for the interannual variations of VFC and TPV, respectively, during 2001-2018.

4.3.4. Computation of environmental variables

We computed a suite of topographical and climatic variables through GEE (Gorelick et al., 2017). Four topographical variables (elevation, slope, northness, and eastness) were generated using the SRTM DEM at 30 m. Northness and eastness were calculated as the cosine and sine of aspect, respectively. Both variables ranged from -1 to 1, with 1 being due north or due east and -1 being due south or due west, respectively.

Two types of climatic variables, preseason climates and dates of specific weather events, were computed using Daymet and MOD10A1 products. Preseason climates were weather variables that were either temporally averaged or accumulated during periods immediately preceding SOS and EOS. The temporally averaged climatic variables were daily maximum (TMax) and minimum (TMin) of air temperature during a preseason. These two variables could have different impacts on LSP because SOS may respond more strongly to TMax than TMin (Piao et al., 2015) and TMax and TMin may have inverse effects on EOS (Wu et al., 2018). The temporally accumulated climatic variables were growing degree days (GDD), the number of chilling days (CD), precipitation (Prcp), and shortwave radiation (SRad). GDD and CD have been widely used to characterize the

forcing and chilling requirements, respectively, for vegetation phenology development (Cong et al., 2017; Delpierre et al., 2018; Fu et al., 2015; Richardson et al., 2006). GDD was computed as the sum of daily mean temperatures (TMean; calculated as the average value of TMax and TMin here) above 0 ℃ and the CD was calculated as the number of days with TMean below 0 ℃ over a preseason. To calculate the preseason climates of GDD, CD, TMax, TMin, Prcp, and SRad, the preseason lengths were needed. Practically, the preseason length for each variable was determined by selecting the optimal preseason length from candidates of 30, 60, 90, 120, 150, and 180 days based on the phenological model performance (see Section 3.5).

The dates of specific weather events included three metrics of snow seasonality that included the first snow date (FSD), last snow date (LSD), and duration of snow (DS). For SOS in a given year, we searched for FSD and LSD in an observation window starting on June 21st (the day with the longest day in a year) in the preceding year and ending on June 20th in the given year; and DS was defined as the number of days between FSD and LSD. For EOS in a given year, we searched for FSD in an observation window from June 21st in the given year to June 20th in the succeeding year. Similarly, we generated the metrics of freeze seasonality, which were the first freeze date (FFD), last freeze date (LFD), duration of freeze (DF). Freeze events were defined as dates with a TMin lower than -2 ℃ (Schwartz et al., 2006).

4.3.5. Machine learning for LSP modeling

The machine learning algorithm used to model the spatial and interannual variations of SOS and EOS was the boosted regression tree (BRT) in the “dismo” R package (Hijmans et al., 2017). BRT combines decision tree algorithms and boosting

methods and is able to handle the complex non-linearity and interactions among a large number of continuous and discrete predictors (Elith et al., 2008). BRT employs the strategy of cross-validation to minimize overfitting and optimizes the number of trees based on the deviance reduction in the cross-validation datasets. The performance of BRT modeling is usually evaluated by measuring the pseudo R^2 that is calculated as the percentage of deviance in the cross-validation datasets explained by the model. In addition, BRT provides the relative importance (or contribution) of each predictor variable by measuring the percentage of improvements to the model with the splits of a variable average over all trees (Friedman and Meulman, 2003). Higher values of relative importance indicate stronger influences of a predictor on the response variable. Lastly, BRT can be used to generate the partial dependence plots that show the effect of a predictor on the response after accounting for the average effects of all other variables in the model.

This study investigated SOS and EOS by developing three sets of BRT models, *i.e.*, MODIS spatial models, HLS spatial models, and MODIS interannual models, separately. The predictor variables used in these models were stratified into six categories (Table 4-2): land cover composition, preseason climates, specific weather events, topography, fire-related factors (BS only), and phenological events (SOS only for modeling EOS). Predictors exclusively used for modeling SOS were CD, LFD, DF, LSD, and DS. Because spring phenology may have a positive effect on autumn phenology (Fu et al., 2018; Liu et al., 2016b), SOS was also used as a predictor for modeling EOS. Although all the categories were used in the spatial models, only predictors with interannual variations were applied for the interannual models, which were land cover

composition, preseason climates, specific weather events, and phenological events (for EOS modeling only).

Table 4-2. Predictors used to model the spatial and interannual variations of SOS and EOS.

Category	Predictors	Unit	SOS	EOS
Land cover composition	Vegetation fractional coverage (VFC)*	1	YES	YES
	Tree proportion to vegetation (TPV)*	1	YES	YES
Climate (preseason climates)	Growing degree days (GDD) +*	℃•days	YES	YES
	Chilling days (CD)+*	days	YES	NO
	Maximum temperature (TMax)+*	℃	YES	YES
	Minimum temperature (TMin)+*	℃	YES	YES
	Precipitation (Prcp)+*	mm	YES	YES
	Shortwave radiation (SRad)+*	kW/m2	YES	YES
Climate (specific weather events)	First freeze date (FFD)*	DOY	YES	YES
	Last freeze date (LFD)*	DOY	YES	NO
	Duration of freeze (DF)*	days	YES	NO
	First snow date (FSD)*	DOY	YES	YES
	Last snow date (LSD)*	DOY	YES	NO
	Duration of freeze (DS)*	days	YES	NO
Topography	Elevation	m	YES	YES
	Slope	°	YES	YES
	Northness	1	YES	YES
	Eastness	1	YES	YES
Fire-related factors	Burn severity (BS)	No unit	YES	YES
Phenological events	SOS*	DOY	NO	YES

+These variables with all the six preseason lengths were used in an initial model and the ones with the respective optimal preseason lengths were used in the final model.

*These variables were normalized and used in the MODIS interannual models.

Before developing the models, all the data used in the HLS spatial model were reprojected to the UTM 13N projection with a spatial resolution of 30 m, and all the data used in the MODIS spatial and interannual models were reprojected to the UTM 13N projection with an actual resolution of 480 m (close to the original MODIS pixel size 463.32 m) using nearest neighbor resampling. To develop the HLS spatial models, we randomly selected 10,000 pixels from the total 337,714 pixels with valid observations to reduce computational requirements. For MODIS spatial models, 1,346 pixels with valid observations in 2018 were used to model SOS and EOS. For MODIS interannual models, only the pixels with valid observations in all the years (2001-2018) were used, resulting in a total 21,624 samples (pixel-years).

To develop the interannual models, all the predictor and response variables were normalized within each pixel across years to attenuate the spatial variations(Rodriguez-Galiano et al., 2016). The normalization was a linear transformation conducted for each pixel using the formula:

$$Z_{var_{y,p}} = \frac{var_{y,p} - \overline{var_p}}{SD_p} \quad (1)$$

where $var_{y,p}$ is a variable observed in year y and pixel p, $\overline{var_p}$ is the multi-year average of the variable in pixel p, SD_p is the corresponding standard deviation across years in pixel p, and $Z_{var_{y,p}}$ is the normalized value of the variable in year y and pixel p. The normalized GMax and GRatio were directly used as surrogates of interannual variations of VFC and TPV during 2001-2018, respectively. This was reasonable because linear relationships existed between GMax and VFC as well as between GRatio and TPV (see Sections 3.3 and 4.2).

From the six preseason lengths ranging from 30 to 180 days (Section 3.4), the optimal preseason length was determined using the relative importance in the BRT modeling. Specifically, initial modeling was performed by including all the preseason lengths and the optimal preseason length for each preseason climate predictor was selected as the one with the largest relative importance. The BRT model was performed again using the preseason climates with the selected preseason lengths and other predictor variables.

From the final BRT models, we computed the pseudo-R^2 to evaluate the model performance and the relative importance to assess the contributions of individual variables. Based on the relative importance, we selected the most important variables that presented relative importance above the average (100%/n; n is the number of predictors) (Thorn et al., 2016). The partial dependence plots were generated for these most important variables in each model. We also generated partial dependence plots for TPV and VFC in each BRT model because land cover composition on LSP variations is one of the foci in this study.

4.4. Results

4.4.1. LSP detections from MODIS and HLS

Figure 4-3 displays the spatial pattern of the SOS and EOS in 2018 derived from the 500-m MODIS and 30-m HLS. From both MODIS and HLS, most pixels showed an SOS ranging from DOY 90 to 150 with an average of around DOY 124. Most EOS values ranged from DOY 270 to 330 with an average of around DOY 300. Extremely late SOS (around DOY 200) was located in the western and southwestern edge of the study area from MODIS but scattered in the central and north parts from HLS. Extremely early

EOS (around DOY 240) was mainly found in the west edge from MODIS but the north parts from HLS. SOS and EOS also varied with burn severity (Figure 4-1b). An earlier SOS and later EOS pattern occurred in the high-severity regions to the south and west, while a later SOS and earlier EOS pattern was found in the areas with the unburned/low-severity in the central and northern regions. Although these spatial patterns were similar in both MODIS- and HLS-derived phenology, HLS data revealed larger local variations in SOS and EOS varying with burn severity levels.

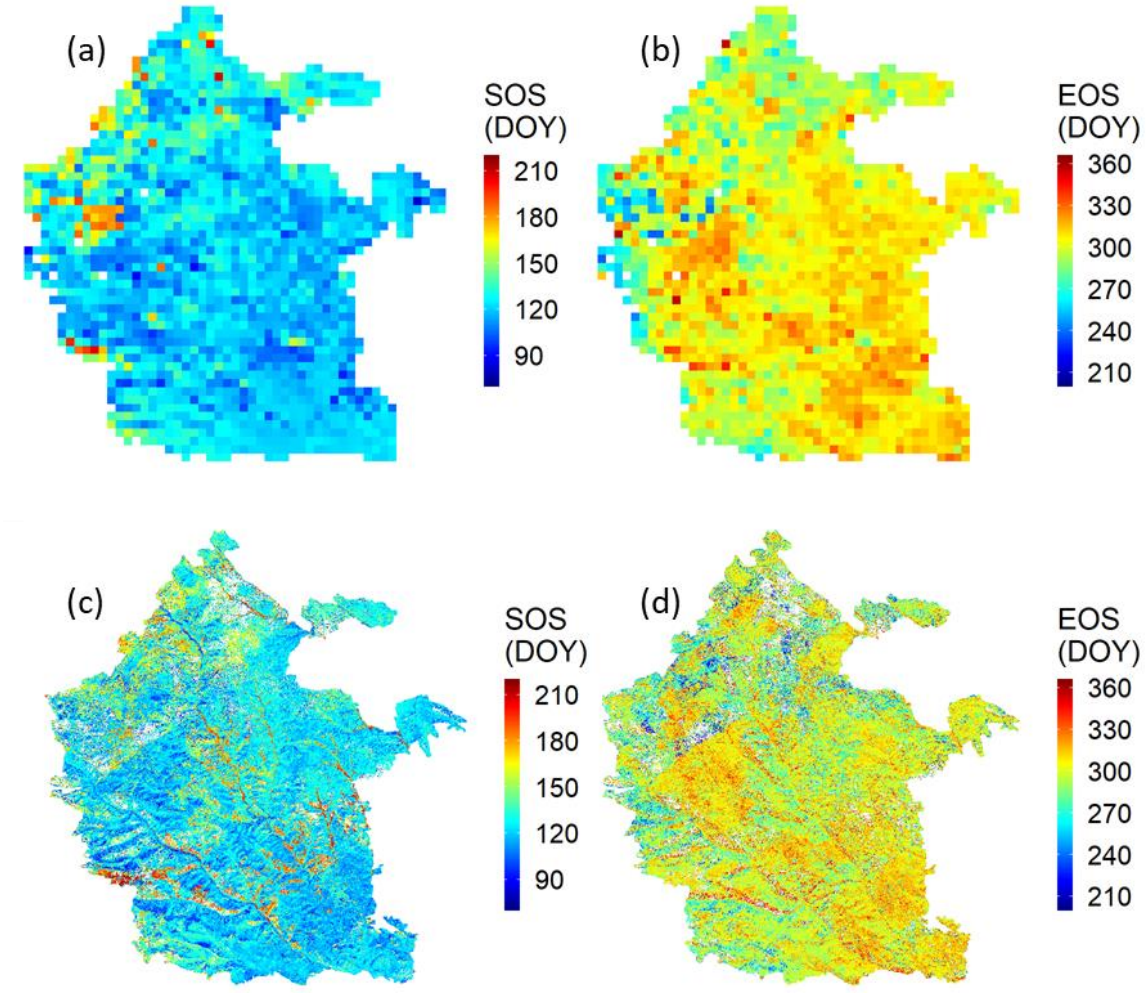

Figure 4-3. Spatial patterns of MODIS-derived SOS (a) and EOS (b) and HLS-derived SOS (c) and EOS (d) in 2018.

SOS and EOS retrieved from the 500-m MODIS were comparable with those aggregated from the 30-m HLS using the "percentile aggregation". For SOS, the 40th percentile obtained the lowest mean absolute deviation (9.4 days) and mean deviation (0.7 days); for EOS, the 60th percentile obtained the lowest mean absolute deviation (8.6 days) and mean deviation (-0.4 days) (Figure 4-4). Larger discrepancies between the two datasets tended to occur in pixels with a later SOS (> DOY 150) and earlier EOS (< DOY 270), where the land cover was mainly the unburned forests.

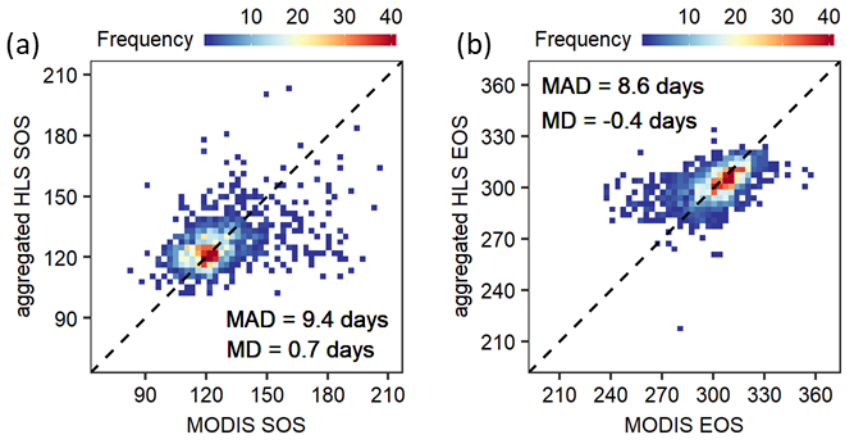

Figure 4-4. Comparisons of SOS (a) and EOS (b) between MODIS and the aggregated HLS in 2018. HLS SOS and EOS were aggregated to the MODIS scale using the 40th and 60th percentile values, respectively, in the sorted HLS observations within a MODIS pixel. The dashed line indicates the 1:1 line. Notations: MAD = mean absolute deviation; and MD = mean deviation.

Figure 4-5 shows the interannual variation of area-aggregated (using average) SOS and EOS across the burned area from MODIS during 2001-2018. LSP detection was

not performed in 2002 because of the interruption of the wildfire occurrence. Before the fire occurrence in 2001, average SOS was on DOY 127. After the fire occurrence, SOS increased slightly with an average value of DOY 130 during 2003-2018 but there was a high interannual variation. The earliest SOS (DOY 116) occurred in 2012 while the latest (DOY 158) occurred in 2013. In contrast, EOS occurred on DOY 277 in 2001 and was largely delayed after the wildfire with an average of DOY 300 and a relatively smaller interannual variation (ranging from DOY 293 and 311).

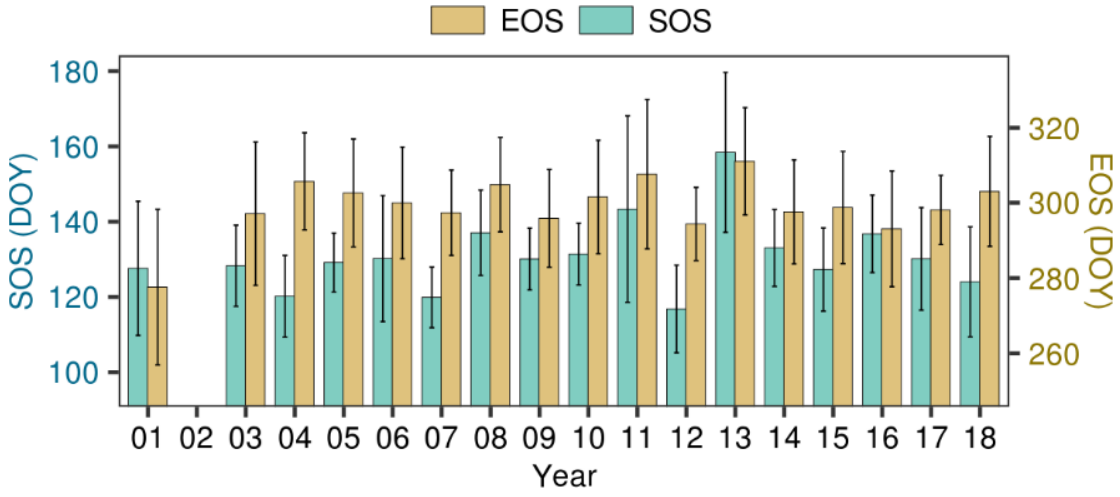

Figure 4-5. Interannual variation in area-aggregated SOS and EOS from MODIS data during 2001-2018. The error bars indicate the spatial standard deviation in each year. The detection was not made in 2002 because of the wildfire occurrence.

4.4.2. Land cover composition and greenness metrics

Maps of land cover composition, i.e., vegetation fractional coverage (VFC) and tree proportion to vegetation (TPV), were developed by aggregating the 3-m classification of 2018 imagery (overall accuracy is 93.9%) (Figure 4-6). Spatial patterns

of VFC and TPV at 30 m and 500 m were similar despite a smoother appearance at the coarser resolution (500 m). The VFC and TPV were closely related to burn severity. In the areas that were unburned/low-severity, VFC and TPV tended to be higher because tree cover was relatively unaffected by the 2002 fire event. In severely burned areas in the southeastern and northwestern regions, TPV was lower due to near-total canopy loss during the fire and a slow rate of tree regeneration (Figures 4-6b, d); VFC was comparatively higher in the southeast part of the fire, indicating faster vegetation recovery than that in the northwest (Figures 4-6a, c). The southeastern portion of the burn area has greater dominance of Gambel oak, a species capable of quickly resprouting from established root systems after fire. The regression analysis indicated that VFC was significantly correlated to the seasonal greenness maximum (GMax; Figure 4-7a, R^2 = 0.31) and TPV was a function of the ratio of greenness minimum to maximum (GRatio; Figure 4-7b, R^2 = 0.56) in 2018 MODIS pixels (500 m). These regressions suggest that GMax and GRatio could be used as proxies of VFC and TPV, respectively, during the 2001-2018 MODIS era.

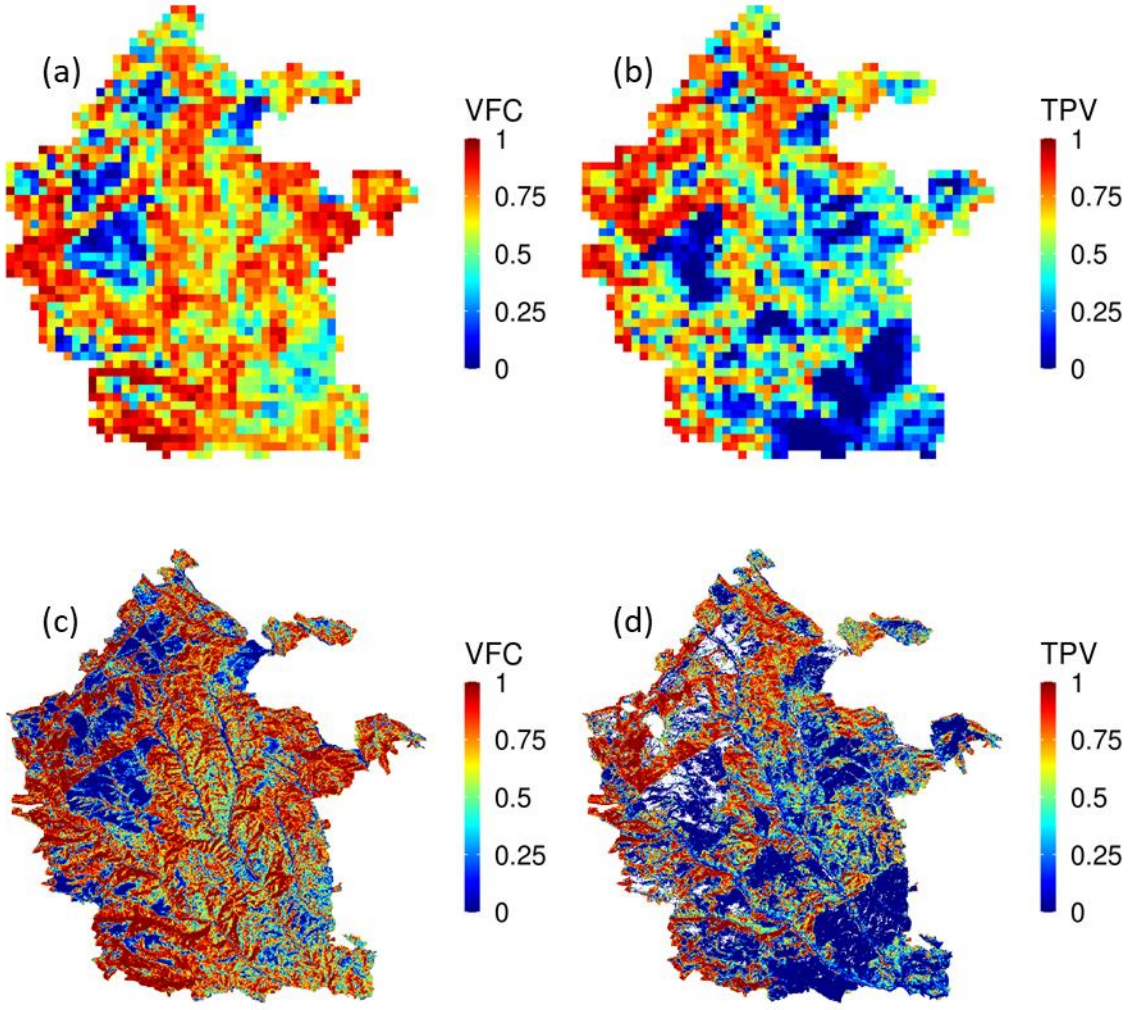

Figure 4-6. Spatial patterns of land cover composition from high-resolution imagery in 2018: VFC (a) and TPV (b) at 500 m and VFC (c) and TPV (d) at 30 m. Note that the gaps in TPV at 30 m (d) were caused by a VFC value of 0.

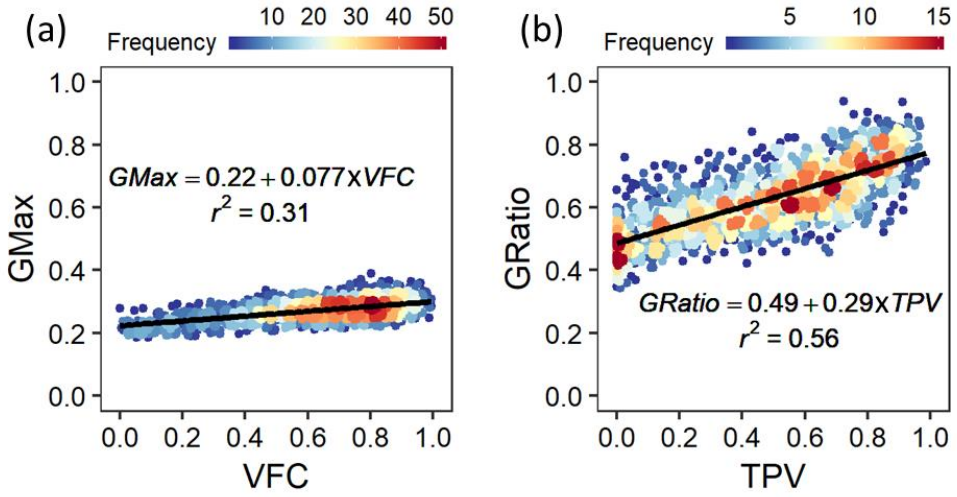

Figure 4-7. The relationships between land cover composition from high-resolution imagery and MODIS-derived greenness metrics in 2018: GMax vs VFC (a) and GRatio vs TPV (b).

Figure 4-8 presents the interannual variation of area-aggregated (using average) greenness of GMax and GRatio from MODIS data during 2001-2018. The range of variation is 0.21-0.31 for GMax and 0.53 to 0.71 for GRatio. The greenness abruptly decreased from 2001 to 2003 because of the fire in 2002, where the reduction was 29% and 8% for GMax and GRatio, respectively. In post-fire years of 2003-2018, GMax increased rapidly while GRatio slightly decreased and had a high interannual variation.

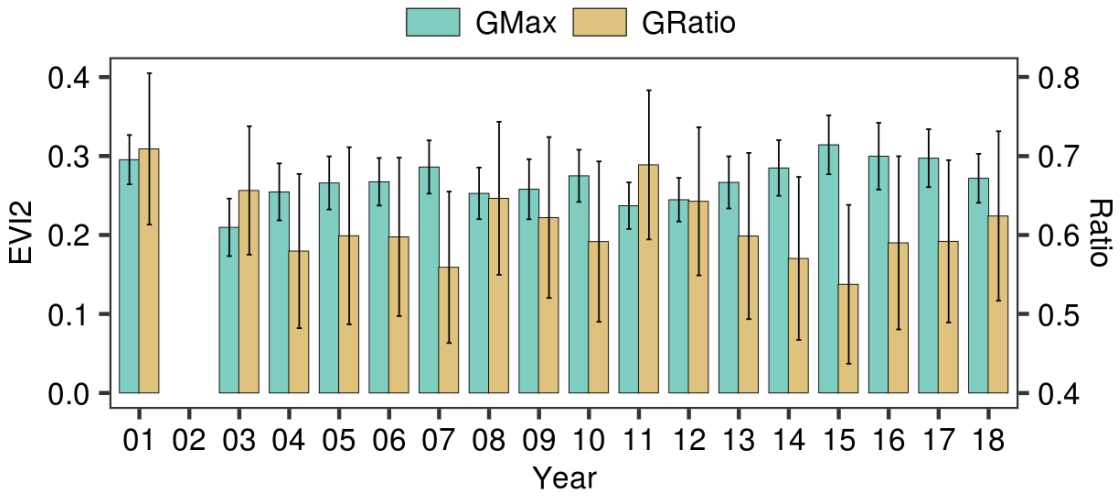

Figure 4-8. Interannual variation in area-aggregated GMax and GRatio from the 500-m MODIS data during 2001-2018. The error bars indicate the spatial standard deviation in each year. The detection was not made in 2002 because of the wildfire occurrence.

4.4.3. MODIS and HLS spatial models

Figure 4-9 shows the pseudo-R^2 and relative importance of each predictor variable in MODIS and HLS spatial models for predicting SOS and EOS. For brevity, the four spatial models are abbreviated as MODIS-SOS for the MODIS spatial model for SOS, MODIS-EOS for the MODIS spatial model for EOS, HLS-SOS for the HLS spatial model for SOS, and HLS-EOS for the HLS spatial model for EOS. Our results indicated that MODIS models had higher pseudo-R^2 values than HLS models. The highest pseudo-R^2 (0.63) was found in the MODIS-EOS, suggesting all the predictors explained 63% of the total deviances in the cross-validation datasets. In contrast, the lowest pseudo-R^2 (0.30) was found in the HLS-EOS.

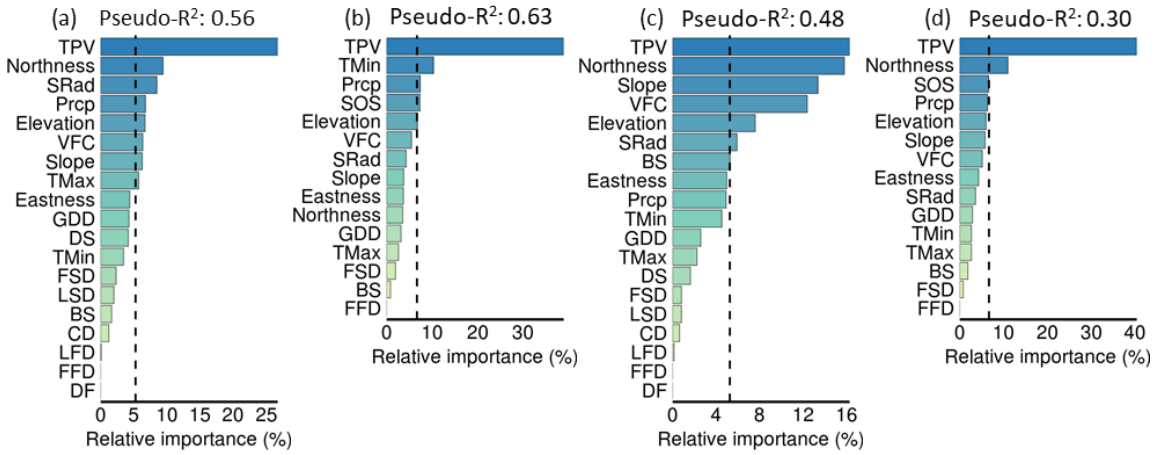

Figure 4-9. The relative importance of predictor variables in MODIS and HLS spatial models derived from BRT analyses of the spatial variation in LSP: MODIS-SOS (a), MODIS-EOS (b), HLS-SOS (c), and HLS-EOS (d). The vertical dashed line marks the average importance. The pseudo-R^2 is shown on the top of each sub-figure. Please refer to Table 4-2 for the full name of each variable.

All the six categories of predictor variables (Table 4-2) were used for EOS modeling and five (SOS itself was excluded) for SOS. Combining the relative importance values from TPV and VFC indicated that land cover composition was the most important factor explaining the spatial variation in all models except for HLS-SOS, with the relative importance value of 33.1% (MODIS-SOS), 44.4% (MODIS-EOS), 28.7% (HLS-SOS), and 45.5% (HLS-EOS). In particular, TPV was the most important predictor in all models with relative importance values of 26.7% (MODIS-SOS), 38.9% (MODIS-EOS), 16.3% (HLS-SOS), and 40.4% (HLS-EOS). VFC also had above-average relative importance in explaining SOS (Figures 4-9a, c) but not EOS (Figures 4-9b, d) from MODIS and HLS.

Northness, a topographic variable, was the second most important predictor of MODIS-SOS (9.4%), HLS-SOS (15.8%), and HLS-EOS (11.0%). Elevation also had

above-average relative importance in all the spatial models except for HLS-EOS. Summing the relative importance values of elevation, slope, northness, and eastness indicated that the topographic variables together explained 26.8% (rank 3 among 5 categories), 17.8% (rank 3/6), 41.8% (rank 1/5), and 45.5% (rank 2/6) of deviance, respectively, in modeling MODIS-SOS, MODIS-EOS, HLS-SOS, and HLS-EOS.

The preseason climates had relative importance values of 29.9% (rank 2/5), 27.8% (rank 2/6), 20.9% (rank 3/5), and 18.2% (rank 3/6) in the four models, respectively. Though no single preseason climate variable had above-average relative importance in all the four models, precipitation and SRad were the two most important variables in the preseason climate category. Other categories of predictors including dates of specific weather events, fire-related factors (burn severity), and phenological factors (SOS) together explained 10.2%, 10.1%, 8.7%, and 9.2% of the deviance of the response variable in modeling MODIS-SOS, MODIS-EOS, HLS-SOS, and HLS-EOS.

Figure 4-10 shows the partial dependence plots of the most important predictors (relative importance value is above average) of MODIS-derived SOS and EOS values. In the MODIS-EOS model, VFC was also included although the importance value was below average. SOS occurred later as TPV increased (Figure 4-10a). Similarly, increases in precipitation (Figure 4-10d) and elevation (Figure 4-10e) were associated with a later SOS. In contrast, increasing northness (Figure 4-10b) and TMax (Figure 4-10h) were associated with an earlier SOS. SOS was earlier at intermediate levels of SRad (Figure 4-10c), and SOS had no clear relationship with VFC (Figure 4-10f) or slope (Figure 4-10g). EOS occurred later with increases in TMin (Figure 4-10j), higher precipitation (Figure 4-10k), and lower values of TPV (Figure 4-10i). Similarly, EOS occurred later with earlier

SOS (Figure 4-10l), at higher elevations (Figure 4-10m), and higher values of VFC (Figure 4-10n). Note that partial dependence plots for HLS models are not presented here because they showed similar trends to MODIS models for the most important variables.

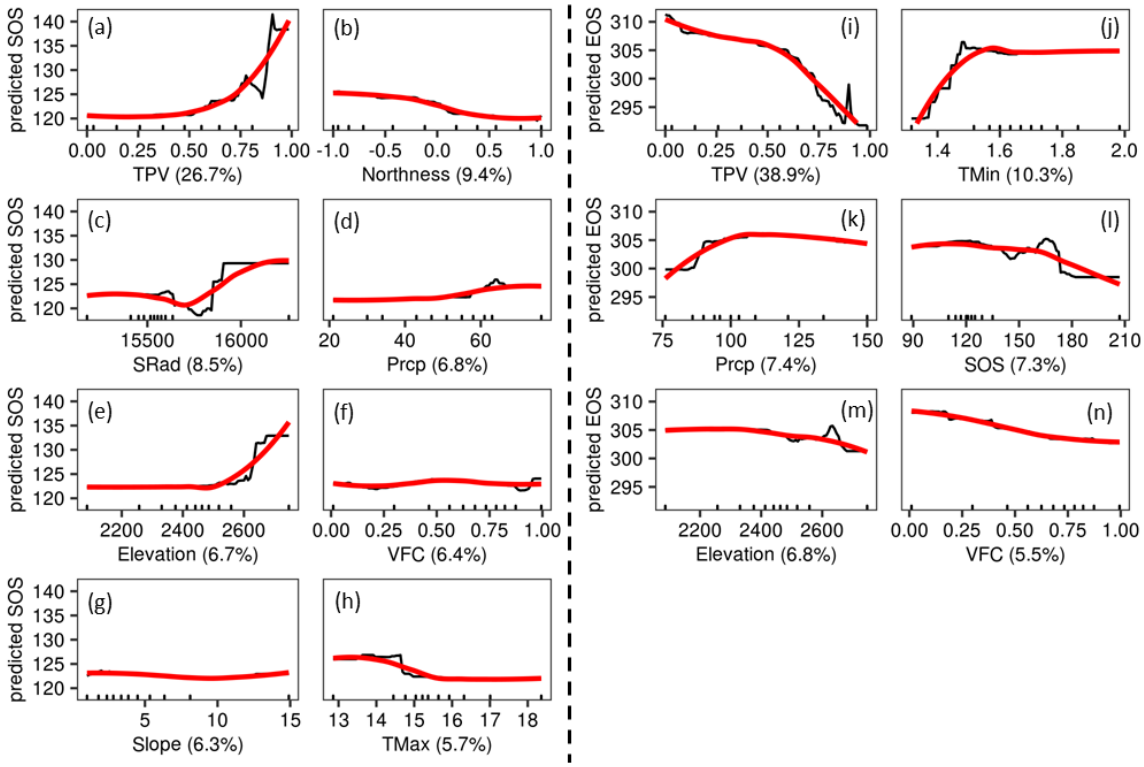

Figure 4-10. Partial dependence plots for the most important predictors in BRT analyses of spatial variation in MODIS-derived SOS (the left panel) and EOS (the right panel). Variables for SOS include TPV (a), northness (b), SRad (c), Prcp (d), elevation (e), VFC (f), slope (g), and TMax (h); variables for EOS include TPV (i), TMin (j), Prcp (k), SOS (l), elevation (m), and VFC (n). The unit of each variable can be found in Table 4-2. The numbers in the parentheses are the relative importance values. The red lines are the smoothed partial dependence functions. X-axis rugs mark the deciles in the distribution of values for each predictor variable. Please refer to Table 4-2 for the full name of each variable.

4.4.4. MODIS interannual models

Figure 4-11 shows the pseudo-R^2 and relative importance of each predictor variable in the interannual models of MODIS-SOS and EOS. Compared to the BRT models of spatial variation in LSP (Figure 4-9), MODIS interannual models had higher pseudo-R^2 values (0.80 and 0.76 for SOS and EOS, respectively). We used three categories of predictors (land cover composition, preseason climates, specific events) for the SOS model and four categories (adding the phenological variable - SOS) for EOS. Summing up the relative importance values in each predictor category, we found that predictors related to preseason climate were most important in modeling interannual variations of SOS (64.5%) and EOS (49%), followed by specific weather events (21.3% for SOS and 23.7% for EOS), land cover composition (14.1% for SOS and 20.1% for EOS), and phenological (7.21% for EOS). The predictors with above-average importance values in modeling SOS were the growing degree days (GDD; 25.1%), TMax (11.3%), chilling days (CD; 10.6%), and vegetation fractional coverage (VFC; 7.8%). The predictors with above-average importance values in modeling EOS were the first freeze date (FFD; 18.2%), SRad (14.8%), VFC (11.3%), and GDD (11.1%).

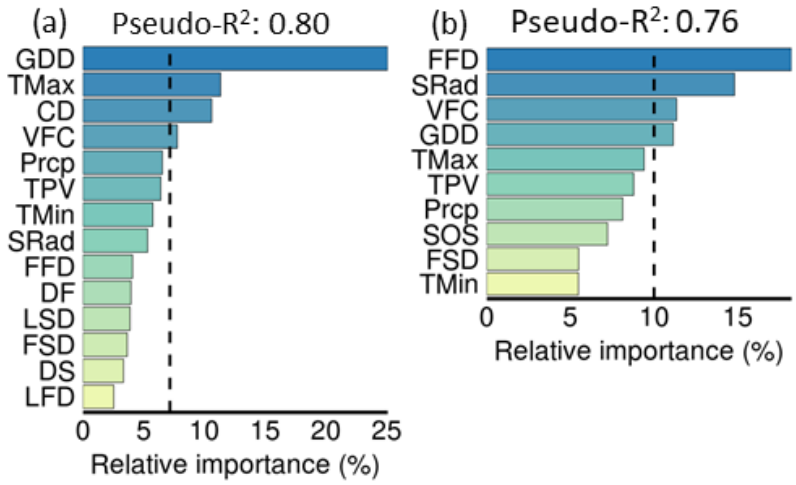

Figure 4-11. The relative importance of the predictor variables in MODIS interannual models: SOS (a) and EOS (b). The vertical dashed line marks the average importance. The pseudo-R2 is shown on the top of each sub-figure. Please refer to Table 4-2 for the full name of each variable.

Figure 4-12 gives the partial dependence plots for the most important variables (above-average relative importance) of interannual variation in MODIS-SOS and EOS (normalized using pixel-specific means and standard deviations). TPV (for SOS and EOS) and SOS (for EOS) were also included although the importance values were below average. SOS occurred later with increases in VFC (Figure 4-12d) and TPV (Figure 4-12e). In contrast, SOS occurred earlier with lower GDD (Figure 4-12a), lower TMax (Figure 4-12b), and fewer CD (Figure 4-12c). EOS occurred later with a later FFD (Figure 4-12f) and SOS (Figure 4-12k), and occurred earlier with higher SRad (Figure 4-12g), VFC (Figure 4-12h), more GDD (Figure 4-12i), and greater TPV (Figure 4-12j).

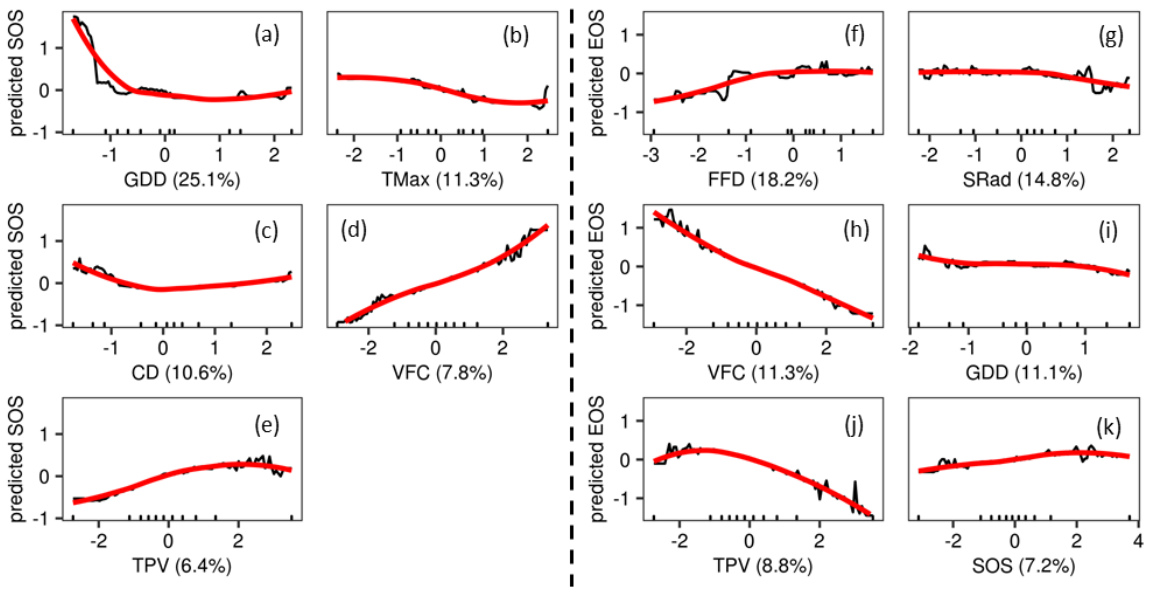

Figure 4-12. Partial dependence plots of the normalized SOS (the left panel) and EOS (the right panel) predicted using the MODIS interannual models with the selected important variables. Variables for SOS include GDD (a), TMax (b), CD (c), VFC (d), and TPV (e); variables for EOS include FFD (f), SRad (g), VFC (h), GDD (i), TPV (j), and SOS (k). The numbers in the parentheses are the relative importance values. The red lines are the smoothed partial dependence functions. X-axis rugs mark the deciles in the distribution of values in each predictor variable. Please refer to Table 4-2 for the full name of each variable.

4.5. Discussion

Using the site of the 2002 Ponil Complex Fire, a dynamic landscape with broad spatial and interannual variation in land cover composition, this study for the first time quantitatively explored the role of land cover composition (vegetation fractional coverage and tree proportion to vegetation) – alongside factors related to climate, topography, and disturbance severity – in shaping spatial and interannual variation in SOS and EOS. For this purpose, we used boosted regression tree (BRT), a machine learning method, to

model the LSP derived from the 500-m MODIS and 30-m HLS data with six categories of predictor variables: land cover composition, preseason climates, specific weather events, topography, fire-related factors (BS only), and phenological events (SOS only). The novelty of this study lies in three aspects. First, the usage of BRT allowed for LSP modeling to link phenological responses to a large number of predictors with nonlinear relationships and interactions among predictors (Figures 4-10 and 12). Moreover, BRT allows the calculation of relative importance with which the contribution of each predictor can be easily ranked and partial dependence plots with which the relationship between each predictor and LSP can be analyzed after accounting for the effects of all other predictors. Second, the modeling of spatial variation in LSP was compared at two scales: 500 m (MODIS) and 30 m (HLS), which deepens the understanding of the effects of phenological drivers across spatial scales. Last, the innovative usage of greenness metrics (GMax and GRatio) in the interannual LSP modeling effectively characterized the contribution of interannual variation in land cover composition, which is particularly important in post-disturbance landscapes.

4.5.1. Modelling of LSP spatial variations

Land cover composition plays a significant role in the spatial variation of LSP (Cho et al., 2017; Misra et al., 2018). The present study also found that land cover composition was the most important of the six categories considered and TPV was the most important variable among the 20 predictors of spatial variation in SOS and EOS. The pixels with higher TPVs are likely to have a later SOS and an earlier EOS, which indicates the difference in timing of greenness development between the understory and canopy vegetation in the study area and aligns with a previous study (Wang and Zhang,

2017). Moreover, land cover composition is more important in influencing the spatial variation in EOS than that in SOS, because EOS exhibits much larger variations among different species than SOS does (Cho et al., 2017; Hill et al., 2010; Misra et al., 2018; Pasquarella et al., 2018; Wang and Zhang, 2020).

Topography is also considered as an important driver of spatial variation in LSP (An et al., 2018). It affects LSP by influencing topoclimate, soil nutrients, and moisture, and plant species distributions (Berryman et al., 2015; Dobrowski, 2011; Hwang et al., 2011; Rodman et al., 2019). Topography in this study was ranked as the second or third important predictor category (depending on the scale of 30 m or 500 m of the data used) in modeling LSP spatial variations. As expected, SOS occurred later and EOS occurred earlier at higher elevations. This study also found that SOS was earlier on north-facing slopes, which may be associated with the higher soil moisture inherent to north slopes (An et al., 2018; Rodman et al., 2019).

Preseason climates also play a significant role in controlling the spatial variations of LSP. Not surprisingly, SOS tended to be earlier with higher TMax and EOS tended to be later with increasing TMin. Interestingly, SOS tended to be earlier at intermediate levels of shortwave radiation (SRad), which could be due to the balance between the required radiation forcing and soil moisture (excessive radiation could reduce the soil moisture) (Lutz et al., 2010).

Other categories of variables have relatively small contributions to variation in LSP. In particular, EOS has a negative relationship with SOS in space (Figure 4-10l), because an earlier greenup is likely to occur in shrub/grass which tends to have a later senescence in the study area (Figures 4-10a and i). It is also worth noting that this study

found little effect of burn severity on the spatial LSP variations, which seems to contradict previous findings from burned areas throughout the western US (Wang and Zhang, 2020). This is because this study separated burn severity from other variables (land cover composition, climate, and topography) in LSP modeling while Wang and Zhang (2020) used the burn severity as a surrogate of wildfire-caused land cover change and minimized the effects of climate and topography by using the pre-fire unburned buffer as an LSP reference. In particular, land cover composition is a more direct representation of the pathway by which fire alters LSP by altering vegetation.

The MODIS and HLS spatial models show the scale-dependent effects of environmental variables on LSP. The spatial models explained more LSP variations at the 500-m scale (56% for SOS and 63% for EOS) than the 30-m scale (48% for SOS and 30% for EOS). This finding could be because the 1-km resolution climate variables more closely align with the analytical scale of the 500-m LSP than the 30-m LSP. Moreover, LSP could also be related to several additional factors not included in this study, such as soil nutrients and water availability (Arend et al., 2015; Estiarte and Peñuelas, 2015; Fay et al., 2012). A coarse pixel could smooth the variation in these fine-scale drivers and increase the explanatory power of macroclimate.

4.5.2. Modelling of LSP interannual variations

Overall, the MODIS interannual models explained 76-80% of LSP variation from 2001-2018. Noticeably, land cover composition still plays an important role in controlling the interannual variations of LSP (Figure 4-11). Both VFC and TPV had above-average relative importance for modeling interannual variation in SOS and EOS. Similar to the spatial models, the increase in TPV led to non-linear trends of a later SOS

and earlier EOS. Moreover, the increase in VFC caused trends of a later SOS and earlier EOS. This influence is biophysically unclear, but one possible cause is that denser vegetation could cool down the land surface (Liu et al., 2019) and reduce light availability for herbaceous plants. Like the spatial models, land cover composition played a more important role in affecting EOS than SOS.

As expected, preseason climate factors were the main drivers of the interannual variation in LSP. The three climatic variables with above-average relative importance for SOS were all temperature-based: GDD, TMax, and CD, suggesting the dominant role of temperature on the interannual variations of SOS in the study area. In particular, the considerable contributions of GDD and CD indicate the importance of forcing and chilling requirements in modeling the interannual variations of SOS (Cong et al., 2017; Delpierre et al., 2018; Richardson et al., 2006). The larger contribution of TMax than TMin confirms the finding that daytime temperature has a stronger effect than nighttime temperature on SOS (Piao et al., 2015). Interestingly, the most important driver of interannual variation in EOS is the first freeze date (FFD). The FFD impact has been rarely considered in previous studies (Rodriguez-Galiano et al., 2016). Following FFD, the preseason SRad and GDD also play a role in controlling the interannual EOS variations. The earlier EOS with the increase of SRad and GDD could be related to the soil moisture reduction (Wu et al., 2018).

This study also revealed that the early phenological events could have an influence on later events during a vegetation growing season. Specifically, a positive relationship of interannual variations of EOS against SOS was found in this study (Figure 4-12), which is supported by previous research (Fu et al., 2018; Liu et al., 2016b). An

earlier EOS could result from the risks of spring frost and summer drought that are increased by an earlier SOS (Buermann et al., 2013; Hufkens et al., 2012; Lian et al., 2020). The within-year relationship of a later SOS and EOS maintains a relatively stable growing season length and may reduce the effect of climate warming on terrestrial carbon sequestration (Richardson et al., 2012).

4.5.3. Implications and limitations.

This study significantly improves the understanding of drivers and mechanisms of phenological dynamics with several interesting and important findings. First and most importantly, land cover composition plays a non-negligible role in both spatial and interannual variations of LSP. This is particularly important in predicting future phenological changes because land cover changes are occurring across much of the Earth. Overlooking the effects of land cover composition is likely to lead to biases in vegetation phenology prediction and further impair the reliability of terrestrial biosphere models (Richardson et al., 2012). Thus, caution is needed to predict or relate the LSP with climate in areas where land cover composition tends to be dynamic, such as disturbed areas (Wang and Zhang, 2020), agricultural areas (Zhang et al., 2019), and arid/semi-arid areas where degradation is common (Diouf and Lambin, 2001).

Second, we found that the first freeze date was the most important predictor of interannual variations of EOS (Figure 4-11), with greater importance than preseason radiation (a proxy of photoperiod), temperature, and precipitation that have been found to be the main drivers of EOS variation in previous studies (Liu et al., 2016a; Yang et al., 2015). Here we recommend that future studies should take the first freeze date into

account when modeling EOS and test the influence of freeze seasonality in different areas across the globe.

Last, the influence of a driver to LSP depends on the applied scale and dimension (temporal or spatial). For example, topography has more contribution to controlling the LSP variation at a resolution of 30 m than 500 m; the relationship between EOS and SOS is negative in the spatial model (Figure 4-10), while it is positive in the interannual model (Figure 4-12). Thus, clear definitions of scale and dimension are crucial in future studies that evaluate the influence of different drivers on LSP variation.

We also acknowledge there are still a few limitations in this study. First, the effectiveness of using GMax and GRatio as surrogates of VFC and TPV has not been directly evaluated because of the limited availability of high-resolution imagery. Future studies may take advantage of the continual accumulation of high-resolution imagery to perform a strict evaluation. Second, the spatial models were based on data in the single year of 2018, which could cause some uncertainties. However, using a multi-year average of LSP to reduce uncertainty as done in previous studies (e.g., Misra et al., 2018) was not a reasonable approach for our study because land cover composition is dynamic in post-fire landscapes (Rodman et al., 2019). Third, although Daymet data is one of the highest-resolution climate datasets available in the study area, the resolution (1 km) is still relatively coarse which may have impacts on model performance. Last, the analysis was performed at a landscape scale, which might not be enough to obtain a general conclusion on the way that different factors drive LSP across heterogeneous regions. A larger-scale study might be needed in the future.

4.6. Conclusions

Using a machine learning approach, this study for the first time quantitatively assessed the contributions of two important land cover composition metrics, *i.e.*, vegetation fractional coverage (VFC) and tree proportion to vegetation (TPV), to both spatial and interannual variations of SOS and EOS with the comparison with other factors mainly including climate and topography. Spatial models for SOS and EOS using HLS and MODIS data in 2018 revealed that land cover composition, particularly TPV, was the most important driver of spatial variation in LSP, immediately followed by topography (in the HLS spatial models) and preseason climates (in the MODIS spatial models). In the topographical variables, northness and elevation showed above-average importance in three of the four spatial models. In the preseason climates, shortwave radiation and precipitation were the most important drivers of LSP although none of them showed dominance. All the other drivers including dates of specific weather events, fire-related factors, and phenological factors contributed little to LSP variations. Based on the interannually normalized predictors and responses, the interannual models of SOS and EOS from MODIS in 2001-2018 found the growing degree days (GDD) and the first freeze date (FFD) were the most important drivers, respectively, for SOS and EOS. However, VFC played a non-negligible role with above-average relative importance in modeling SOS and EOS. Moreover, the models for both spatial and interannual LSP variations also revealed a stronger influence of land cover composition in EOS than SOS. Overall, this study suggests that land cover composition metrics have a substantial effect on spatial and interannual variations of LSP and should not be overlooked in predicting land surface phenology.

Acknowledgments

This work was supported by NASA contract 80NSSC18K0626. Thanks to the google earth engine (GEE) team.

Reference

An, S., Zhang, X., Chen, X., Yan, D., Henebry, G.M., 2018. An exploration of terrain effects on land surface phenology across the Qinghai–Tibet plateau using Landsat ETM+ and OLI data. Remote Sens. 10, 1069.

Arend, M., Gessler, A., Schaub, M., 2015. The influence of the soil on spring and autumn phenology in European beech. Tree Physiol. 36, 78–85.

Arthur, D., Vassilvitskii, S., 2006. k-means++: The advantages of careful seeding. Stanford.

Augspurger, C.K., Cheesman, J.M., Salk, C.F., 2005. Light gains and physiological capacity of understorey woody plants during phenological avoidance of canopy shade. Funct. Ecol. 19, 537–546. https://doi.org/10.1111/j.1365-2435.2005.01027.x

Berryman, E.M., Barnard, H.R., Adams, H.R., Burns, M.A., Gallo, E., Brooks, P.D., 2015. Complex terrain alters temperature and moisture limitations of forest soil respiration across a semiarid to subalpine gradient. J. Geophys. Res. Biogeosciences 120, 707–723. https://doi.org/10.1002/2014JG002802

Betancourt, J.L., Schwartz, M.D., Breshears, D.D., Cayan, D.R., Dettinger, M.D., Inouye, D.W., Post, E., Reed, B.C., 2005. Implementing a US national phenology network. Eos, Trans. Am. Geophys. Union 86, 539.

Bond-Lamberty, B., Rocha, A. V, Calvin, K., Holmes, B., Wang, C., Goulden, M.L.,

2014. Disturbance legacies and climate jointly drive tree growth and mortality in an intensively studied boreal forest. Glob. Chang. Biol. 20, 216–227.

Buermann, W., Bikash, P.R., Jung, M., Burn, D.H., Reichstein, M., 2013. Earlier springs decrease peak summer productivity in North American boreal forests. Environ. Res. Lett. 8, 24027.

Cao, R., Chen, J., Shen, M., Tang, Y., 2015. An improved logistic method for detecting spring vegetation phenology in grasslands from MODIS EVI time-series data. Agric. For. Meteorol. 200, 9–20. https://doi.org/10.1016/j.agrformet.2014.09.009

Chen, J., Jönsson, P., Tamura, M., Gu, Z., Matsushita, B., Eklundh, L., 2004. A simple method for reconstructing a high-quality NDVI time-series data set based on the Savitzky-Golay filter. Remote Sens. Environ. 91, 332–344. https://doi.org/10.1016/j.rse.2004.03.014

Chen, X., Wang, D., Chen, J., Wang, C., Shen, M., 2018. The mixed pixel effect in land surface phenology: A simulation study. Remote Sens. Environ. 211, 338–344. https://doi.org/10.1016/j.rse.2018.04.030

Chmielewski, F.-M., Rötzer, T., 2001. Response of tree phenology to climate change across Europe. Agric. For. Meteorol. 108, 101–112. https://doi.org/https://doi.org/10.1016/S0168-1923(01)00233-7

Cho, M.A., Ramoelo, A., Dziba, L., 2017. Response of Land Surface Phenology to Variation in Tree Cover during Green-Up and Senescence Periods in the Semi-Arid Savanna of Southern Africa. Remote Sens. 9, 689. https://doi.org/10.3390/rs9070689

Claverie, M., Ju, J., Masek, J.G., Dungan, J.L., Vermote, E.F., Roger, J.C., Skakun, S. V.,

Justice, C., 2018. The Harmonized Landsat and Sentinel-2 surface reflectance data set. Remote Sens. Environ. 219, 145–161. https://doi.org/10.1016/j.rse.2018.09.002

Cober, E.R., Curtis, D.F., Stewart, D.W., Morrison, M.J., 2014. Quantifying the effects of photoperiod, temperature and daily irradiance on flowering time of soybean isolines. Plants 3, 476–497.

Cong, N., Shen, M., Piao, S., Chen, X., An, S., Yang, W., Fu, Y.H., Meng, F., Wang, T., 2017. Little change in heat requirement for vegetation green-up on the Tibetan Plateau over the warming period of 1998-2012. Agric. For. Meteorol. 232, 650–658. https://doi.org/10.1016/j.agrformet.2016.10.021

Czernecki, B., Nowosad, J., Jabłońska, K., 2018. Machine learning modeling of plant phenology based on coupling satellite and gridded meteorological dataset. Int. J. Biometeorol. 62, 1297–1309. https://doi.org/10.1007/s00484-018-1534-2

Dai, W., Jin, H., Zhang, Y., Liu, T., Zhou, Z., 2019. Detecting temporal changes in the temperature sensitivity of spring phenology with global warming: Application of machine learning in phenological model. Agric. For. Meteorol. 279, 107702. https://doi.org/10.1016/j.agrformet.2019.107702

De'ath, G., 2007. Boosted trees for ecological modeling and prediction. Ecology 88, 243–251. https://doi.org/10.1890/0012-9658(2007)88[243:BTFEMA]2.0.CO;2

de Beurs, K.M., Henebry, G.M., 2004. Land surface phenology, climatic variation, and institutional change: Analyzing agricultural land cover change in Kazakhstan. Remote Sens. Environ. 89, 497–509. https://doi.org/10.1016/j.rse.2003.11.006

Delbart, N., Kergoat, L., Le Toan, T., Lhermitte, J., Picard, G., 2005. Determination of phenological dates in boreal regions using normalized difference water index.

Remote Sens. Environ. 97, 26–38.

Delpierre, N., Lireux, S., Hartig, F., Camarero, J.J., Cheaib, A., Čufar, K., Cuny, H., Deslauriers, A., Fonti, P., Gričar, J., Huang, J.-G.J., Krause, C., Liu, G., de Luis, M., Mäkinen, H., Martinez del Castillo, E., Morin, H., Nöjd, P., Oberhuber, W., Prislan, P., Rossi, S., Saderi, S., Treml, V., Vavrick, H., Rathgeber, C.B.K., Luis, M. de, Mäkinen, H., Castillo, E.M. del, Morin, H., Nöjd, P., Oberhuber, W., Prislan, P., Rossi, S., Saderi, S., Treml, V., Vavrick, H., Rathgeber, C.B.K., 2018. Chilling and forcing temperatures interact to predict the onset of wood formation in Northern Hemisphere conifers. Glob. Chang. Biol. 0. https://doi.org/10.1111/gcb.14539

Diouf, A., Lambin, E.F., 2001. Monitoring land-cover changes in semi-arid regions: remote sensing data and field observations in the Ferlo, Senegal. J. Arid Environ. 48, 129–148. https://doi.org/https://doi.org/10.1006/jare.2000.0744

Dobrowski, S.Z., 2011. A climatic basis for microrefugia: the influence of terrain on climate. Glob. Chang. Biol. 17, 1022–1035. https://doi.org/10.1111/j.1365-2486.2010.02263.x

Eidenshink, J., Schwind, B., Brewer, K., Zhu, Z., Quayle, B., Howard, S., 2007. A Project for Monitoring Trends in Burn Severity. Fire Ecol. 3, 3–21. https://doi.org/10.4996/fireecology.0301003

Elith, J., Leathwick, J.R., Hastie, T., 2008. A working guide to boosted regression trees. J. Anim. Ecol. 77, 802–813. https://doi.org/10.1111/j.1365-2656.2008.01390.x

Estiarte, M., Peñuelas, J., 2015. Alteration of the phenology of leaf senescence and fall in winter deciduous species by climate change: effects on nutrient proficiency. Glob. Chang. Biol. 21, 1005–1017.

Farr, T.G., Rosen, P.A., Caro, E., Crippen, R., Duren, R., Hensley, S., Kobrick, M., Paller, M., Rodriguez, E., Roth, L., Seal, D., Shaffer, S., Shimada, J., Umland, J., Werner, M., Oskin, M., Burbank, D., Alsdorf, D., 2007. The Shuttle Radar Topography Mission. Rev. Geophys. 45. https://doi.org/10.1029/2005RG000183

Fay, P.A., Jin, V.L., Way, D.A., Potter, K.N., Gill, R.A., Jackson, R.B., Polley, H.W., 2012. Soil-mediated effects of subambient to increased carbon dioxide on grassland productivity. Nat. Clim. Chang. 2, 742–746.

Friedman, J.H., Meulman, J.J., 2003. Multiple additive regression trees with application in epidemiology. Stat. Med. 22, 1365–1381.

Fu, Y., He, H.S., Zhao, J., Larsen, D.R., Zhang, H., Sunde, M.G., Duan, S., 2018. Climate and spring phenology effects on autumn phenology in the Greater Khingan Mountains, northeastern China. Remote Sens. 10. https://doi.org/10.3390/rs10030449

Fu, Y.H., Piao, S., Op de Beeck, M., Cong, N., Zhao, H., Zhang, Y., Menzel, A., Janssens, I.A., 2014. Recent spring phenology shifts in western Central Europe based on multiscale observations. Glob. Ecol. Biogeogr. 23, 1255–1263. https://doi.org/10.1111/geb.12210

Fu, Y.H., Piao, S., Vitasse, Y., Zhao, H., De Boeck, H.J., Liu, Q., Yang, H., Weber, U., Hänninen, H., Janssens, I.A., 2015. Increased heat requirement for leaf flushing in temperate woody species over 1980–2012: effects of chilling, precipitation and insolation. Glob. Chang. Biol. 21, 2687–2697. https://doi.org/10.1111/gcb.12863

Gao, B.-C., 1996. NDWI—A normalized difference water index for remote sensing of vegetation liquid water from space. Remote Sens. Environ. 58, 257–266.

Geng, X., Fu, Y.H., Hao, F., Zhou, X., Zhang, X., Yin, G., Vitasse, Y., Piao, S., Niu, K., De Boeck, H.J., Menzel, A., Peñuelas, J., 2020. Climate warming increases spring phenological differences among temperate trees. Glob. Chang. Biol. n/a. https://doi.org/10.1111/gcb.15301

Gorelick, N., Hancher, M., Dixon, M., Ilyushchenko, S., Thau, D., Moore, R., 2017. Google Earth Engine: Planetary-scale geospatial analysis for everyone. Remote Sens. Environ. 202, 18–27. https://doi.org/10.1016/j.rse.2017.06.031

Hall, D.K., Riggs, G.A., Salomonson, V. V, DiGirolamo, N.E., Bayr, K.J., 2002. MODIS snow-cover products. Remote Sens. Environ. 83, 181–194.

Hijmans, R.J., Phillips, S., Leathwick, J., Elith, J., Hijmans, M.R.J., 2017. Package 'dismo.' Circles 9, 1–68.

Hill, R.A., Wilson, A.K., George, M., Hinsley, S.A., 2010. Mapping tree species in temperate deciduous woodland using time-series multi-spectral data. Appl. Veg. Sci. 13, 86–99. https://doi.org/10.1111/j.1654-109X.2009.01053.x

Huete, A., Didan, K., Miura, T., Rodriguez, E.P., Gao, X., Ferreira, L.G., 2002. Overview of the radiometric and biophysical performance of the MODIS vegetation indices. Remote Sens. Environ. 83, 195–213. https://doi.org/http://dx.doi.org/10.1016/S0034-4257(02)00096-2

Hufkens, K., Friedl, M.A., Keenan, T.F., Sonnentag, O., Bailey, A., O'Keefe, J., Richardson, A.D., 2012. Ecological impacts of a widespread frost event following early spring leaf-out. Glob. Chang. Biol. 18, 2365–2377.

Hwang, T., Song, C., Vose, J.M., Band, L.E., 2011. Topography-mediated controls on local vegetation phenology estimated from MODIS vegetation index. Landsc. Ecol.

26, 541–556.

Jeong, S.J., Ho, C.H., Gim, H.J., Brown, M.E., 2011. Phenology shifts at start vs. end of growing season in temperate vegetation over the Northern Hemisphere for the period 1982-2008. Glob. Chang. Biol. 17, 2385–2399. https://doi.org/10.1111/j.1365-2486.2011.02397.x

Jiang, Z., Huete, A.R., Didan, K., Miura, T., 2008. Development of a two-band enhanced vegetation index without a blue band. Remote Sens. Environ. 112, 3833–3845. https://doi.org/http://dx.doi.org/10.1016/j.rse.2008.06.006

Jolly, W.M., Running, S.W., 2004. Effects of precipitation and soil water potential on drought deciduous phenology in the Kalahari. Glob. Chang. Biol. 10, 303–308.

Laughlin, D.C., Bakker, J.D., Stoddard, M.T., Daniels, M.L., Springer, J.D., Gildar, C.N., Green, A.M., Covington, W.W., 2004. Toward reference conditions: wildfire effects on flora in an old-growth ponderosa pine forest. For. Ecol. Manage. 199, 137–152. https://doi.org/10.1016/j.foreco.2004.05.034

Li, J., Roy, D.P., 2017. A global analysis of Sentinel-2A, Sentinel-2B and Landsat-8 data revisit intervals and implications for terrestrial monitoring. Remote Sens. 9, 902. https://doi.org/10.3390/rs9090902

Lian, X., Piao, S., Li, L.Z.X., Li, Y., Huntingford, C., Ciais, P., Cescatti, A., Janssens, I.A., Peñuelas, J., Buermann, W., 2020. Summer soil drying exacerbated by earlier spring greening of northern vegetation. Sci. Adv. 6, eaax0255.

Liang, L., Schwartz, M.D., Fei, S., 2011. Validating satellite phenology through intensive ground observation and landscape scaling in a mixed seasonal forest. Remote Sens. Environ. 115, 143–157. https://doi.org/https://doi.org/10.1016/j.rse.2010.08.013

Liu, Q., Fu, Y.H., Liu, Y., Janssens, I.A., Piao, S., 2018. Simulating the onset of spring vegetation growth across the Northern Hemisphere. Glob. Chang. Biol. 24, 1342–1356. https://doi.org/10.1111/gcb.13954

Liu, Q., Fu, Y.H., Zeng, Z., Huang, M., Li, X., Piao, S., 2016a. Temperature, precipitation, and insolation effects on autumn vegetation phenology in temperate China. Glob. Chang. Biol. 22, 644–655. https://doi.org/10.1111/gcb.13081

Liu, Q., Fu, Y.H., Zhu, Z., Liu, Y., Liu, Z., Huang, M., Janssens, I.A., Piao, S., 2016b. Delayed autumn phenology in the Northern Hemisphere is related to change in both climate and spring phenology. Glob. Chang. Biol. 22, 3702–3711. https://doi.org/10.1111/gcb.13311

Liu, Z., Ballantyne, A.P., Cooper, L.A., 2019. Biophysical feedback of global forest fires on surface temperature. Nat. Commun. 10, 214. https://doi.org/10.1038/s41467-018-08237-z

Luedeling, E., Gassner, A., 2012. Partial Least Squares Regression for analyzing walnut phenology in California. Agric. For. Meteorol. 158–159, 43–52. https://doi.org/https://doi.org/10.1016/j.agrformet.2011.10.020

Lutz, J.A., van Wagtendonk, J.W., Franklin, J.F., 2010. Climatic water deficit, tree species ranges, and climate change in Yosemite National Park. J. Biogeogr. 37, 936–950. https://doi.org/10.1111/j.1365-2699.2009.02268.x

Melaas, E.K., Friedl, M.A., Richardson, A.D., 2016. Multiscale modeling of spring phenology across Deciduous Forests in the Eastern United States. Glob. Chang. Biol. 22, 792–805. https://doi.org/10.1111/gcb.13122

Melaas, E.K., Friedl, M.A., Richardson, A.D., 2015. Multi-scale modeling of spring

phenology across Deciduous Forests in the Eastern United States. Glob. Chang. Biol. n/a-n/a. https://doi.org/10.1111/gcb.13122

Misra, G., Buras, A., Heurich, M., Asam, S., Menzel, A., 2018. LiDAR derived topography and forest stand characteristics largely explain the spatial variability observed in MODIS land surface phenology. Remote Sens. Environ. 218, 231–244. https://doi.org/10.1016/j.rse.2018.09.027

Morin, X., Roy, J., Sonié, L., Chuine, I., 2010. Changes in leaf phenology of three European oak species in response to experimental climate change. New Phytol. 186, 900–910. https://doi.org/10.1111/j.1469-8137.2010.03252.x

Park, I.W., Mazer, S.J., 2018. Overlooked climate parameters best predict flowering onset: Assessing phenological models using the elastic net. Glob. Chang. Biol. 24, 5972–5984. https://doi.org/10.1111/gcb.14447

Pasquarella, V.J., Holden, C.E., Woodcock, C.E., 2018. Improved mapping of forest type using spectral-temporal Landsat features. Remote Sens. Environ. 210, 193–207. https://doi.org/10.1016/j.rse.2018.02.064

Persson, M., Lindberg, E., Reese, H., 2018. Tree species classification with multi-temporal Sentinel-2 data. Remote Sens. 10, 1794.

Piao, S., Fang, J., Zhou, L., Ciais, P., Zhu, B., 2006. Variations in satellite-derived phenology in China's temperate vegetation. Glob. Chang. Biol. 12, 672–685. https://doi.org/10.1111/j.1365-2486.2006.01123.x

Piao, S., Tan, J., Chen, A., Fu, Y.H., Ciais, P., Liu, Q., Janssens, I. a, Vicca, S., Zeng, Z., Jeong, S.-J., Li, Y., Myneni, R.B., Peng, S., Shen, M., Peñuelas, J., 2015. Leaf onset in the northern hemisphere triggered by daytime temperature. Nat. Commun. 6,

6911. https://doi.org/10.1038/ncomms7911

Planet Labs Inc, 2020. Planet Imagery and Archive.

Primack, R.B., Ibáñez, I., Higuchi, H., Lee, S.D., Miller-Rushing, A.J., Wilson, A.M., Silander, J.A., 2009. Spatial and interspecific variability in phenological responses to warming temperatures. Biol. Conserv. 142, 2569–2577. https://doi.org/https://doi.org/10.1016/j.biocon.2009.06.003

Qiu, T., Song, C., Clark, J.S., Seyednasrollah, B., Rathnayaka, N., Li, J., 2020. Understanding the continuous phenological development at daily time step with a Bayesian hierarchical space-time model: impacts of climate change and extreme weather events. Remote Sens. Environ. 247, 111956.

Richardson, A.D., Anderson, R.S., Arain, M.A., Barr, A.G., Bohrer, G., Chen, G., Chen, J.M., Ciais, P., Davis, K.J., Desai, A.R., Dietze, M.C., Dragoni, D., Garrity, S.R., Gough, C.M., Grant, R., Hollinger, D.Y., Margolis, H. a., Mccaughey, H., Migliavacca, M., Monson, R.K., Munger, J.W., Poulter, B., Raczka, B.M., Ricciuto, D.M., Sahoo, A.K., Schaefer, K., Tian, H., Vargas, R., Verbeeck, H., Xiao, J., Xue, Y., 2012. Terrestrial biosphere models need better representation of vegetation phenology: Results from the North American Carbon Program Site Synthesis. Glob. Chang. Biol. 18, 566–584. https://doi.org/10.1111/j.1365-2486.2011.02562.x

Richardson, A.D., Bailey, A.S., Denny, E.G., Martin, C.W., O'KEEFE, J., 2006. Phenology of a northern hardwood forest canopy. Glob. Chang. Biol. 12, 1174–1188.

Rodman, K.C., Veblen, T.T., Chapman, T.B., Rother, M.T., Wion, A.P., Redmond, M.D., 2019. Limitations to recovery following wildfire in dry forests of southern Colorado

and northern New Mexico, USA. Ecol. Appl. 0, 1–20. https://doi.org/10.1002/eap.2001

Rodriguez-Galiano, V.F., Sanchez-Castillo, M., Dash, J., Atkinson, P.M., Ojeda-Zujar, J., 2016. Modelling interannual variation in the spring and autumn land surface phenology of the European forest. Biogeosciences 13, 3305–3317. https://doi.org/10.5194/bg-13-3305-2016

Schaaf, C.B., Gao, F., Strahler, A.H., Lucht, W., Li, X., Tsang, T., Strugnell, N.C., Zhang, X., Jin, Y., Muller, J.-P.P., Lewis, P., Barnsley, M., Hobson, P., Disney, M., Roberts, G., Dunderdale, M., Doll, C., D'Entremont, R.P., Hu, B., Liang, S., Privette, J.L., Roy, D., 2002. First operational BRDF, albedo nadir reflectance products from MODIS. Remote Sens. Environ. 83, 135–148. https://doi.org/10.1016/S0034-4257(02)00091-3

Schwartz, M.D., Ahas, R., Aasa, A., 2006. Onset of spring starting earlier across the Northern Hemisphere. Glob. Chang. Biol. 12, 343–351. https://doi.org/10.1111/j.1365-2486.2005.01097.x

Shen, M., Piao, S., Jeong, S.-J., Zhou, L., Zeng, Z., Ciais, P., Chen, D., Huang, M., Jin, C.-S., Li, L.Z.X., 2015. Evaporative cooling over the Tibetan Plateau induced by vegetation growth. Proc. Natl. Acad. Sci. 112, 9299–9304.

Shen, M., Tang, Y., Chen, J., Zhu, X., Zheng, Y., 2011. Influences of temperature and precipitation before the growing season on spring phenology in grasslands of the central and eastern Qinghai-Tibetan Plateau. Agric. For. Meteorol. 151, 1711–1722. https://doi.org/10.1016/j.agrformet.2011.07.003

Sparks, T.H., Jeffree, E.P., Jeffree, C.E., 2000. An examination of the relationship

between flowering times and temperature at the national scale using long-term phenological records from the UK. Int. J. Biometeorol. 44, 82–87. https://doi.org/10.1007/s004840000049

Tarantino, C., Casella, F., Adamo, M., Lucas, R., Beierkuhnlein, C., Blonda, P., 2019. Ailanthus altissima mapping from multi-temporal very high resolution satellite images. ISPRS J. Photogramm. Remote Sens. 147, 90–103. https://doi.org/https://doi.org/10.1016/j.isprsjprs.2018.11.013

Thomas, N., Neigh, C.S.R., Carroll, M.L., McCarty, J.L., Bunting, P., 2020. Fusion Approach for Remotely Sensed Mapping of Agriculture (FARMA): A Scalable Open Source Method for Land Cover Monitoring Using Data Fusion. Remote Sens. 12, 3459. https://doi.org/10.3390/rs12203459

Thorn, A.M., Thompson, J.R., Plisinski, J.S., 2016. Patterns and predictors of recent forest conversion in New England. Land 5, 30.

Thornton, P.E., Thornton, M.M., Mayer, B.W., Wei, Y., Devarakonda, R., Vose, R.S., Cook, R.B., 2017. Daymet: Daily Surface Weather Data on a 1-km Grid for North America, Version 3. https://doi.org/10.3334/ornldaac/1328

USDA, 2015. National Agriculture Imagery Program [WWW Document]. URL https://www.fsa.usda.gov/programs-and-services/aerial-photography/imagery-programs/naip-imagery/

Van Wijk, M.T., Williams, M., JA, GR, 2003. Interannual variability of plant phenology in tussock tundra: modelling interactions of plant productivity, plant phenology, snowmelt and soil thaw. Glob. Chang. Biol. 9, 743–758.

Wang, J., Zhang, X., 2020. Investigation of wildfire impacts on land surface phenology

from MODIS time series in the western US forests. ISPRS J. Photogramm. Remote Sens. 159, 281–295. https://doi.org/10.1016/j.isprsjprs.2019.11.027

Wang, J., Zhang, X., 2017. Impacts of wildfires on interannual trends in land surface phenology: an investigation of the Hayman Fire. Environ. Res. Lett. 12, 054008. https://doi.org/10.1088/1748-9326/aa6ad9

Wang, Z., Schaaf, C.B., Sun, Q., Shuai, Y., Román, M.O., 2018. Capturing rapid land surface dynamics with Collection V006 MODIS BRDF/NBAR/Albedo (MCD43) products. Remote Sens. Environ. 207, 50–64. https://doi.org/https://doi.org/10.1016/j.rse.2018.02.001

White, M.A., De Beurs, K.M., Didan, K., Inouye, D.W., Richardson, A.D., Jensen, O.P., O'keefe, J., Zhang, G., Nemani, R.R., Van Leeuwen, W.J.D., Brown, J.F., De Wit, A., Schaepman, M., Lin, X., Dettinger, M., Bailey, A.S., Kimball, J., Schwartz, M.D., Baldocchi, D.D., Lee, J.T., Lauenroth, W.K., 2009. Intercomparison, interpretation, and assessment of spring phenology in North America estimated from remote sensing for 1982-2006. Glob. Chang. Biol. 15, 2335–2359. https://doi.org/10.1111/j.1365-2486.2009.01910.x

Wu, C., Hou, X., Peng, D., Gonsamo, A., Xu, S., 2016. Land surface phenology of China's temperate ecosystems over 1999–2013: Spatial–temporal patterns, interaction effects, covariation with climate and implications for productivity. Agric. For. Meteorol. 216, 177–187. https://doi.org/10.1016/j.agrformet.2015.10.015

Wu, C., Wang, X., Wang, H., Ciais, P., Peñuelas, J., Myneni, R.B., Desai, A.R., Gough, C.M., Gonsamo, A., Black, A.T., Jassal, R.S., Ju, W., Yuan, W., Fu, Y., Shen, M., Li, S., Liu, R., Chen, J.M., Ge, Q., 2018. Contrasting responses of autumn-leaf

senescence to daytime and night-time warming. Nat. Clim. Chang. 8, 1. https://doi.org/10.1038/s41558-018-0346-z

Xie, J., Kneubühler, M., Garonna, I., Notarnicola, C., De Gregorio, L., De Jong, R., Chimani, B., Schaepman, M.E., 2017. Altitude-dependent influence of snow cover on alpine land surface phenology. J. Geophys. Res. Biogeosciences 122, 1107–1122. https://doi.org/10.1002/2016JG003728

Yang, Y., Guan, H., Shen, M., Liang, W., Jiang, L., 2015. Changes in autumn vegetation dormancy onset date and the climate controls across temperate ecosystems in China from 1982 to 2010. Glob. Chang. Biol. 21, 652–665. https://doi.org/10.1111/gcb.12778

Zhang, X., 2015. Reconstruction of a complete global time series of daily vegetation index trajectory from long-term AVHRR data. Remote Sens. Environ. 156, 457–472. https://doi.org/10.1016/j.rse.2014.10.012

Zhang, X., Friedl, M.A., Schaaf, C.B., Strahler, A.H., Hodges, J.C.F.F., Gao, F., Reed, B.C., Huete, A., 2003. Monitoring vegetation phenology using MODIS. Remote Sens. Environ. 84, 471–475. https://doi.org/10.1016/S0034-4257(02)00135-9

Zhang, X., Liu, L., Henebry, G.M., 2019. Impacts of land cover and land use change on long-term trend of land surface phenology: A case study in agricultural ecosystems. Environ. Res. Lett. 14. https://doi.org/10.1088/1748-9326/ab04d2

Zhang, X., Liu, L., Liu, Y., Jayavelu, S., Wang, J., Moon, M., Henebry, G.M., Friedl, M.A., Schaaf, C.B., 2018. Generation and evaluation of the VIIRS land surface phenology product. Remote Sens. Environ. 216, 212–229. https://doi.org/10.1016/j.rse.2018.06.047

Zhang, X., Tarpley, D., Sullivan, J.T., 2007. Diverse responses of vegetation phenology to a warming climate. Geophys. Res. Lett. 34, 1–5. https://doi.org/10.1029/2007GL031447

Zhang, X., Wang, J., Gao, F., Liu, Y., Schaaf, C., Friedl, M., Yu, Y., Jayavelu, S., Gray, J., Liu, L., Yan, D., Henebry, G.M., 2017. Exploration of scaling effects on coarse resolution land surface phenology. Remote Sens. Environ. 190, 318–330. https://doi.org/10.1016/j.rse.2017.01.001

Zhang, X., Wang, J., Henebry, G.M., Gao, F., 2020. Development and evaluation of a new algorithm for detecting 30 m land surface phenology from VIIRS and HLS time series. ISPRS J. Photogramm. Remote Sens. 161, 37–51. https://doi.org/10.1016/j.isprsjprs.2020.01.012

CHAPTER 5: Summary of the research

5.1. Research summary

The research aims to gain a comprehensive understanding of the responses of land surface phenology (LSP) to wildfires in the western US forests. To reach this goal, three hypotheses were developed. Below summarize the three studies (detailed in Chapters 2, 3, and 4, respectively) that test the hypotheses.

5.1.1. Hypothesis 1: the magnitude and interannual trend of SOS are influenced by the 2002 Hayman Fire, Colorado, USA.

5.1.1.1. Summary of the methods

This study quantified the impacts of the 2002 Hayman Fire on SOS and its trend by using a buffer that was not influenced by wildfire surrounding the burned area as a reference. The burned area and burn severity were obtained from Landsat-based MTBS. The start of growing season (SOS) and annual greenness maximum (GMax) and minimum (GMin) were detected by applying the hybrid piecewise-logistic-model-based LSP detection algorithm (HPLM-LPSD) on the 250-m MODIS EVI2 time series from 2001-2014. Wildfire impact on SOS was quantified by calculating the difference of the spatial anomaly between the post-fire years (2003-2014) and pre-fire year (2001) with the spatial anomaly defined as the SOS difference between the entire burned area (or area burned with a specified severity level) and reference for each year. SOS trends during 2001-2014 were calculated using simple linear regression and compared between burned and reference areas. The post-fire recovery was evaluated with GMax and GMin using simple linear regression in the post-fire years (2003-2014).

5.1.1.2. Results and conclusions

The Hayman Fire advanced SOS by 15.2 days while the change in SOS increased with burn severity. The wildfire-caused SOS change was also influenced by extreme weather events. Particularly, SOS was >21 days earlier in the burned area than the reference area in 2012 when the contiguous US experienced an exceptionally warm spring and a severe drought. Moreover, the Hayman Fire converted SOS from a delaying trend of 3.9 days/decade to an advancing trend of -1.9 days/decade from 2001-2014. The vegetation greenness could recover to the pre-fire status in 2022 and 2053 for GMax and GMin, respectively. Based on the field survey of post-fire recovery for the Hayman Fire from the existing literature (Chambers et al., 2016; Fornwalt and Kaufmann, 2014; Rhoades et al., 2011), the post-fire temporal trajectory of GMax and GMin coincided with the post-fire recovery process of total vegetation and evergreen tree, respectively.

5.1.1.3. Implications and limitations

This study, for the first time, quantitatively analyzed wildfire impacts on SOS trend, suggesting that it should be cautious against simply viewing LSP trends as indicative of climate change. The slow recovery rate of greenness indicates that the fire impacts on the satellite-derived SOS variability and interannual trends could continue in the next few decades. However, as the area-integrated SOS was used in the analysis, an additional error bar (indicating the spatial variation) could have been used to provide more insights on the significance of wildfire impacts on LSP. Moreover, the burn severity based LSP variation could have some uncertainties because the burn severity in the MTBS map was obtained from remotely-sensed Normalized Burn Ratio (NBR) without strong supports of field investigations (French et al., 2008; Roy et al., 2006). Last,

considering that this study is based only on a single wildfire and a single LSP metric, evidence of wildfire impacts on LSP is needed from investigations involving other LSP metrics and more wildfires.

5.1.2. Hypothesis 2: wildfires in the western US forests change the LSP timing in two divergent directions (advance and delay) with the extent of change depending on burn severity.

5.1.2.1. Summary of the methods

Wildfire impacts on LSP and its trend were systematically analyzed using 838 forest fires that occurred from 2002-2014 across the western US obtained from MTBS. Three LSP timing metrics that are start (SOS), end (EOS), and length (LOS) of growing season and two LSP greenness metrics that are seasonal greenness maximum (GMax) and minimum (GMin) were derived from daily time series of 250-m MODIS two-band enhanced vegetation index (EVI2) during 2001-2015. Abrupt LSP changes by wildfires were quantified using the average LSP in the first three years after wildfire occurrence and that in all pre-fire years. LSP trends were determined for the entire time series from 2001-2015 and post-fire time series using a Sen's slope and Mann-Kendall test and compared between the burned and buffer areas.

5.1.2.2. Results and conclusions

Wildfires decreased LSP greenness while changed LSP timing in two opposite directions. Overall, an absolute abrupt shift of > 2 days occurred in 73% wildfires for SOS, 80% for EOS, and 85% for LOS. More wildfires caused an advance in SOS, delay in EOS, and prolongation in LOS. Moreover, wildfires showed stronger impacts on EOS

than SOS indicating a larger variation in autumn phenology than spring phenology among different species. This is likely related to the facts: (1) the vegetation species are more diverse in the burned area after fire occurrences; (2) EOS is more complexly controlled by environmental factors than SOS although the underlying mechanism remains to be investigated (Delpierre et al. 2009; Richardson et al 2010; Zhang et al 2020; Wang et al., 2020). In addition, the abrupt LSP changes depended largely on burn severity with the largest impact at the moderate burn severity for LSP timing and the high burn severity for LSP greenness. Finally, the phenological trends from 2001-2015 differed significantly between burned and unburned reference areas. Particularly, the reference areas showed a delaying trend for SOS and a greening trend for GMin, while the burned areas showed an advancing trend for SOS and browning trend for GMin with the trend value depending on the wildfire occurrence year.

5.1.2.3. Implications and limitations

This study provides stronger evidence of wildfire impacts on LSP trends by using a large number of wildfires and multiple LSP metrics. Changes in trends of both the entire time series from 2001-2015 and post-fire time series indicate that the wildfires occurred either during or before a given study period can influence the interannual trends. Therefore, historical fires could also have considerable impacts on LSP trends at a regional scale. Moreover, the wildfire frequency and size across the globe are expected to increase in this century because of the changing climate (Liu et al., 2010). As a result, LSP trends responding to climate change may have been largely interrupted and the interruption could become broader in the future decades. It suggests that land disturbance,

such as wildfire, should be considered when using satellite-derived phenological trends to interpret global climate change.

We acknowledge there are a few limitations in this study. First, besides the burn severity investigated in this study, other factors can also influence the wildfire-caused abrupt LSP changes. For example, different fire types cause different changes in vegetation species, soil conditions, and surface temperature, which in turn influence the abrupt LSP changes. Second, this study only discussed the wildfire impacts on evergreen forests impeding a statistically meaningful analysis of the wildfire impacts on LSP among different forest types. Third, this study used unburned forest pixels as an LSP reference that was not influenced by wildfires. However, the environmental conditions between the reference and burned areas could differ largely, which interrupts the quantification of wildfire impacts. Future studies are recommended to select reference areas with environmental conditions (e.g., topography, climate, and plant species) similar to burned areas. Fourth, although the direct influence of climate and topography on LSP variation was largely removed using references, their interactions with wildfire impacts could still influence LSP variation (Alexander et al., 2006; Davis et al., 2019) which impedes a complete separation of wildfire impacts from other factors. Last, the potential uncertainty from MTBS map discussed in Section 5.1.1.3. still exists, although MTBS is a convenient resource and field investigation of fire effect is difficult in a large area like western US.

5.1.3. Hypothesis 3: land cover composition, climate, and topography co-determine the LSP variation in the burned area of the 2002 Ponil Complex Fire, New Mexico.

5.1.3.1. Summary of the methods

The 2002 Ponil Complex Fire in New Mexico, USA was selected as the study area because it is a large wildfire in the western US and the wildfire-caused plant species change was acquirable. This study quantified the contributions of land cover composition change (caused by the fire) and other environmental factors to the spatial and interannual variations of LSP using a machine learning approach of the Boosted Regression Tree (BRT). SOS and EOS were derived from the 500-m MODIS data from 2001-2018 and 30-m Harmonized Landsat Sentinel-2 (HLS) data in 2018. Two metrics of land cover composition, i.e., vegetation fractional coverage (VFC) and tree proportion to vegetation (TPV), were derived from the high-resolution imagery in 2018 and from MODIS greenness during a growing season from 2001-2018. Using BRT, LSP spatial variations in 2018 were modeled with land cover composition and other predictors mainly including climate and topography, while LSP interannual variations during 2001-2018 were modeled with land cover composition and climate. These BRT models quantified the contribution of each predictor to spatial and interannual variations in LSP.

5.1.3.2. Results and conclusions

For LSP spatial variations, land cover composition, particularly TPV, was the most important driver, immediately followed by topography (in the HLS LSP spatial models) and preseason climates (in the MODIS LSP spatial models). In contrast, for the LSP interannual variations, the growing degree days (GDD) and the first freeze date (FFD) were the most important drivers for SOS and EOS, respectively. However, VFC

played a non-negligible role with above-average relative importance in modeling SOS and EOS. Moreover, the models for both spatial and interannual LSP variations revealed a stronger influence of land cover composition in EOS than SOS.

5.1.3.3. Implications and limitations

Some implications can be derived from the findings. The substantial effects on both spatial and interannual variations of LSP suggest that land cover composition should not be overlooked in predicting land surface phenology in the disturbed areas. Second, the largest contribution of the FFD to controlling the interannual variations of EOS indicates that EOS models could be potentially improved by adding FFD into current models that are mainly based on the preseason photoperiod, temperature, and precipitation (Liu et al., 2016; Yang et al., 2015). Third, the scale effect on HLS and MODIS LSP models suggests that the scale and dimension need to be clearly defined when evaluating the drivers of LSP variation.

There are also a few limitations. First, the effectiveness of using GMax and GRatio as surrogates of VFC and TPV has not been directly evaluated because of the limited availability of high-resolution imagery. Second, although Daymet record is one of the highest-resolution climate datasets available in the study area, the resolution (1 km) is still relatively coarse and could have an impact on the modeling performance. Last, the analysis was performed at a landscape scale, which might not be enough to obtain a general conclusion on the way that different factors drive LSP.

5.2. Key findings

The key findings of this dissertation are:

1. SOS trend was changed to be earlier by the 2002 Hayman Fire comparing an unburned reference.

2. Wildfires in the western US forests changed the LSP timing in both earlier and later directions depending on individual wildfire events.

3. The largest shifts of LSP timing occur at moderate burn severity.

4. Wildfire has a stronger impact on EOS than SOS.

5. LSP trends are interrupted by wildfires with the degree of impacts largely dependent on the wildfire occurrence year.

6. Land cover composition variation caused by a wildfire plays a dominant role in the LSP spatial variations and a non-negligible role in the LSP interannual variations in a recently burned landscape.

5.3. Recommendations and future directions

Based on the discussions of implications and limitations in the three studies (see Sections 5.1.1.3, 5.1.2.3, and 5.1.3.3), I recommend the following three main directions for future research work.

First, the underlying mechanism of the divergent response of LSP to wildfires remains unclear and needs a thorough investigation in the future. While this research found burn severity influences wildfire-caused LSP changes, other factors, such as fire type, forest type, soil conditions, and human management, can also affect post-fire LSP and should be analyzed in future studies.

Second, other land disturbances than wildfire could also interrupt the LSP trends and their impacts on LSP need to be investigated. Considering the human populations and

their use of land have modified about one-third to one-half of the land surface and transformed another third or more of the terrestrial biosphere into rangelands and seminatural anthromes (Ellis, 2011; Vitousek et al., 1997), land disturbance is likely to have broader impacts on LSP.

Third, as the current LSP trends are often interrupted by disturbances like wildfire, future studies are recommended to explore the possibility of extracting LSP variation only responses to climate change. While some studies analyzed the LSP by excluding the areas with land cover changes (Jönsson et al., 2018; Melaas et al., 2016), the completely pure and homogenous pixels are rare in nature and difficult to identify in moderate to coarse resolution remote sensing data (Misra et al., 2018). Although high-resolution (<10 m) data, such as PlanetScope, are less suffered from this issue, LSP trend analysis based on those data is currently limited because of the relatively short data record and can be studied with the accumulation of high-resolution data in the future. On the other hand, the change detection methods recently developed based on time series analysis, such as Breaks For Additive Seasonal and Trend (Verbesselt et al., 2010) and Detecting Breakpoints and Estimating Segments in Trend (Jamali et al., 2015), provide an opportunity to separate the gradual trend from abrupt changes. However, these methods are still not able to separate the LSP responses to climate change from the disturbance impacts, which calls for new approaches. A possible way could be incorporating the pattern of LSP responses to disturbances to the change detection methods, which relies on a thorough and comprehensive analysis of LSP responses to different disturbance agents.

References

Alexander, J.D., Seavy, N.E., Ralph, C.J., Hogoboom, B., 2006. Vegetation and topographical correlates of fire severity from two fires in the Klamath-Siskiyou region of Oregon and California. Int. J. Wildl. Fire 15, 237–245.

Chambers, M.E., Fornwalt, P.J., Malone, S.L., Battaglia, M.A., 2016. Patterns of conifer regeneration following high severity wildfire in ponderosa pine-dominated forests of the Colorado Front Range. For. Ecol. Manage. 378, 57–67. https://doi.org/10.1016/j.foreco.2016.07.001

Davis, K.T., Dobrowski, S.Z., Higuera, P.E., Holden, Z.A., Veblen, T.T., Rother, M.T., Parks, S.A., Sala, A., Maneta, M.P., 2019. Wildfires and climate change push low-elevation forests across a critical climate threshold for tree regeneration. Proc. Natl. Acad. Sci. 116, 6193 LP – 6198. https://doi.org/10.1073/pnas.1815107116

Delpierre, N., Dufrêne, E., Soudani, K., Ulrich, E., Cecchini, S., Boé, J., François, C., 2009. Modelling interannual and spatial variability of leaf senescence for three deciduous tree species in France. Agric. For. Meteorol. 149, 938–948. https://doi.org/https://doi.org/10.1016/j.agrformet.2008.11.014Ellis, E.C., 2011. Anthropogenic transformation of the terrestrial biosphere. Philos. Trans. R. Soc. London A Math. Phys. Eng. Sci. 369, 1010–1035.

Fornwalt, P.J., Kaufmann, M.R., 2014. Understorey plant community dynamics following a large, mixed severity wildfire in a Pinus ponderosa-Pseudotsuga menziesii forest, Colorado, USA. J. Veg. Sci. 25, 805–818. https://doi.org/10.1111/jvs.12128

French, N.H.F., Kasischke, E.S., Hall, R.J., Murphy, K.A., Verbyla, D.L., Hoy, E.E., Allen, J.L., 2008. Using Landsat data to assess fire and burn severity in the North American boreal forest region : an overview and summary of results 443–462. https://doi.org/10.1071/WF08007Jamali, S., Jönsson, P., Eklundh, L., Ardö, J., Seaquist, J., 2015. Detecting changes in vegetation trends using time series segmentation. Remote Sens. Environ. 156, 182–195. https://doi.org/10.1016/j.rse.2014.09.010

Jönsson, P., Cai, Z., Melaas, E., Friedl, M.A., Eklundh, L., 2018. A method for robust estimation of vegetation seasonality from Landsat and Sentinel-2 time series data. Remote Sens. 10. https://doi.org/10.3390/rs10040635

Li, J., Roy, D.P., 2017. A global analysis of Sentinel-2A, Sentinel-2B and Landsat-8 data revisit intervals and implications for terrestrial monitoring. Remote Sens. 9, 902. https://doi.org/10.3390/rs9090902

Liu, Q., Fu, Y.H., Zeng, Z., Huang, M., Li, X., Piao, S., 2016. Temperature, precipitation, and insolation effects on autumn vegetation phenology in temperate China. Glob. Chang. Biol. 22, 644–655. https://doi.org/10.1111/gcb.13081

Liu, Y., Stanturf, J., Goodrick, S., 2010. Trends in global wildfire potential in a changing climate. For. Ecol. Manage. 259, 685–697.

Melaas, E.K., Sulla-Menashe, D., Gray, J.M., Black, T.A., Morin, T.H., Richardson, A.D., Friedl, M.A., 2016. Multisite analysis of land surface phenology in North American temperate and boreal deciduous forests from Landsat. Remote Sens. Environ. 186, 452–464. https://doi.org/10.1016/j.rse.2016.09.014

Misra, G., Buras, A., Heurich, M., Asam, S., Menzel, A., 2018. LiDAR derived topography and forest stand characteristics largely explain the spatial variability observed in MODIS land surface phenology. Remote Sens. Environ. 218, 231–244. https://doi.org/10.1016/j.rse.2018.09.027

Rhoades, C.C., Entwistle, D., Butler, D., 2011. The influence of wildfire extent and severity on streamwater chemistry, sediment and temperature following the Hayman Fire, Colorado. Int. J. Wildl. Fire 20, 430–442. https://doi.org/10.1071/WF09086

Roy, D.P., Boschetti, L., Trigg, S.N., 2006. Remote sensing of fire severity: Assessing the performance of the normalized burn ratio. IEEE Geosci. Remote Sens. Lett. 3, 112–116. https://doi.org/10.1109/LGRS.2005.858485

Richardson, A.D., Andy Black, T., Ciais, P., Delbart, N., Friedl, M.A., Gobron, N., Hollinger, D.Y., Kutsch, W.L., Longdoz, B., Luyssaert, S., 2010. Influence of spring and autumn phenological transitions on forest ecosystem productivity. Philos. Trans. R. Soc. B Biol. Sci. 365, 3227–3246.Verbesselt, J., Hyndman, R., Newnham, G., Culvenor, D., 2010. Detecting trend and seasonal changes in satellite image time series. Remote Sens. Environ. 114, 106–115. https://doi.org/10.1016/j.rse.2009.08.014

Vitousek, P.M., Aber, J.D., Howarth, R.W., Likens, G.E., Matson, P.A., Schindler, D.W., Schlesinger, W.H., Tilman, D.G., 1997. Human alteration of the global nitrogen cycle: sources and consequences. Ecol. Appl. 7, 737–750.

Wang, X., Dannenberg, M.P., Yan, D., Jones, M.O., Kimball, J.S., Moore, D.J.P., van Leeuwen, W.J.D., Didan, K., Smith, W.K., 2020. Globally Consistent Patterns of

Asynchrony in Vegetation Phenology Derived From Optical, Microwave, and Fluorescence Satellite Data. J. Geophys. Res. Biogeosciences 125. https://doi.org/10.1029/2020JG005732

Yang, Y., Guan, H., Shen, M., Liang, W., Jiang, L., 2015. Changes in autumn vegetation dormancy onset date and the climate controls across temperate ecosystems in China from 1982 to 2010. Glob. Chang. Biol. 21, 652–665. https://doi.org/10.1111/gcb.12778

Zhang, Y., Parazoo, N.C., Williams, A.P., Zhou, S., Gentine, P., 2020. Large and projected strengthening moisture limitation on end-of-season photosynthesis. Proc. Natl. Acad. Sci. 117, 9216–9222.